



HAL
open science

Bioinformatics analysis and consensus ranking for biological high throughput data

Bo Yang

► **To cite this version:**

Bo Yang. Bioinformatics analysis and consensus ranking for biological high throughput data. Bioinformatics [q-bio.QM]. Université Paris Sud - Paris XI; Université de Wuhan (Chine), 2014. English. NNT : 2014PA112250 . tel-01207489

HAL Id: tel-01207489

<https://theses.hal.science/tel-01207489v1>

Submitted on 1 Oct 2015

HAL is a multi-disciplinary open access archive for the deposit and dissemination of scientific research documents, whether they are published or not. The documents may come from teaching and research institutions in France or abroad, or from public or private research centers.

L'archive ouverte pluridisciplinaire **HAL**, est destinée au dépôt et à la diffusion de documents scientifiques de niveau recherche, publiés ou non, émanant des établissements d'enseignement et de recherche français ou étrangers, des laboratoires publics ou privés.



Comprendre le monde,
construire l'avenir®

UNIVERSITÉ PARIS-SUD

ÉCOLE DOCTORALE 427 :
INFORMATIQUE PARIS SUD

Laboratoire : Laboratoire de Recherche en Informatique

THÈSE DE DOCTORAT

INFORMATIQUE

par

Bo YANG

Analyses bioinformatiques et classements consensus
pour les données biologiques à haut débit

Date de soutenance : 30/09/2014

Composition du jury :

Directeur de thèse :
Co-directeur de thèse :

Alain DENISE
Xiang-Dong Fu

Co-directeur de thèse
Co-directeur de thèse

Rapporteurs :
Examineurs :

Daowen WANG
Sarah COHEN-BOULAKIA
Stéphane VIALETTE
Min Wu

Examineur
Examinatrice
Examineur
Examineur

Content

Content	I
Résumé	III
Abstract	V
Chapter 1: Introduction	1
Chapter 2: Genome-wide Analysis of U2AF Functions in pre-mRNA Splicing	5
2.1 Introduction.....	5
2.1.1 RNA splicing.....	5
2.1.2 Alternative splicing	11
2.1.3 Splicing regulation	13
2.1.4 Splicing and disease	16
2.1.5 Motivation.....	18
2.2 Methods.....	21
2.2.1 High throughput sequencing	21
2.2.2 Bioinformatics analysis.....	27
2.3 Results.....	38
2.3.1 Genome-wide mapping of U2AF-RNA interactions.....	38
2.3.2 U2AF recognition of ~88% functional 3' splice sites in the human genome	44
2.3.3 Additional U2AF binding events beyond functional 3' splice sites	47
2.3.4 Critical roles of U2AF in regulated splicing	49
2.3.5 Multiple mechanisms underlying U2AF-regulated alternative splicing.....	52
2.3.6 Polar effect of U2AF65 binding on downstream 3' splice site recognition.....	56
2.3.7 Coordinated action of U2AF65 and U2AF35 in regulated splicing.....	59
2.3.8 U2AF65 binding scores.....	63
2.4 Discussion	66
Chapter 3: Consistent-Pivot: A New effective Pivot Algorithms for Ranking Aggregation Problem	69
3.1 Introduction.....	69

3.2 Notations	73
3.2.1 Ranking with ties.....	73
3.2.2 Unifying a set of partial rankings.....	73
3.2.3 Distance measures.....	74
3.2.4 Kemeny optimal aggregations.....	76
3.3 Previous algorithms.....	78
3.3.1 Some heuristics and approximation algorithms	78
3.3.2 Other algorithms.....	82
3.3.3 Pivot Algorithms	82
3.4 Methods.....	91
3.4.1 Consistent-Pivot algorithm.....	91
3.4.2 Experiments on the algorithms.....	94
3.5 Results.....	98
3.5.1 Results on real biological data	98
3.5.2 Results on WebSearch data	100
3.5.3 Results on synthetic data	103
3.6 Discussion	105
Reference	106
Appendix : List of the publications.....	120
Acknowledgement	121

Résumé

Cette thèse aborde deux problèmes relatifs à l'analyse et au traitement des données biologiques à haut débit: le premier touche l'analyse bioinformatique des génomes à grande échelle, le deuxième est consacré au développement d'algorithmes pour le problème de la recherche d'un classement consensus de plusieurs classements.

L'épissage des ARN est un processus cellulaire qui modifie un ARN pré-messager en en supprimant les introns et en raboutant les exons. L'hétérodimère U2AF a été très étudié pour son rôle dans processus d'épissage lorsqu'il se fixe sur des sites d'épissage fonctionnels. Cependant beaucoup de problèmes critiques restent en suspens, notamment l'impact fonctionnel des mutations de ces sites associées à des cancers. Par une analyse des interactions U2AF-ARN à l'échelle génomique, nous avons déterminé qu'U2AF a la capacité de reconnaître environ 88% des sites d'épissage fonctionnels dans le génome humain. Cependant on trouve de très nombreux autres sites de fixation d'U2AF dans le génome. Nos analyses suggèrent que certains de ces sites sont impliqués dans un processus de régulation de l'épissage alternatif. En utilisant une approche d'apprentissage automatique, nous avons développé une méthode de prédiction des sites de fixation d'U2AF, dont les résultats sont en accord avec notre modèle de régulation. Ces résultats permettent de mieux comprendre la fonction d'U2AF et les mécanismes de régulation dans lesquels elle intervient.

Le classement des données biologiques est une nécessité cruciale. Nous nous sommes intéressés au problème du calcul d'un classement consensus de plusieurs classements de données, dans lesquels des égalités (*ex-aequo*) peuvent être présentes. Plus précisément, il s'agit de trouver un classement dont la somme des distances aux classements donnés en entrée est minimale. La mesure de distance utilisée le plus fréquemment pour ce problème est la distance de Kendall-tau généralisée. Or, il a été montré que, pour cette distance, le problème du consensus est NP-difficile dès lors qu'il y a plus de quatre classements en entrée. Nous proposons pour le résoudre une heuristique qui est une nouvelle variante d'algorithme à pivot. Cette heuristique,

appelée Consistent-pivot, s'avère à la fois plus précise et plus rapide que les algorithmes à pivot qui avaient été proposés auparavant.

Abstract

It is thought to be more and more important to solve biological questions using Bioinformatics approaches in the post-genomic era. This thesis focuses on the Bioinformatics analysis and algorithms development of consensus ranking for biological high throughput data.

In molecular biology and genetics, RNA splicing is a modification of the nascent pre-messenger RNA (pre-mRNA) transcript in which introns are removed and exons are joined. The U2AF heterodimer has been well studied for its role in defining functional 3' splice sites in pre-mRNA splicing, but multiple critical problems are still outstanding, including the functional impact of their cancer-associated mutations. Through genome-wide analysis of U2AF-RNA interactions, we report that U2AF has the capacity to define ~88% of functional 3' splice sites in the human genome. Numerous U2AF binding events also occur in other genomic locations and metagene and minigene analysis suggests that upstream intronic binding events interfere with the immediate downstream 3' splice site associated with either the alternative exon to cause exon skipping or competing constitutive exon to induce inclusion of the alternative exon. We further build up a U2AF65 scoring scheme for prediction its target sites base on the high throughput sequencing data using a Maximum Entropy machine learning method, and the scores on the up and down regulated cases are consistent with our regulation model. These findings reveal the genomic function and regulatory mechanism of U2AF, which facilitates us understanding those associated diseases.

Ranking biological data is a crucial need. Instead of developing new ranking methods, Cohen-Boulakia and her colleagues proposed to generate a consensus ranking to highlight the common points of a set of rankings while minimizing their disagreements to combat the noise and error for biological data. However, it is a NP-hard question even for only four rankings based on the Kendall-tau distance. In this thesis, we propose a new variant of pivot algorithms named as Consistent-Pivot. It uses a new strategy of pivot selection and other elements assignment, which performs better

both on computation time and accuracy than previous pivot algorithms.

Key words: Bioinformatics analysis; High throughput sequencing; U2AF; RNA splicing; Algorithm; Consensus ranking;

Chapter 1: Introduction

As said by Eric Green who is the director of American National Human Genome Research Institute, “Generating the data is not the bottleneck..... The bottleneck is analyzing the data”, it is thought to be more and more important to solve biological questions using Bioinformatics approaches in the post-genomic ear. Bioinformatics is an interdisciplinary scientific field of computer and biology sciences. It uses computer to better understand biology, especially important in this biological big data era (see Figure 1.1).

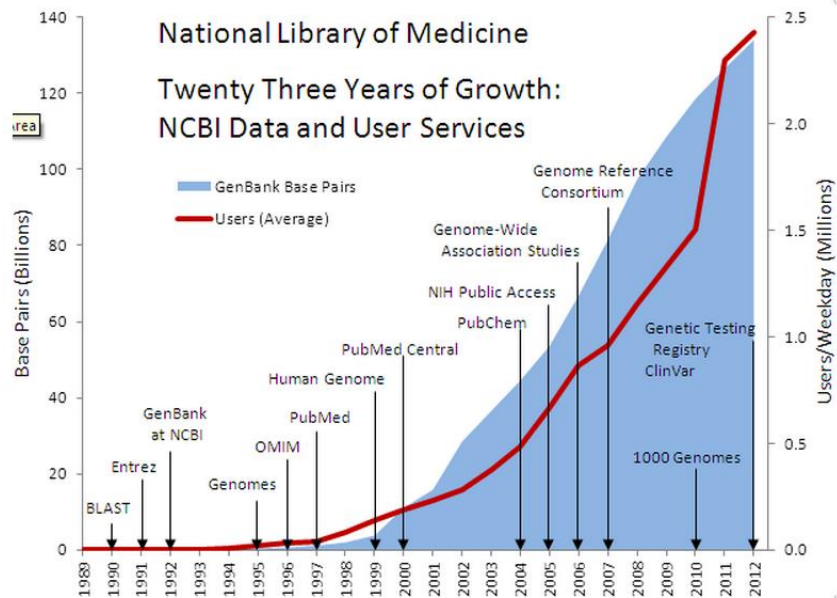


Figure 1.1. The amount of base pairs and users in GenBank database in twenty three years. Many important events are also indicated. Figure from (<http://www.nlm.nih.gov/about/2014CJ.html>).

Bioinformatics starts from sequencing alignment and annotation, while it appears in every aspect in biological research now (see Figure 1.2), as shown in below:

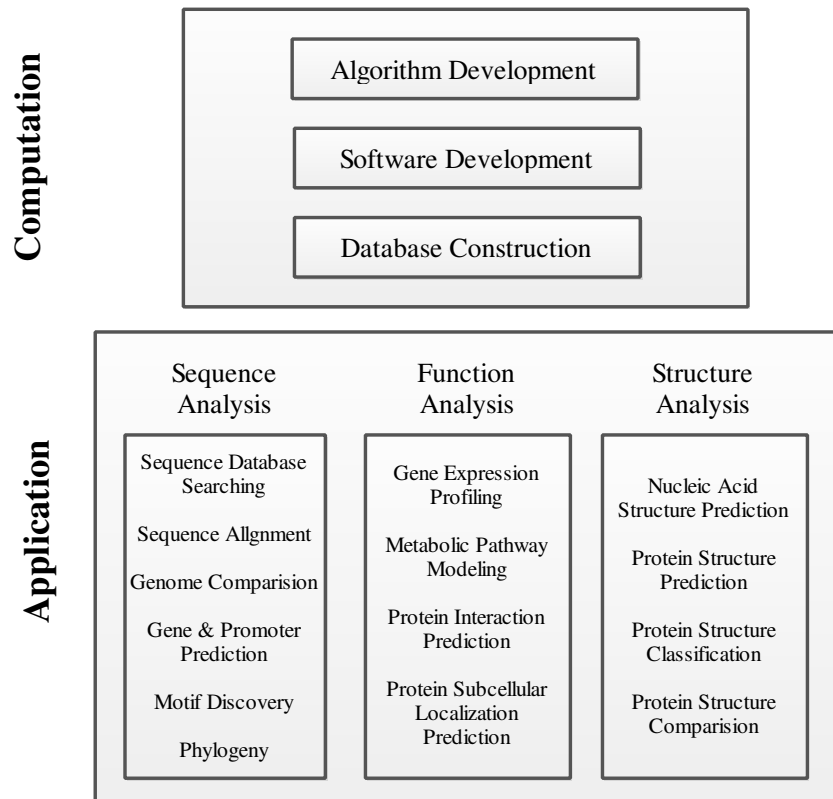


Figure 1.2. Overview of various of subfields of bioinformatics

1. Sequence analysis: Genome annotation to predict unknown genes; comparative genomics to understand gene function and evolution; genome wide associate study (GWAS) to find disease genes or mutation sites.
2. High throughput sequencing analysis: Data analysis of ChIP-seq, CLIP-seq, RNA-seq, Ribo-Seq and so on, to reveal the gene and protein expression profiles, protein and DNA/RNA interaction and regulation.
3. Structure prediction: Structures of RNAs and proteins are always related with their functions. Structure prediction helps to understand the function, and then guides drug design
4. Network and systems biology: Attempts to integrate many different data types, to understand biology process in a network view.
5. Software and tools: Rang from simple tools to design PCR primer, to complex platform or web-server for searching various types of data.

6. Algorithms development: Big data means a large amount of calculation. It cannot be accepted, if it should run for a long time. Developing an effective algorithm to correctly solve problem in a short time, is also a big challenge.
7. Databases: It is very important for biological research, because it is mainly based on a large amount of knowledge. Storing in database facilitate searching, modification and utilization.

Bioinformatics has become an important part of many areas of biology. In experimental molecular biology, bioinformatics techniques such as image and signal processing allow extraction of useful results from large amounts of raw data. In the field of genetics and genomics, it aids in sequencing and annotating genomes and their observed mutations. It plays a role in the text mining of biological literature and the development of biological and gene ontologies to organize and query biological data. It also plays a role in the analysis of gene and protein expression and regulation. Bioinformatics tools aid in the comparison of genetic and genomic data and more generally in the understanding of evolutionary aspects of molecular biology. At a more integrative level, it helps analyze and catalogue the biological pathways and networks that are an important part of systems biology. In structural biology, it aids in the simulation and modeling of DNA, RNA, and protein structures as well as molecular interactions.

This thesis focuses on the Bioinformatics data analysis in Chapter 2 and algorithms development of consensus ranking for biological high throughput data in Chapter 3, to solve biological questions.

In molecular biology and genetics, RNA splicing is a modification of the nascent pre-messenger RNA (pre-mRNA) transcript in which introns are removed and exons are joined. The U2AF heterodimer has been well studied for its role in defining functional 3' splice sites in pre-mRNA splicing, but multiple critical problems are still outstanding, including the functional impact of their cancer-associated mutations. In Chapter 2, we aim to find out the function of U2AF65 to define 3' splice sites and

regulate alternative splicing using high throughput sequencing data, to facilitate the research of related disease.

Ranking biological data is a crucial need. For example, in the research of RNA alternative splicing regulation, we always want to know which splice site is weaker or stronger. There have been many tools for scoring the splice sites signal strength. But the rankings of these tools are always very different. Instead of developing new ranking methods, Cohen-Boulakia and her colleagues proposed to generate a consensus ranking to highlight the common points of a set of rankings while minimizing their disagreements to combat the noise and error for biological data. However, it is a NP-hard question even for only four rankings based on the Kendall-tau distance. In Chapter 3, we propose a new variant of pivot algorithms named as Consistent-Pivot. It uses a new strategy of pivot selection and other elements assignment, which performs better both on computation time and accuracy than previous pivot algorithms.

Chapter 2: Genome-wide Analysis of U2AF Functions in pre-mRNA Splicing

2.1 Introduction

The genetic information is stored in DNA, which is transferred from one generation to the next generation. During the life of a cell, the DNA information is transferred as RNA, and then the RNA is translated as protein. This is the central dogma of molecular biology, describing the flow of genetic information within a biological system (Crick, 1970). However, RNA does not simply copy the genetic information, as the primary RNA transcript generated from DNA should undergo processing.

2.1.1 RNA splicing

As we know, the DNA coding sequence of a protein-coding gene is a series of three-nucleotide codons, which specifies the linear sequence of amino acids in its polypeptide product. In the vast majority of cases in bacteria and their phages, the coding sequence is contiguous: the codon for one amino acid is immediately adjacent to the codon for the next amino acid in the polypeptide chain. But it is rarely so for eukaryotic genes. In those cases, the coding sequence is periodically interrupted by stretches of non-coding sequence.

Most eukaryotic genes are thus mosaics, consisting of blocks of coding sequences separated from each other by blocks of non-coding sequences. The coding sequences are called exons, and the intervening sequences are called introns. Once DNA is transcribed into an RNA transcript, the introns must be removed and the exons are joined together to create the messenger RNA (mRNA) for that gene, which is then exported into the cytoplasm. So the term exon technically names for exported regions,

and applies to any region retained in a mature RNA, whether or not it is coding. Non-coding exons include the 5' and 3' untranslated regions of an mRNA.

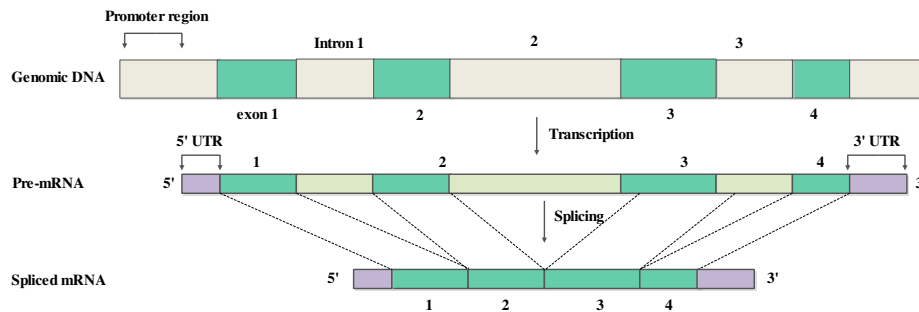


Figure 2.1.1. A typical eukaryotic gene. The depicted gene contains four coding exons separated by three introns. Transcription from the promoter generates a pre-mRNA, shown in the middle line, which contains all of the exons and introns. Splicing removes the introns and fuses the exons to generate the mature mRNA. Technically, the 5' and 3' untranslated regions are also exons because they are retained in the mature mRNA. They are shown here in light purple to indicate their status as non-coding exons.

Figure 2.1.1 shows a typical eukaryotic gene in which the coding region is interrupted by three introns, splitting it into four exons. The number of introns found within a gene varies enormously, from one in the case of most intron-containing yeast genes (and a few human genes), to as many as 363 in the case of the *Titin* gene of humans. Figure 2.1.2 shows the average number of introns per gene for a range of organisms. Interestingly, the average number increases as one looks from simple single-celled eukaryotes, such as yeast, through higher organisms such as worms and flies, all the way up to humans (Roy and Gilbert, 2006).

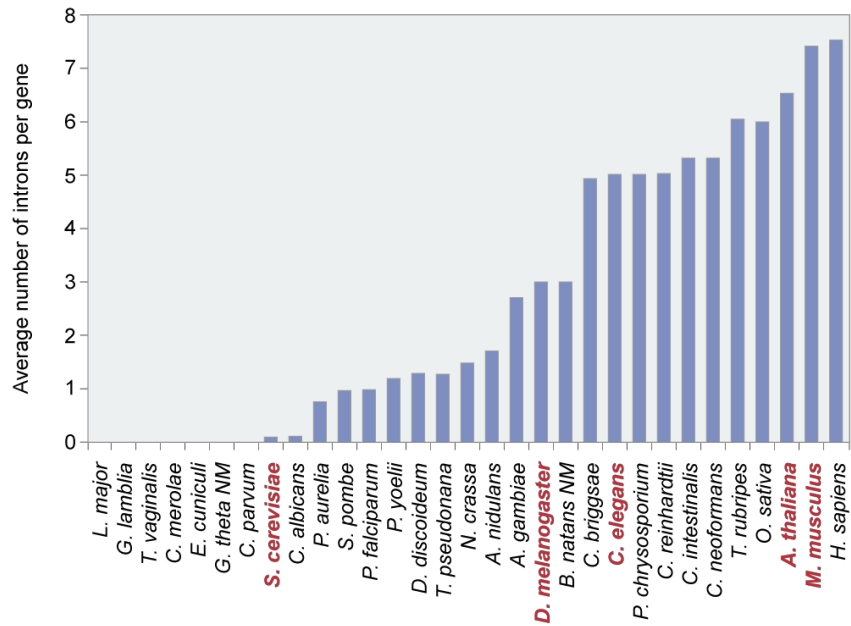


Figure 2.1.2. Number of introns per gene in various eukaryotic species. The average number of introns per gene is shown for a selection of eukaryotic species. The names in red are those of the common model organisms. Figure revised from (Roy and Gilbert 2006).

The primary transcripts of intron-containing genes must have their introns removed before they can be translated into proteins. The process of introns removal, called RNA splicing, converts the pre-mRNA into mature mRNA. It must occur with great precision to avoid the loss, or addition, of even a single nucleotide at the sites at which the exons are joined, because the triplet-nucleotide codons of mRNA are translated in a fixed reading frame that is set by the first codon in the protein-coding sequence (Dietz and Kendzior, 1994). Lack of precision in splicing, would throw the reading frames of exons out of frame: downstream codons would be incorrectly selected and the wrong amino acids incorporated into proteins.

So, how are the introns and exons distinguished from each other? How are introns removed? How are exons joined with high precision?

2.1.1.1 Consensus splicing signals

The borders between introns and exons are marked by specific nucleotide sequences within the pre-mRNAs. These sequences delineate where splicing will occur.

Thus, as shown in Figure 2.1.3, the exon-intron boundary, which is the boundary at the 5' end of the intron, is marked by a sequence called the 5' splice site. The intron-exon boundary at the 3' end of the intron is marked by the 3' splice site. The figure shows a third sequence necessary for splicing. This is called the branch point site (or branch point sequence, BPS). It is found entirely within the intron, usually close to its 3' end, and is followed by a polypyrimidine tract (Py tract) (Will and Lührmann, 2011).

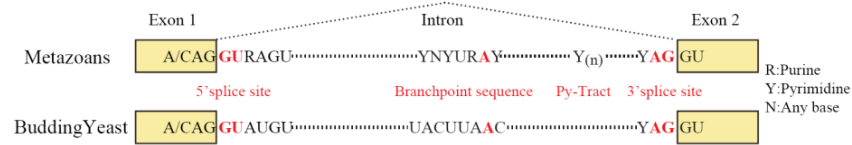


Figure 2.1.3. Sequences at intron-exon boundaries. The consensus sequences for both the 5' and 3' splice sites, and also the conserved A at the branch site. Figure revised from (Will and Lührmann, 2011).

The consensus sequence for each of these elements is shown in Figure 2.1.3. The most highly conserved sequences are the GU in the 5' splice site, the AG in the 3' splice site, and the A at the branch site. These highly conserved nucleotides are all found within the intron itself. Indeed the sequence of most exons, in contrast to the introns, is constrained by the need to encode the specific amino acids of the protein product.

As consensus sequences related with splicing are also a type of crucial features for eukaryotic gene prediction, series of splicing sites and branch site prediction tools have been developed recently: GeneSplicer (Pertea et al., 2001), MaxEntScan (Yeo and Burge, 2004), Human Splicing Finder (HSF) (Desmet et al., 2009), NetGene2 (Brunak et al., 1991), NNSplice (Reese et al., 1997), based on high throughput data, comparative genomics or mutation analysis.

Most introns have the GT-AG termini, so they are also called GT-AG introns. It is worth noting that in higher eukaryotes, there are also a few AT-AC introns, which contain AU at the 5' splice site and AC at the 3' splice site. The two types of introns are spliced by different spliceosomes (see below). GT-AG introns use the major splicing machinery, called U2-dependent spliceosome. While AT-AC introns are spliced by an

alternative, low-abundance spliceosome, called U12-dependent spliceosome (Levine and Durbin, 2001).

2.1.1.2 Spliceosome

An intron is removed through two successive transesterification reactions in which phosphodiester linkages within the pre-mRNA are broken and new ones are formed.

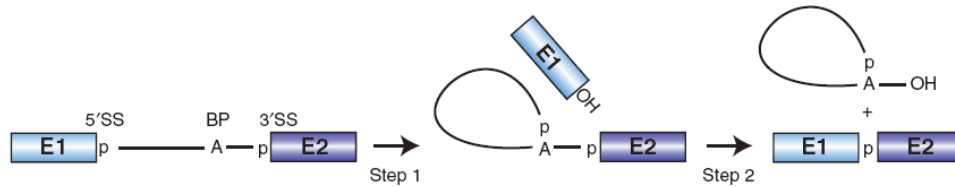


Figure 2.1.4. Schematic representation of the two-step mechanism of pre-mRNA splicing. Boxes and solid lines represent the exons (E1, E2) and the intron, respectively. The branch site adenosine is indicated by the letter A and the phosphate groups (p) at the 5' and 3' splice sites, which are conserved in the splicing products, are also shown. Figure from (Will and Lührmann, 2011)

The transesterification reactions are mediated by a huge molecular machine called the spliceosome. This complex comprises about 150 proteins and five RNAs. The five RNAs (U1, U2, U4, U5, and U6) are collectively called small nuclear RNAs (snRNAs). Each of these RNAs is between 100 and 300 nucleotides long in most eukaryotes and is complexed with several proteins. These RNA-protein complexes are called small nuclear ribonuclear proteins (snRNPs). The spliceosome is the large complex made up of these snRNPs and also many other proteins, but the exact makeup differs at different stages of the splicing reaction: different snRNPs come and go at different times, each performing particular functions in the reaction.

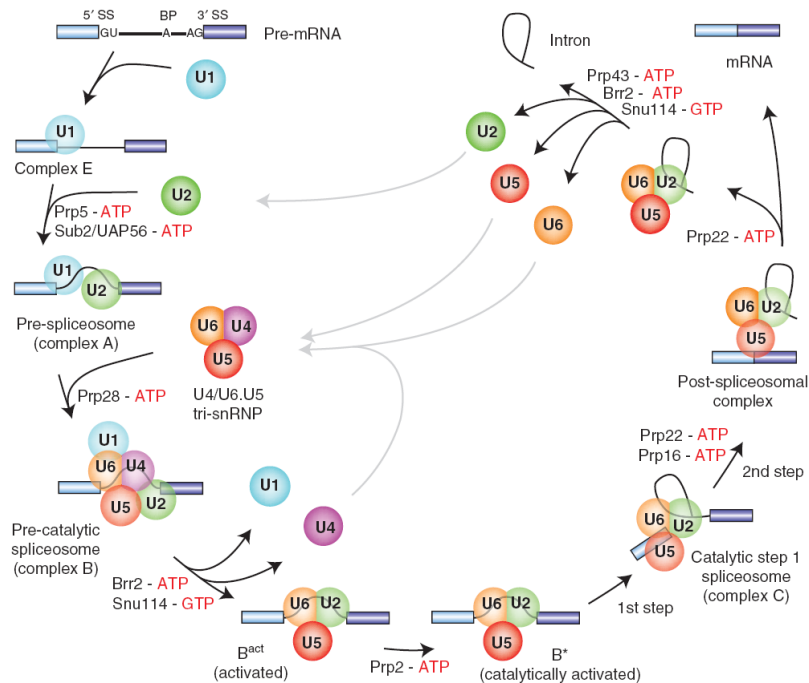


Figure 2.1.5. Canonical cross-intron assembly and disassembly pathway of the U2-dependent spliceosome. For simplicity, the ordered interactions of the snRNPs (indicated by circles) are shown, but not those of non-snRNP proteins. The various spliceosomal complexes are named according to the metazoan nomenclature. Exon and intron sequences are indicated by boxes and lines, respectively. The stages at which the evolutionarily conserved DExH/D-box RNA ATPases/helicases Prp5, Sub2/UAP56, Prp28, Brr2, Prp2, Prp16, Prp22 and Prp43, or the GTPase Snu114, act to facilitate conformational changes are indicated. Figure from (Will and Lührmann, 2011)

As shown in Figure 2.1.5, initially the 5' splice site is recognized by the U1 snRNP, using base pairing between its snRNA and the pre-mRNA. U2AF is made up of two subunits, the larger of which, called U2AF65, binds to the Py tract and the smaller, called U2AF35, binds to the 3' splice site. The former subunit interacts with BBP (SF1) and helps that protein bind to the branch site. This arrangement of proteins and RNA is called the early (E) complex. U2 snRNP then binds to the branch site, aided by U2AF and displacing BBP (SF1). This arrangement is called the A complex. Binding of the U4/U6-U5 tri-snRNP then forms the B complex. Several structural rearrangements in the B complex lead to loss of the U1 and U4 snRNPs, resulting in the C complex. Here

the U6 snRNA is base-paired to the 5' splice site, and the base-pairing between the U4/U6 snRNAs is replaced with a U2-U6 snRNA interaction. This creates the active conformation of the spliceosome, and the two-transesterification reactions of splicing occur in it (Will and Lührmann, 2011).

2.1.2 Alternative splicing

Most pre-mRNAs in higher eukaryotes can be spliced in more than one way. Thus, mRNAs containing different selections of exons can be generated from a given pre-mRNA. Called alternative splicing (AS), this strategy enables a gene to give rise to more than one polypeptide product. These alternative products are called isoforms.

There are several different types of alternative splicing events, which can be classified into four main subgroups. The first type is exon skipping, in which a type of exon known as a cassette exon is spliced out of the transcript together with its flanking introns (see the Figure 2.1.6, Cassette exon). Exon skipping accounts for nearly 40% of alternative splicing events in higher eukaryotes (Alekseyenko et al., 2007 and Sugnet et al., 2004), but is extremely rare in lower eukaryotes. The second and third types are alternative 3' splice site (3' SS) and 5' SS selection. These types of AS events occur when two or more splice sites are recognized at one end of an exon. Alternative 3' SS and 5' SS selection account for 18.4% and 7.9% of all AS events in higher eukaryotes, respectively. The fourth type is intron retention, in which an intron remains in the mature mRNA transcript. This is the rarest AS event in vertebrates and invertebrates, accounting for less than 5% of known events (Alekseyenko et al., 2007; Kim et al., 2008; and Sugnet et al., 2004). By contrast, intron retention is the most prevalent type of AS in plants, fungi and protozoa (Kim et al., 2008). Less frequent, complex events that give rise to alternative transcript variants include mutually exclusive exons, alternative promoter usage and alternative polyadenylation (Black, 2003).

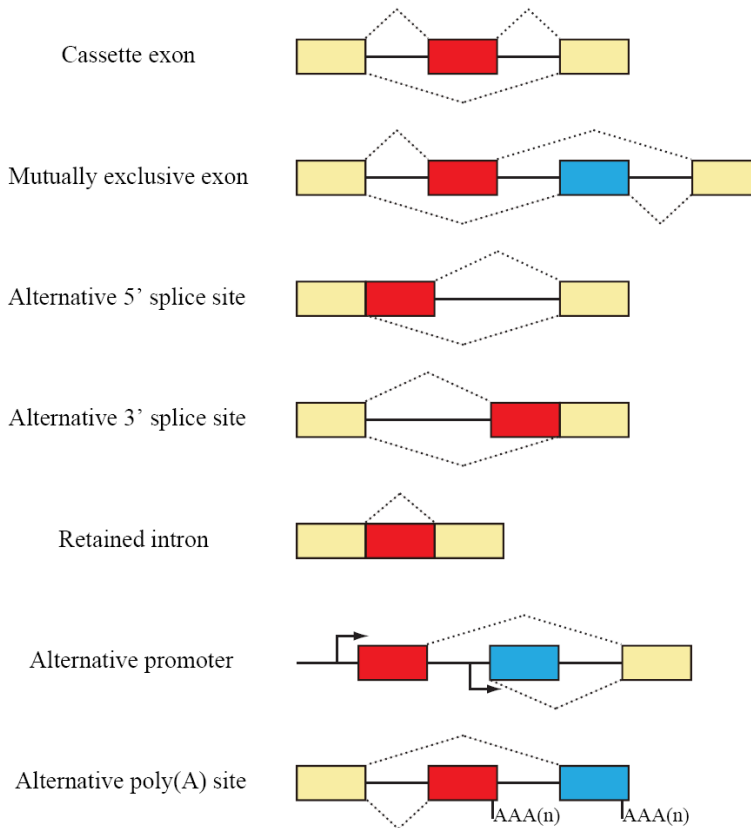


Figure 2.1.6. Types of alternative splicing events. Constitutive exons are shown in yellow and alternatively spliced regions in red or blue. Introns are represented by solid lines, and dashed lines indicate splicing options. Figure revised from (Keren, Lev-Maor and Ast, 2010).

Alternative splicing is a major cellular mechanism in metazoans for generating proteomic diversity (Nilsen and Graveley, 2010). A large proportion of protein-coding genes in multicellular organisms undergo alternative splicing, and in humans, it has been estimated that nearly 90 % of protein-coding genes-much larger than expected-are subject to alternative splicing (Black, 2003; Pan et al., 2008; Chen and Manley, 2009). Genomic analyses of alternative splicing have illuminated its universal role in shaping the evolution of genomes, in the control of developmental processes, and in the dynamic regulation of the transcriptome to influence phenotype. Disruption of the splicing machinery has been found to drive pathophysiology, and indeed reprogramming of aberrant splicing can provide novel approaches to the development of molecular therapy.

2.1.3 Splicing regulation

Splicing is regulated by trans-acting proteins (repressors and activators) and corresponding cis-acting regulatory sites (silencers and enhancers) on the pre-mRNA. However, as part of the complexity of alternative splicing, it is noted that the effects of a splicing factor are frequently position-dependent. It means that a splicing factor that serves as splicing activator when bound to an intronic enhancer element may serve as a repressor when bound to its splicing element in the context of an exon, and vice versa (Lim et al., 2011).

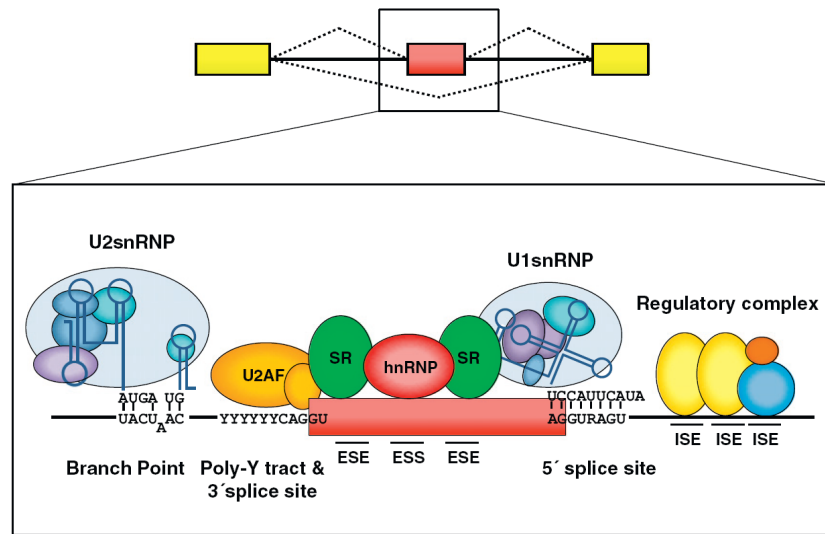


Figure 2.1.7. Schematic representation of core spliceosomal components that bind to the canonical splicing signals (5' splice site, branch point, polypyrimidine tract, and 3' splice site). Additional cis-acting elements in exons and introns that control splice site recognition are also shown. Although the diagram depicts positive and negative acting roles for SR and hnRNP proteins, respectively, depending on the location of the binding sites of these factors, they can also act in the opposite manner. Similarly, various tissue-dependent splicing factors can either promote or repress splice site selection depending on the location of their binding sites with respect to splicing signals. ISE, intronic splicing enhancer; ISS, intronic splicing silencer; ESE, exonic splicing enhancer; ESS, exonic splicing silencer; SR, Ser/Arg-repeat containing protein; hnRNP, heterogeneous ribonucleoprotein (hnRNP); and U2AF, U2 snRNP auxiliary factor. Figure from (Irimia and

Blencowe, 2012).

There are two major types of cis-acting RNA sequence elements present in pre-mRNAs and they have corresponding trans-acting RNA-binding proteins (see Figure 2.1.7). Splicing silencers are sites to which splicing repressor proteins bind, reducing the probability that a nearby site will be used as a splice junction. These can be located in the intron (intronic splicing silencers, ISS) or in a neighboring exon (exonic splicing silencers, ESS). They vary in sequence, as well as in the types of proteins that bind to them. The majority of splicing repressors are heterogeneous nuclear ribonucleoproteins (hnRNPs) such as hnRNPA1 and polypyrimidine tract binding protein (PTB) (Matlin, Clark and Smith, 2005; Wang and Burge, 2008).

Splicing enhancers are sites to which splicing activator proteins bind, increasing the probability that a nearby site will be used as a splice junction. These also may locate in the intron (intronic splicing enhancers, ISE) or exon (exonic splicing enhancers, ESE). Most of the activator proteins that bind to ISEs and ESEs are members of the SR protein family. Such proteins contain RNA recognition motifs and arginine and serine-rich (RS) domains (Matlin, Clark and Smith, 2005; Wang and Burge, 2008).

The secondary structure of the pre-mRNA transcript also plays a role in regulating splicing, such as by bringing together splicing elements or by masking a sequence that would otherwise serve as a binding element for a splicing factor (Warf and Berglund, 2010; Reid et al., 2009).

Mechanisms of alternative splicing are highly variable, and new examples are constantly being found, particularly through the use of high-throughput techniques. Researchers hope to fully elucidate the regulatory systems involved in splicing, so that alternative splicing products from a given gene under particular conditions could be predicted by a “splicing code” (Matlin, Clark and Smith, 2005; David and Manley, 2008).

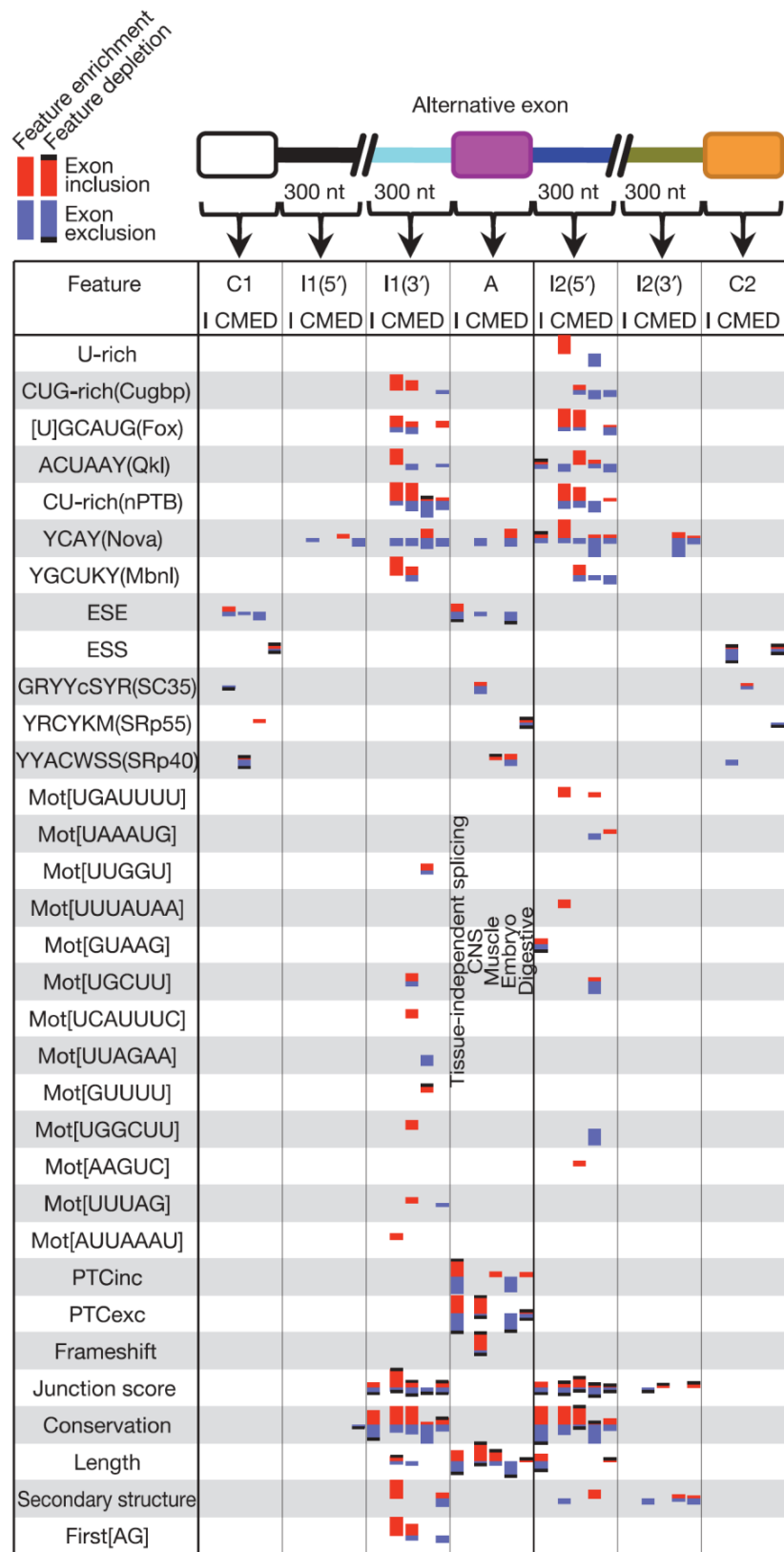


Figure 2.1.8. Graphical depiction of the splicing code. The region-specific activity of each feature

in increased exon inclusion (red bar) or exclusion (blue bar) is shown for CNS (C), muscle (M), embryo (E) and digestive (D) tissues, plus a tissue-independent mixture (I). A bar with/without a black hat indicates activity due to feature depletion/enrichment. Bar size conveys enrichment P-value < 0.005 in all cases. Potential feature binding proteins are shown in parentheses. Figure from (Barash et al. 2010)

Barash and colleagues tried to describe the assembly of splicing code, which uses method of association analysis between hundreds of RNA features (including structural features) and alternative splicing outcome in 3665 exons from microarray data in 27 tissues (Barash et al. 2010). As shown in Figure 2.1.8, most splicing codes locate in the local regions around the alternative splicing exons with a distance of 300 nucleotides.

2.1.4 Splicing and disease

Abnormal variations in splicing are also implicated in disease. A large proportion of human genetic disorders result from splicing variants. A study in 2005 involving probabilistic analyses indicated that more than 60% of human disease-causing mutations affect splicing rather than directly affecting coding sequences (López-Bigas et al., 2005). A more recent study indicates that one-third of all hereditary diseases are likely to have a splicing component (Lim et al., 2011). Regardless of exact percentage, a number of splicing-related diseases do exist (Ward and Cooper, 2010). As described below, a prominent example of splicing-related diseases is cancer.

One example of a specific splicing variant associated with cancers is in one of the human DNMT genes. Three DNMT genes encode enzymes that add methyl groups to DNA, a modification that often has regulatory effects. Several abnormally spliced DNMT3B mRNAs are found in tumors and cancer cell lines. In two separate studies, expression of two of these abnormally spliced mRNAs in mammalian cells caused changes in the DNA methylation patterns in those cells. Cells with one of the abnormal mRNAs also grew twice as fast as control cells, indicating a direct contribution to tumor development by this product (Fackenthal and Godley, 2008).

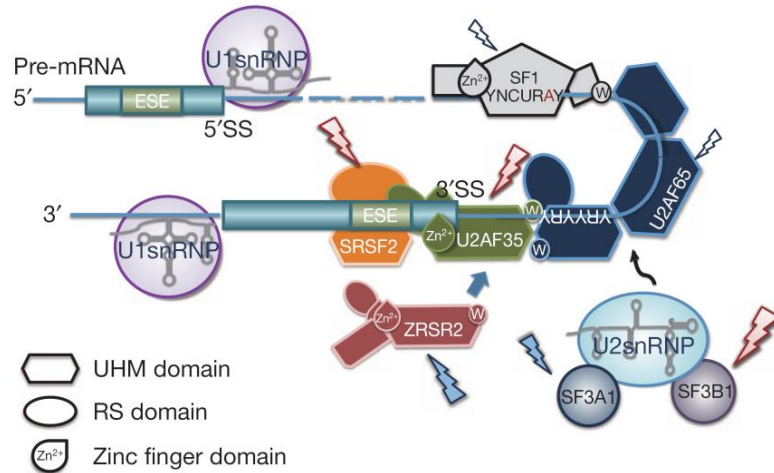


Figure 2.1.9. Components of the splicing E/A complex mutated in myelodysplasia. RNA splicing is initiated by the recruitment of U1 snRNP to the 5' SS. SF1 and the larger subunit of the U2 auxiliary factor (U2AF), U2AF65, bind the branch point sequence (BPS) and its downstream polypyrimidine tract, respectively. The smaller subunit of U2AF (U2AF35) binds to the AG dinucleotide of the 3' SS, interacting with both U2AF65 and a SR protein, such as SRSF2, through its UHM and RS domain, comprising the earliest splicing complex (E complex). ZRSR2 also interacts with U2AF and SR proteins to perform essential functions in RNA splicing. After the recognition of the 3' SS, U2 snRNP, together with SF3A1 and SF3B1, is recruited to the 3' SS to generate the splicing complex A. The mutated components in myelodysplasia are indicated by arrows. Figure from (Yoshida et al., 2011).

Single-nucleotide alterations in splice sites or cis-acting splicing regulatory sites may lead to differences in splicing of a single gene, while changes in the RNA processing machinery may lead to mis-splicing of multiple transcripts. Yoshida and his colleagues report whole-exome sequencing of 29 myelodysplasia specimens, which unexpectedly revealed novel pathway mutations involving multiple components of the RNA splicing machinery, including U2AF35, ZRSR2, SRSF2 and SF3B1. In a large series analysis, these splicing pathway mutations were frequent (~45 to 85%), and highly specific to myeloid neoplasms showing features of myelodysplasia (see Figure 2.1.9). Conspicuously, most of the mutations affect genes involved in the 3' splice site recognition during pre-mRNA processing, which may induce abnormal RNA splicing

and compromised haematopoiesis (Yoshida et al., 2011).

2.1.5 Motivation

Pre-mRNA splicing takes place in the multi-component RNA machinery known as the spliceosome, which is assembled in a step-wise fashion through the sequential addition of U1, U2, and U4/U6/U5 small nuclear ribonucleoprotein particles to the pre-mRNA (Wahl et al., 2009). U1 defines the functional 5' splice site largely through base-pairing interactions, whereas U2 recognizes the functional 3' splice site, which also involves base pairing with the branch point sequence. Because the BPS (branch point site) is quite degenerate in higher eukaryotic cells (see Figure 2.1.3), the addition of U2 snRNP requires multiple auxiliary factors, the most important one being the U2AF heterodimer consisting of a 65kD and 35kD subunit (Zamore et al., 1992; Zhang et al., 1992). Numerous biochemical experiments on model pre-mRNAs have established sequence-specific binding of U2AF65 to the polypyrimidine tract (Py-tract) immediate downstream of the BPS and direct contact of U2AF35 with the AG dinucleotide, which together defines functional 3' splice sites (Singh et al., 1995; Valcárcel et al., 1996). Upon definition of the functional 5' and 3' splice sites by U1 and U2 snRNPs and following a series of ATP-dependent steps, the U4/U6/U5 tri-snRNP complex joins the initial pre-spliceosome to convert it into the mature spliceosome (Wahl et al., 2009).

While the vital role of the U2AF heterodimer in defining 3' splice sites has widely been appreciated, it has been unclear whether it is required for the recognition of all functional 3' splice sites, especially in mammalian cells. In budding yeast, Mud2 has been characterized as the U2AF65 ortholog, but Mud2 is a non-essential gene, likely because of highly invariant BPS in this lower eukaryotic organism (Abovich et al., 1994; Abovich et al., 1997). Similarly, in fission yeast, a significant fraction of intron-containing genes seem to lack typical Py-tract, and indeed, multiple U2AF-independent introns have been reported (Sridharan et al., 2011; Sridharan and Singh, 2007). In mammals, the presence of high levels of splicing enhancer factors, such as SR proteins, appears to be capable of bypassing the requirement for U2AF to initiate spliceosome

assembly (MacMillan et al., 1997). In addition, mammalian genomes also encode for multiple genes with related functions to both U2AF65 (Imai et al., 1993; Hastings et al., 2007; Page-McCaw et al., 1999) and U2AF35 (Tronchre et al., 1997; Shepard et al., 2002; Mollet et al., 2006). Therefore, the functional requirement for U2AF may be bypassed by multiple mechanisms, raising a general question with respect to the degree of the involvement of the U2AF65/35 heterodimer in 3' splice site definition in mammalian genomes. This fundamental question has remained unaddressed despite the availability of genome-wide U2AF65-RNA interaction data (Zarnack et al., 2013).

Secondly, the RNA binding specificity of U2AF65 has been well characterized at the biochemical levels. Introns that contain a strong Py-tract are able to support spliceosome assembly in an AG-independent manner (Reed, 1989), and U2AF65 appears to be sufficient to support splicing of such AG-independent introns, at least in vitro (Zamore and Green, 1991). However, the U2AF35 subunit is responsible for directly contacting the AG dinucleotide on typical functional 3' splice sites and this partnership is enforced by U2AF65-dependent stability control of U2AF35 (Pacheco et al., 2006). Functioning as a heterodimer, U2AF65/35 is thought to provide strong discrimination against pyrimidine-rich exonic as well as intronic sequences that are not part of the functional 3' splice sites in mammalian genomes. Specific RNA binding proteins, such as DEK and hnRNP A1, have been implicated in improving the RNA binding specificity in mammalian genomes (Soares et al., 2006; Tavanez et al., 2012). However, it remains to be directly demonstrated whether the U2AF heterodimer indeed binds preferentially to the Py-tract followed by the AG dinucleotide from genome-wide analysis.

Thirdly, besides the critical role of U2AF in constitutive splicing, both U2AF65 and U2AF35 have been implicated in regulated splicing (Park et al., 2004; Moore et al., 2010). In theory, alternative splice sites are weak in general, and as a result, suboptimal binding may render them particularly sensitive to levels of U2AF, which may be further subjected to such PTB, TIA-1/TIAR, and more recently, hnRNPC (Zarnack et al., 2013; Le Guiner et al., 2001; Xue et al., 2009; Wang et al., 2010). While these mechanisms

appear to readily explain U2AF-dependent exon inclusion, it has been largely unknown why and how depletion of U2AF could also induce a large number of exon inclusion events in vivo (Park et al., 2004). Engineered U2AF binding on exon was recently shown to inhibit the inclusion of the exon (Lim et al., 2011), but it has been unclear how widely this mechanism is used to regulate alternative splicing of endogenous genes.

Last, but not least, multiple mutations in both U2AF65 and U2AF35 have been reported to associate with myelodysplasia (MDS) and related blood disorders (Yoshida et al., 2011; Thol et al., 2012; Cazzola et al., 2013). However, it is unclear how such mutations might affect the normal function of U2AF in regulated splicing, which further underscores the importance in mechanistic understanding of the regulatory role of U2AF in mammalian cells.

Given such a long range of mechanistic issues that remain to be addressed, we have embarked on genome-wide analysis of U2AF-RNA interactions in the human genome. By defining the genomic landscape of U2AF binding and the functional requirement for both U2AF65 and U2AF35 in regulated splicing, we provide a series of mechanistic insights into the function of U2AF in normal and disease states.

2.2 Methods

To reveal the target site of U2AF, my colleagues use UV radiation to link the protein to RNA molecules *in vivo*. U2AF65 is then precipitated by using a specific antibody. With the protein, target RNA attached to the protein is isolated and high throughput sequenced.

On the other hand, RNA-seq or RASL-seq could give us the insights into all the alternative splicing change regulated by knockdown the trans-acting splicing regulatory protein.

I then developed serials of bioinformatics analysis pipelines to parse the rules coding in the high throughput sequencing data.

2.2.1 High throughput sequencing

“It could be argued that the greatest transformative aspect of the Human Genome Project has been not the sequencing of the genome itself, but the resultant development of new technologies”, just as said by Kahvejian in 2008, high throughput sequencing has dramatically changed the way of life sciences research (Kahvejian et al., 2008).

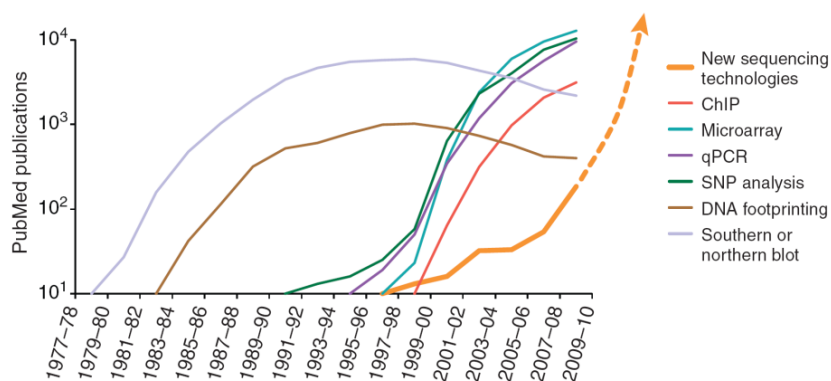


Figure 2.2.1. The number of publications with keywords for nucleic acid detection and sequencing technologies. PubMed (<http://www.ncbi.nlm.nih.gov/sites/entrez>) was searched in two-year increments for key words and the number of hits plotted over time. Figure from (Kahvejian et al., 2008).

As shown in Figure 2.2.1, traditional biological nucleic acid detection methods are used less and less, while high throughput sequencing starts to be widely used from 2008. Consistent with it, the amount of genetic sequencing data stored at the European Bioinformatics Institute takes less than a year to double in size (Marx, 2013) (see Figure 2.2.2).

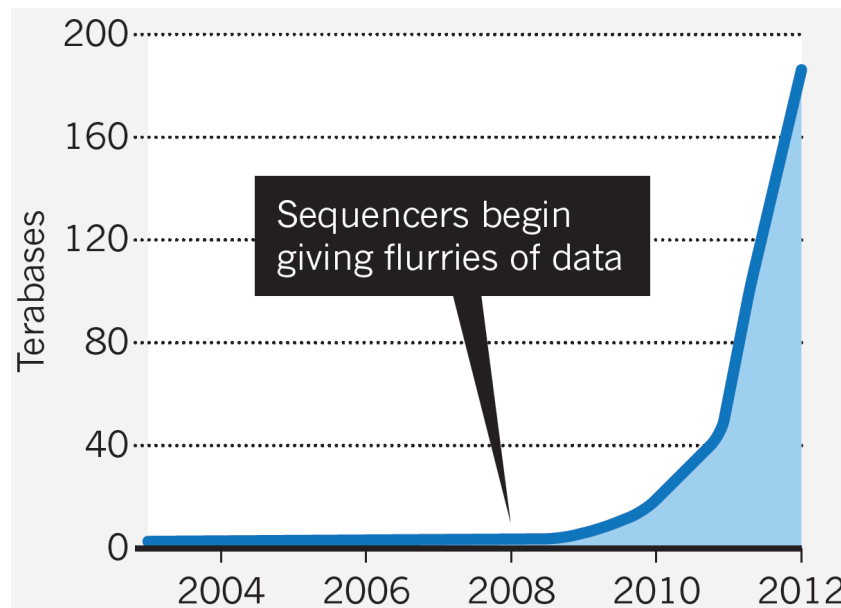


Figure 2.2.2. Data explosion. The amount of genetic sequencing data stored at the European Bioinformatics Institute takes less than a year to double in size. Figure from (Marx, 2013)

In the other hand, the high demand for sequencing has driven the development of several types of efficient high throughput sequencers. There are four platforms dominating the high throughput sequencing field now: 454, illumina, Ion Torrent and PacBio (Quiñones-Mateu et al., 2014). All those four sequencers could generate high quality sequence information, while they each have their own advantages and disadvantages (see Figure 2.2.3).

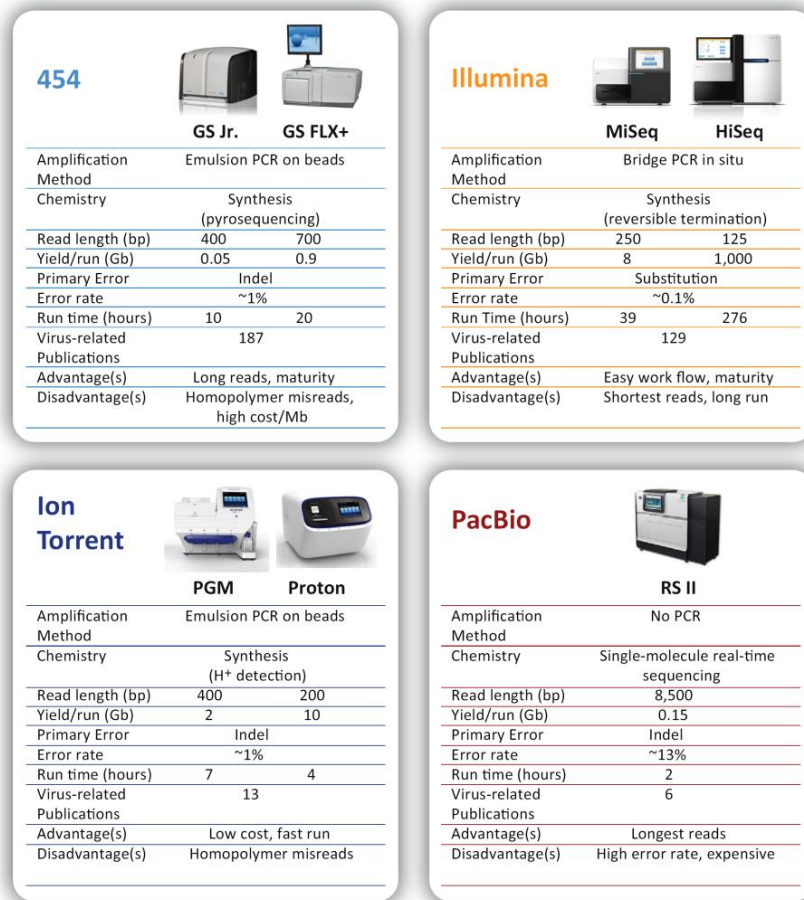


Figure 2.2.3. Principal characteristics of the four most used deep sequencing platforms now: 454 (GS Junior and GS FLX+ systems), Illumina (MiSeq v2 and HiSeq 2500 systems), Ion Torrent (Ion Personal Genome Machine, 318 v2 chip and Ion Proton), and Pacific Biosciences (PacBio RS II SMRT). Figure from (Quiñones-Mateu et al., 2014)

Along with the remarkable improvements in DNA sequencing technologies, the cost of sequencing is decreasing (see Figure 2.2.4). White line in the figure reflects Moore's Law, which describes a long-term trend in the computer hardware industry that involves the doubling of compute power every two years. As shown in the figure, the cost of sequencing a human genome is consistent with the Moore's Law before 2008, while the trend of cost decreasing surpasses the Moore's Law later. Now it only cost 4000 dollars to sequencing a genome.

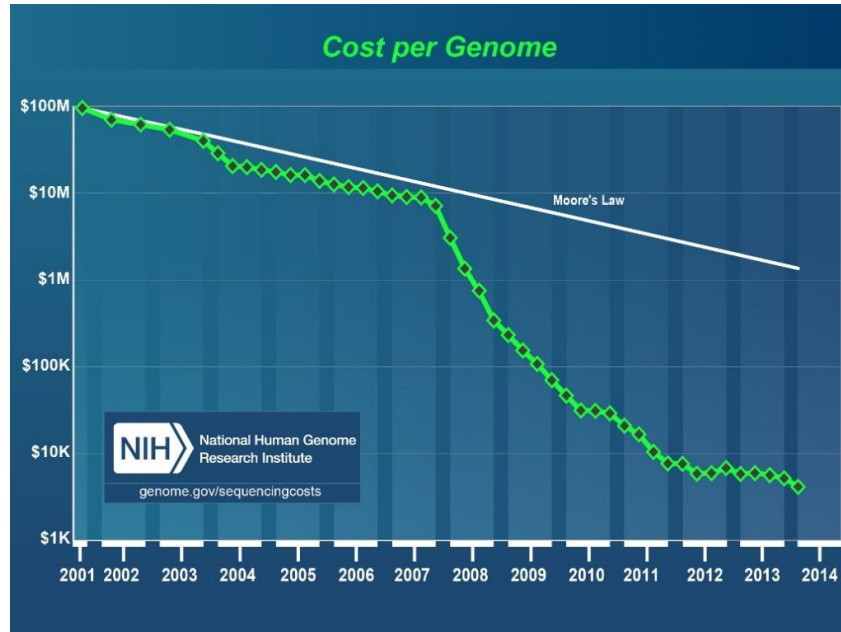


Figure 2.2.4. Total cost of sequencing a human genome over time as calculated by the National Human Genome Research Institute (NHGRI). Figure from (<http://www.genome.gov/sequencingcosts/>).

Biological scientists develop a lot of types of methods base on high throughput sequencing technologies, to get insights of biological molecular' expression and regulation in a large scale. Various high throughput sequencing methods can precisely map and quantify chromatin features, DNA modifications and several specific steps in the cascade of information from transcription to translation (see Figure 2.2.5 and Table 2.2.1).

Feature	Method	Description	Refernce
Transcripts, small RNA and transcribed regions	RNA-seq	Isolate RNA followed by HT sequencing	(Waern et al, 2011)
	CAGE	HT sequencing of 5'-methylated RNA	(Kodzius et al, 2006)
	RNA-PET	CAGE combined with HT sequencing of poly-A tail	(Fullwood et al, 2009c)
	ChIRP-Seq	Antibody-based pull down of DNA bound to lncRNAs followed by HT sequencing	(Chu et al, 2011)
	GRO-Seq	HT sequencing of bromouridinated RNA to identify transcriptionally engaged Pol II and determine direction of transcription	(Core et al, 2008)
	NET-Seq	Deep sequencing of 3' ends of nascent transcripts associated with RNA polymerase, to monitor transcription at nucleotide resolution	(Churchman and Weissman, 2011)
	Ribo-Seq	Quantification of ribosome-bound regions revealed uORFs and non-ATG codons	(Ingolia et al, 2009)
Transcriptional machinery and protein-DNA interactions	ChIP-seq	Antibody-based pull down of DNA bound to protein followed by HT sequencing	(Robertson et al, 2007)
	DNase footprinting	HT sequencing of regions protected from DNaseI by presence of proteins on the DNA	(Hesselberth et al, 2009)
	DNase-seq	HT sequencing of hypersensitive non-methylated regions cut by DNaseI	(Crawford et al, 2006)
	FAIRE	Open regions of chromatin that is sensitive to formaldehyde is isolated and sequenced	(Giresi et al, 2007)
	Histone modification	ChIP-seq to identify various methylation marks	(Wang et al, 2009a)
DNA methylation	RRBS	Bisulfite treatment creates C to U modification that is a marker for methylation	(Smith et al, 2009)
Chromosome-interacting sites	5C	HT sequencing of ligated chromosomal regions	(Dostie et al. 2006)
	ChIA-PET	Chromatin-IP of formaldehyde cross-linked chromosomal regions, followed by HT sequencing	(Fullwood et al, 2009a)

Table 2.2.1. The various high throughput sequencing assays. Table from (Soon et al., 2013).

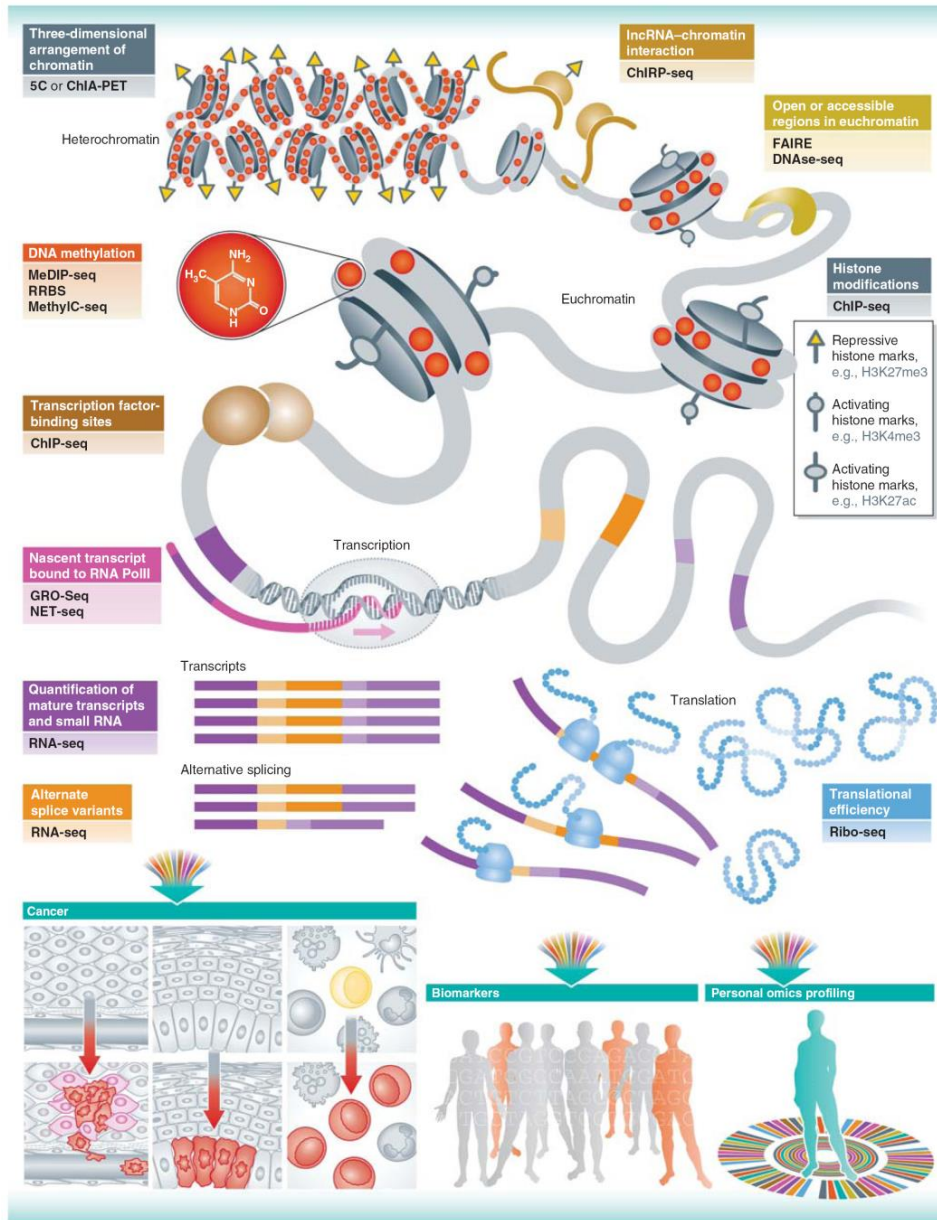


Figure 2.2.5. Sequencing technologies and their uses. Figure from (Soon et al., 2013)

These technologies can be applied in a variety of medically relevant settings, including uncovering regulatory mechanisms and expression profiles that distinguish normal and cancer cells, and identifying disease biomarkers, particularly regulatory variants that fall outside of protein coding regions. Together, these methods can be used for integrated personal omics profiling to map all regulatory and functional elements in an individual. Using this basal profile, dynamics of the various components can be studied in the context of disease, infection, treatment options, and so on. Such studies

will be the cornerstone of personalized and predictive medicine (see Figure 2.2.5).

2.2.2 Bioinformatics analysis

To examine the function of U2AF in pre-mRNA splicing, my colleagues get a high quality library of the protein-RNA interaction by CLIP-seq, and two RNA-seq data for HeLa cells with or without U2AF65 knockdown. In addition, several RASL-seq experiments were done to reveal the cooperative relationship. All these high throughput data are analyzed as below.

The scripts for the analysis were mainly written in Perl or R. All the analysis was done under Linux Ubuntu 10.04.

2.2.2.1 FastQ format

High throughput sequencing results are mostly stored in a text-based format. It is proposed by the Wellcome Trust Sanger Institute. The format includes both the biological sequence and sequencing quality which is encoded as a single American Standard Code for Information Interchange (ASCII) character (Cock et al., 2010).

It uses four lines for one sequence: line 1 and line 3 usually are the identifier of the sequence, which line 1 must begin with a character “@” and line 2 should begin with a character “+”; Only line 2 and line 4 are useful information that line 2 is the raw sequence letters and line 4 is the Phred quality score which is encoded with a ASCII letter (see Figure 2.2.8).

```
@SEQ_ID
GATTTGGGGTTCAAAGCAGTATCGATCAAATAGTAAATCCATTTGTTCAACTCACAGTTT
+
!/*((( (**+))%%%+) (%%%) . 1**+*'/) **55CCF>>>>>CCCCCCC65
```

Figure 2.2.6. An example of a sequence data in FastQ format out of high throughput sequencers.

The Phred quality score Q is used to measure the sequencing accuracy of each nucleotide base of a sequence. It is defined as property which is logarithmically related to the base-calling error probabilities P (Li et al., 2008).

$$Q = -10(\log_{10} P)$$

So, if the error ratio is 0.001, the quality score would be 30. In common, only sequences with an average Phred quality score of 20 or above could be used.

2.2.2.2 Sequencing quality control

Before analyzing the high throughput sequencing data, we always should check the quality of it to make sure there are no problems or biases in data which may affect the way we use it.

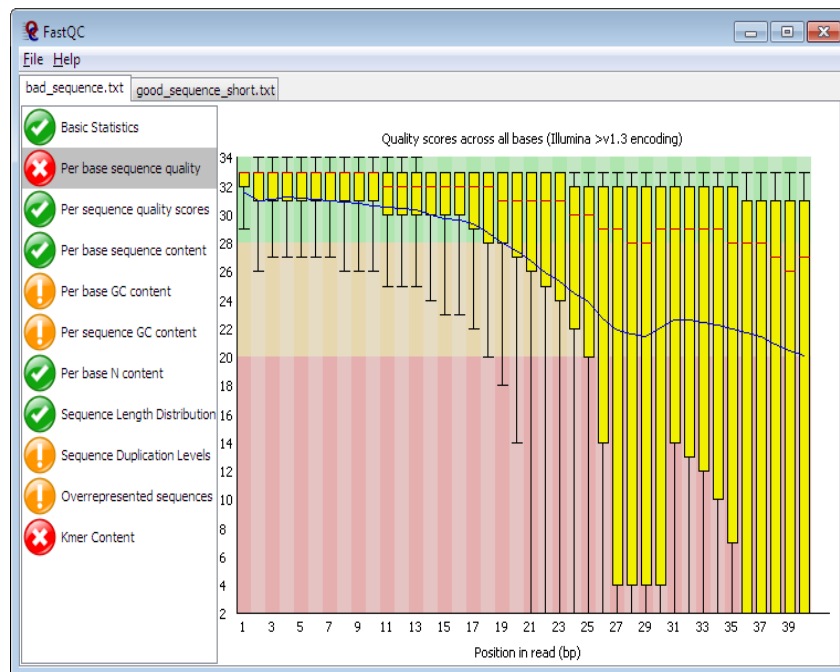


Figure 2.2.7. An interface of the FastQC. It could find out that the quality in the end of the data is bad, mainly because of the sequencing procedure. Figure from (<http://www.bioinformatics.babraham.ac.uk/projects/fastqc/>)

We use a tool named FastQC (Andrews, 2010). The report of it include a lot of summary information of all the sequences: sequence base quality at each position, average quality distribution for all the sequences, nucleotide frequency at each position, and over presented sequence (see Figure 2.2.9). It can be run in a non-interactive mode. So it would be suitable for integrating into a larger analysis pipeline for the systematic

processing of large numbers of files.

2.2.2.3 Mapping

Finding the best alignment of two sequences is an ancient problem. And almost all the books about algorithm would introduce it, because it is a classical application of the algorithm of dynamic programming. Setting reasonable scoring parameters, algorithm of dynamic programming could map the sequencing reads to the genome very well. However, it is still much too slow for mapping, especially for millions of short reads.

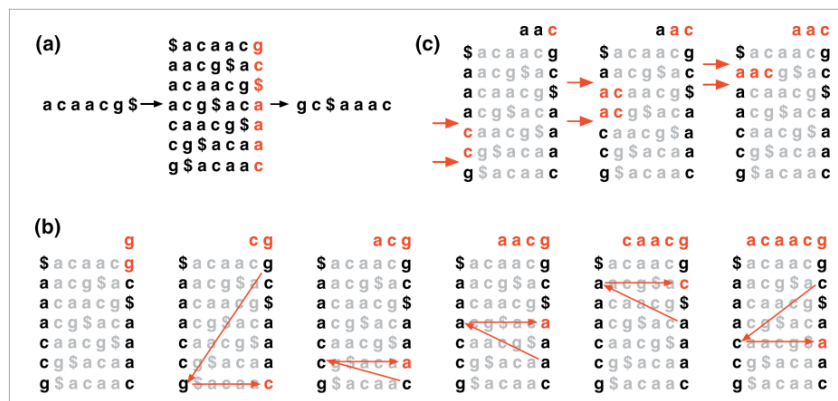


Figure 2.2.8. Burrows-Wheeler transform. (a) The Burrows-Wheeler matrix and transformation for 'acaacg'. (b) Steps taken by EXACTMATCH to identify the range of rows, and thus the set of reference suffixes, prefixed by 'aac'. (c) UNPERMUTE repeatedly applies the last first (LF) mapping to recover the original text (in red on the top line) from the Burrows-Wheeler transform (in black in the rightmost column). Figure from (Langmead et al., 2009)

There are two mostly used for short-reads sequence alignment: Bowtie (Langmead et al., 2009) and BWA (Li and Durbin, 2009). They are both based on a algorithms called Burrows-Wheeler transform to create a compressed, reusable index (table) form genome sequence first (see Figure 2.2.10). Then a new version of Bowtie named Bowtie2 was developed. It allows indels in alignment (Langmead and Salzberg, 2012). As for UV crosslinking would induce deletion in the reads (Zhang and Darnell, 2011), we use Bowtie2 to map our reads to the genome.

For RNA-seq data, we firstly make an index of mRNA, but not genome sequence.

After mapping the pair-end reads separately, we join them together and recalculate the coordinate in the genome.

2.2.2.4 Peak calling

Biological experiments cannot avoid inducing noise. High throughput sequencing also would read out some noisy signals for non-specific binding or sequencing error. So we should find out the real binding site out of the background, called peak calling.

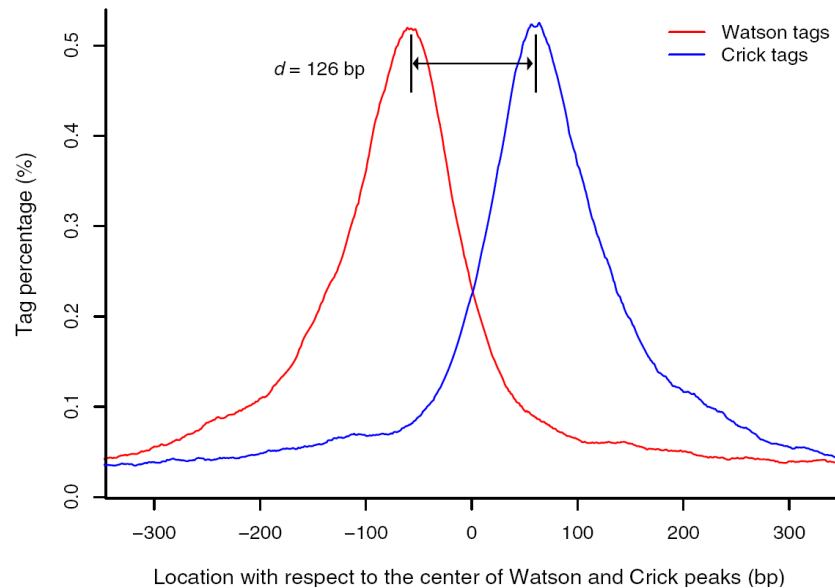


Figure 2.2.9. The double peak pattern in Watson strand and Crick strand around protein binding site from ChIP-Seq data. Figure from (Zhang et al., 2008).

A famous peak calling algorithm for ChIP-seq data is developed by Liu group (Zhang et al., 2008). It is based on a pattern that reads of ChIP-seq are always forming a separate peak in each strand around the binding site with a reasonable distance (see Figure 2.2.11). The center of the peaks is accurately the binding site of proteins. While RNA is single strand, the signal cannot appear a two-peak mode. So it is more difficult to peak calling for the CLIP-seq data. There are mainly two types of methods.

One is developed by Yeo and colleagues (Yeo et al., 2009; Xue et al., 2009). It is based on an intuition that real peaks would have a significant higher height than noise in each gene region. The background frequency of the height for overlapped reads at

every nucleotide was computed by randomly placing the same number of reads within the gene. Based on the sampling background, a threshold peak height could be found out with a pre-set FDR.

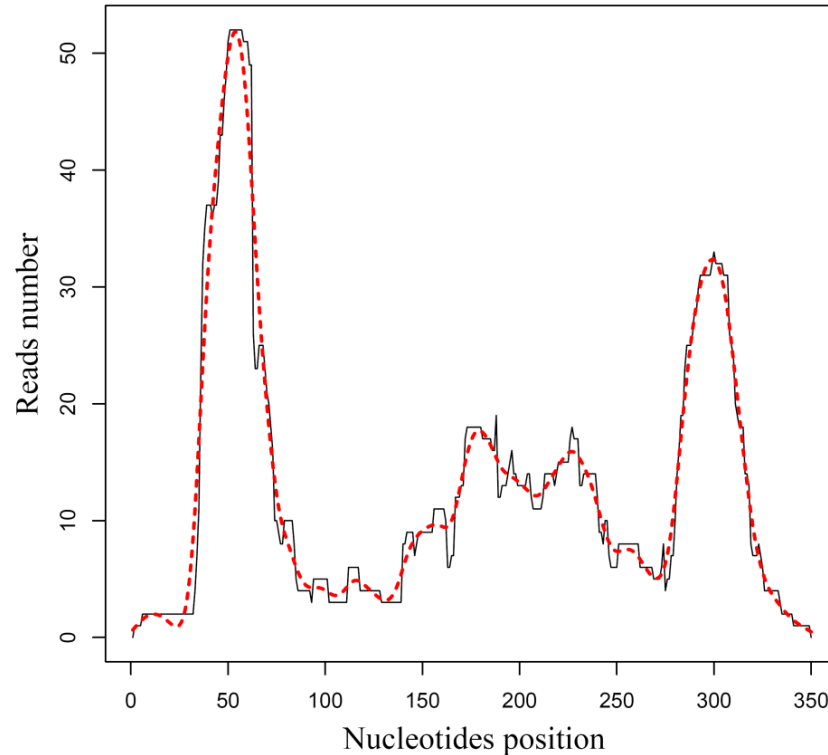


Figure 2.2.10. An example of peak calling base on kurtosis. The black line is the real signal of high throughput sequencing. After cubic spline interpolation, we get a smooth and derivative line (red line).

The other one is proposed by Darnell group (Chi et al., 2008). It is based on the shape value that real peaks always like a mountain that has a bigger kurtosis value. After using cubic spline interpolation, all the potential peaks could be seek out base on derivative value, and then the excess kurtosis could be computed and the threshold kurtosis value for peaks could be find out with a pre-set FDR (see Figure 2.2.12).

In this study, we code and try both the two methods, and find that each method have advantages and disadvantages. Height based method is more reliable, but it can not be used in regions without any annotation gene. Kurtosis based method could be used anywhere, but it perform not well in regions with lots of continuous peaks.

2.2.2.5 Annotation and plotting distribution

Annotation and plotting distribution could directly release a lot of information, including data quality, binding pattern and function. Beside the well-known genes, there are a lot of genes are predicted by varies of algorithms. Corresponding to it, there are several annotation data from different groups for using. The widely used are: UCSC genes (Hsu et al., 2006), RefSeq genes (Pruitt et al., 2007), Ensemble genes (Hubbard et al., 2002), GENCODE genes (Harrow et al., 2006), Genscan genes (Burge and Karlin, 1997) and so on.

2.2.2.6 Motif finding

All of the reads sequences from CLIP experiment were supposed to bind with the protein *in vivo*, although there may exist some non-specific tags. Motif finding is to identify the RNA sequence pattern which is bound with the protein. In short, it tries to find out the overrepresented sequence. It usually calculates the k-mer (like 2-mer, 3-mer, 4-mer, 5-mer) frequency, and find out the most enriched sequence than background.

Here, Motif finding was implemented using RSA tools oligo analysis algorithm (<http://rsat.ulb.ac.be/>) with input U2AF65 peaks (van Helden et al., 1998).

2.2.2.7 Visualization

Pictures contain more information than a serial of numbers, and they are more intuitionist than numbers. People also always like to look at picture but not pure numbers. It is the same for biological data. Many platforms are developed for storing and visualization the high throughput data. Two of those are widely used.

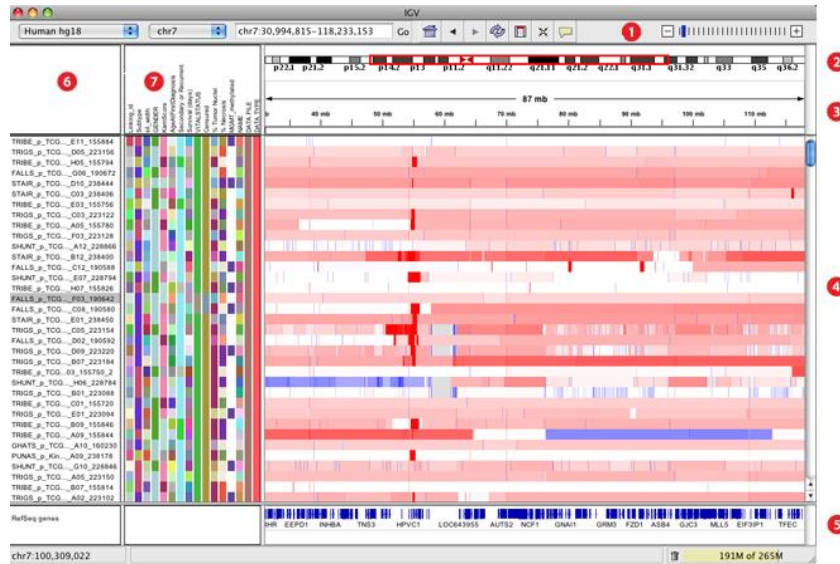


Figure 2.2.11. The interface of Integrative Genomics Viewer. 1: tool bar; 2 and 3: chromosome is displayed; 4: data displays in horizontal rows called tracks; 5: annotation features also display, such as genes, in tracks; 6: track names; 7: attribute names. Figure from (<https://www.broadinstitute.org/software/igv/MainWindow>)

The Integrative Genomics Viewer (IGV) is a high-performance visualization tool for interactive exploration of large, integrated genomic datasets (see Figure 2.2.13). It supports a wide variety of data types, including array-based and next-generation sequence data, and genomic annotations.

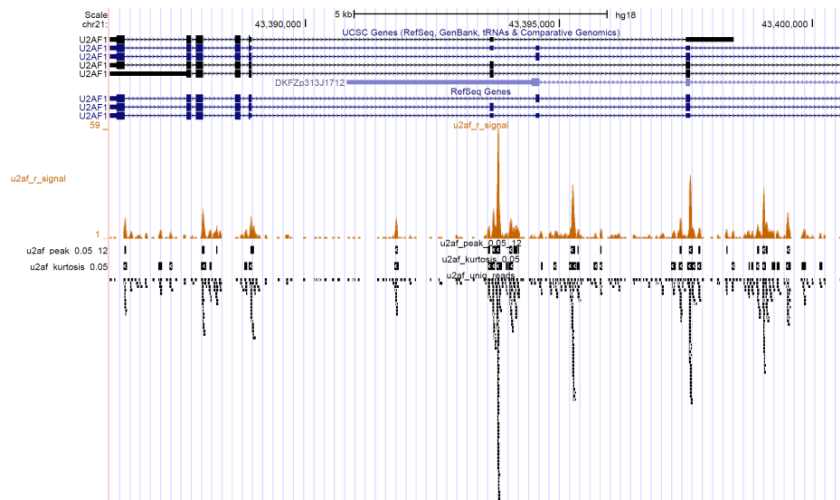


Figure 2.2.12. The interface of UCSC genome browser. The track names are on the right site. Chromosome and genes structure are showed on the up side. Data track could be showed in four

types of ways. Figure from (<https://genome.ucsc.edu/cgi-bin/hgGateway>).

The other one is UCSC genome browser. It is an interactive web server build by University of California, Santa Cruz (UCSC), offering access to genome sequence data from a variety of vertebrate and invertebrate species and major model organisms. Above all, there are a large collection of aligned annotations integrated in the database, and all could be easily used (see Figure 2.2.14).

2.2.2.8 Regulation pattern analysis

Plotting the RNA-map on up- and down-regulated cases is a common way to dig the regulation pattern. However, it is very tricky because of the normalization. Different types of data should be normalized in a commensurate level, and cases in a same type also should be normalized. If not, the final result would be dominant by only few cases.

2.2.2.9 Machine learning and prediction of U2AF65 binding sites

Motif finding only state a general intuition of U2AF65 binding preference, because it just finds out the most frequency k-mer sequence. The base frequency at each position, the neighboring and nonneighboring dependencies of the pattern are all crucial, and should be taken into account for prediction binding site.

As we known, a weight matrix could present the likes and dislikes for nucleotides at each position, and the product of all the probability at each position could be used as a criterion for prediction. More complicated, the first- or higher-order Markov model could reflect the dependencies between neighboring bases in a positional or nonpositional way. All the possibility model cannot contain all the potential patterns, and the nonneighboring dependencies are much more complex (Durbin, 1998).

Yeo and Burge proposed a framework for modeling sequence patterns based on the maximum entropy principle (MEP), which could consider all constraints together, and give insight into the relative importance of different dependencies at different positions (Yeo and Burge, 2004). The Shannon entropy, H , is given by the expression

$$H(p) = -\sum p(x) \log_2(p(x)).$$

Where the sum is taken over all possible sequences, x . It is a measure of the average uncertainty in the random variable X . For example, a rolling of an unbiased dice would get every number from 1 to 6 in a probability $1/6$. So the uncertainty for this thing would be $\log_2 6$.

The principle of maximum entropy states that, the probability distribution which best represents the current state of knowledge is the one with largest entropy. People always automatically use this principle. When we have no prior information of a dice, we would think that every side would appear in a same probability $1/6$, but not other possible. Interestingly, this is just the maximum entropy state in this situation.

The maximum entropy model (MEM) aim to learn two distributions for all kinds of sequences X (the number is 4^n , if the length of target sites is n). They are a signal model ($P^+(X)$) learning from positive training data and a negative probability distribution ($P^-(X)$) learning from negative training data. Given a new sequence, the MEM could be used to judge if it is a real binding site based on the likelihood ratio, L

$$L(X = x) = \frac{P^+(X = x)}{P^-(X = x)}$$

If $L(X = x)$ is not smaller than a threshold which achieved based on a setting FDR, it would be predicted as a true target site.

How to learn the distribution of training data? We begin with a uniform possibility distribution for all the sequences X .

$$p(x) = 4^{-n}$$

In this study, we set the length of predicted binding sequences as 12 nucleotides based on the results of motif finding (see below). And then the technique of iterative scaling is used to learn the positive or negative training data with a set of constraints circularly one by one, to reach a convergence which simultaneously satisfy all the list

of constrains as far as possible.

In detail, represent each member of the ordered list of constraints as Q_i , where i is the order in the list. The sequences relevant to the constraint at the j th step of iteration have the form

$$P^j(X = x) = P^{j-1}(X = x) \frac{Q_i}{Q_i^{j-1}}$$

Where $P^{j-1}(X = x)$ is the probability of the sequence at the $(j-1)$ th step in the iteration. Q_i^{j-1} is the sum of probabilities of the sequences accord with constraint Q_i determined from the distribution at the $(j-1)$ th step. For example, when calculate a nonadjacent constraint $Q_i(X = ANA)$ at the j th step, for all the sequences satisfy the constrains:

$$P^j(X = ANA) = P^{j-1}(X = ANA) \frac{Q_i}{Q_i^{j-1}}, \quad N \in \{A, C, G, T\}.$$

$$Q_i^{j-1} = \sum_{N \in \{A, C, G, T\}} P^{j-1}(X = ANA).$$

While all the sequences not matching ANA are iterated as follows:

$$P^j(X \neq ANA) = P^{j-1}(X \neq ANA) \frac{1 - Q_i}{1 - Q_i^{j-1}}, \quad N \in \{A, C, G, T\}.$$

As the iterations proceed, the entropy H for all the sequences X decreases. For our purposes, we say the entropy has converged when the scope of decreases between iterations becomes very small ($|\Delta H| \leq 10^{-7}$).

	True binding sites	False binding sites
Train	113090	198946
Test	56514	99955
Total	169604	300000

Table 2.2.2. Number of sequences in training and test sets.

We use a total of 169604 real U2AF65 binding sites with crosslink induced deletion sites, taking 3 nucleotides (nt) before, 8 nt after the deletion site and the deletion site itself (12 nt in total) as the target sites. 300000 false binding sites are randomly selected from intronic regions without any U2AF65 binding reads in the genes having U2AF65 binding peaks (see Table 2.2.2).

2.3 Results

2.3.1 Genome-wide mapping of U2AF-RNA interactions

To map the interaction of U2AF65 with RNA in the human genome, my colleagues initially employed the standard CLIP-seq procedure to construct the library (Xue et al., 2009). While we could not efficiently ligate the 3' RNA linker to IPed RNA on the U2AF complex, resulted in a useless high throughput sequencing data full of non-specific PCR product. Reasoning that the U2AF35 subunit might had caused steric hindrance for enzymatic reactions at the 3' end of nuclease-trimmed RNA under our conditions, we modified the CLIP procedure by first ligating the 5' linker to 32P-labeled RNA on the complex (see Figure 2.3.1).

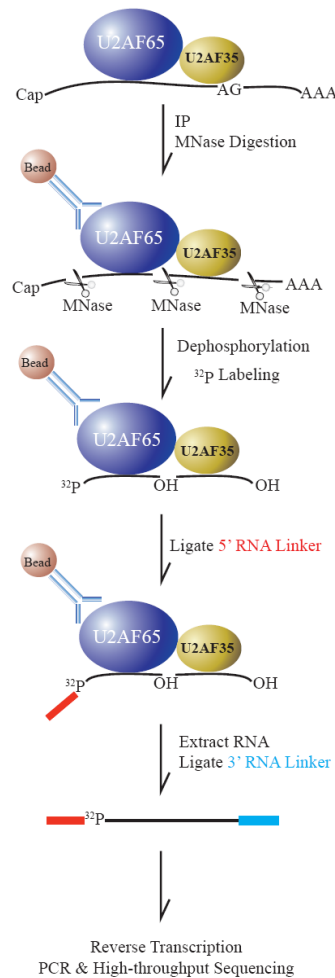


Figure 2.3.1. Schematic illustration of U2AF65 CLIP-seq. U2AF65 was immunoprecipitated with MC3 mAb before Micrococcal Nuclease (MNase) treatment on beads. The associated RNA were dephosphorylated and 5'-labeled with ^{32}P by T4 kinase. Because the 3' end of RNA appears to be protected by U2AF35, we first ligated the RNA linker to the 5' RNA. After SDS-PAGE followed by transfer to nitrocellulose, the isolated U2AF-RNA complexes were deproteinized, and recovered RNA was ligated to the 3' RNA linker, reverse transcribed, amplified by PCR, and analyzed by deep sequencing.

This resulted in U2AF65-RNA complexes that were readily detectable by autoradiography (see Figure 2.3.2). Recovered RNA was next ligated to the 3' linker followed by reverse transcription, PCR amplification, and deep sequencing. This modified CLIP procedure effectively prevented primer dimer formation because both 5' and 3' linkers contain the 5'-OH group.

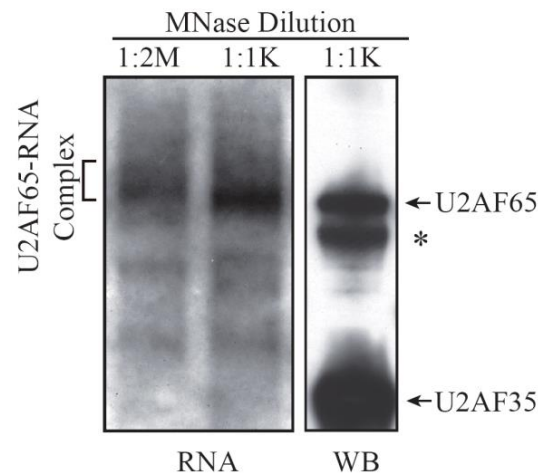


Figure 2.3.2. The U2AF65-RNA complexes trimmed by two different concentration of MNase (1:2,000,000 or 1:10,000 dilution) was detected by autoradiography. The positions of U2AF65 and U2AF35 were determined by Western blotting. * indicates the IgG heavy chain. Bracketed RNA-protein adducts were recovered for CLIP library construction.

We included a randomized barcode in our libraries to help remove PCR products during library amplification. Out of a total of 19.5 million sequenced tags, 12.1 million could be mapped and 9.3 million could be uniquely mapped to the human genome (see Table 2.3.1).

U2AF65 CLIP-Seq data	
total reads	19513772
mapped reads	12088822
mapped ratio	61.95%
uniquely mapped reads	9329565
uniquely mapped ratio	77.18%
crosslink reads	1482140

Table 2.3.1. Mapping result of U2AF65 CLIP-Seq data. Cross-linked reads are reads with deletion site which induced by UV crosslinking.

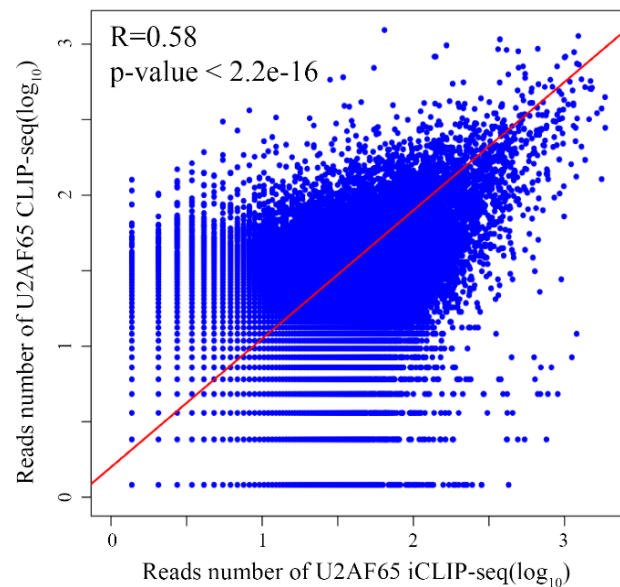


Figure 2.3.3. A reads number correlation of two separate CLIP-seq data. Reads number was counted in windows by 5000 nt length.

Since another iCLIP-seq of U2AF65 work was reported in a recent study (Zarnack et al., 2013), We should examine the overlap of read tags between two works to see whether these two dataset are consistent to each other. It is revealing that $R=0.58$, $p\text{-value}<2.2e-16$ (see Figure 2.3.3). In consideration of the difference of the experiment methods (iCLIP and CLIP) and sequencing depth, the data show a highly reasonable correlation.

After peak calling, we find out that U2AF65 binding was mostly detected in intronic regions of pre-mRNA (80.74%) with an additional fraction (13.24%) corresponding to exon-intron boundaries, which together accounts for 94% of mapped U2AF65 binding events in the human genome (see Figure 2.3.4). We also detected U2AF65 binding to exons (2.3%) and 3'UTRs (2.7%), consistent with the negative impact of exon-bound U2AF65 on splicing (Lim et al., 2011) and with the positive role of U2AF65 in 3' end formation (Danckwardt et al., 2007).

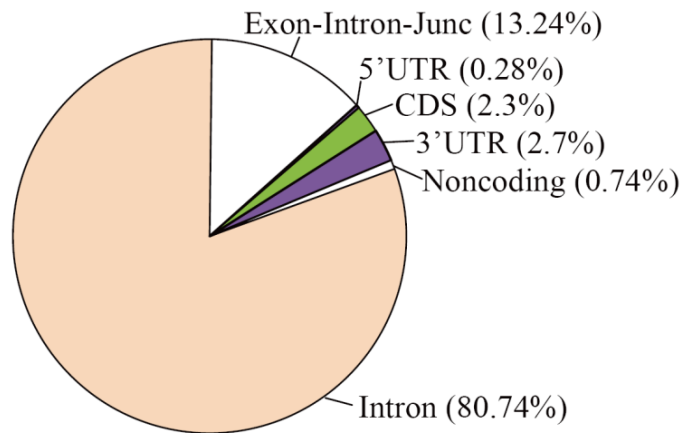


Figure 2.3.4. Genomic distribution of U2AF65 CLIP-seq peaks, the majority of which are located in introns or at exon-intron boundaries.

Chi and his colleagues developed a useful methods to calculate the footprint of a RNA binding protein using CLIP-seq data in 2009 (Chi et al., 2009). We made a similar estimate on the footprint of the U2AF heterodimer. By compiling a set of frequent U2AF65 binding events (8111 tags on 200 top clusters), we estimated the average U2AF65 footprint to be ~36nt (see Figure 2.3.5).

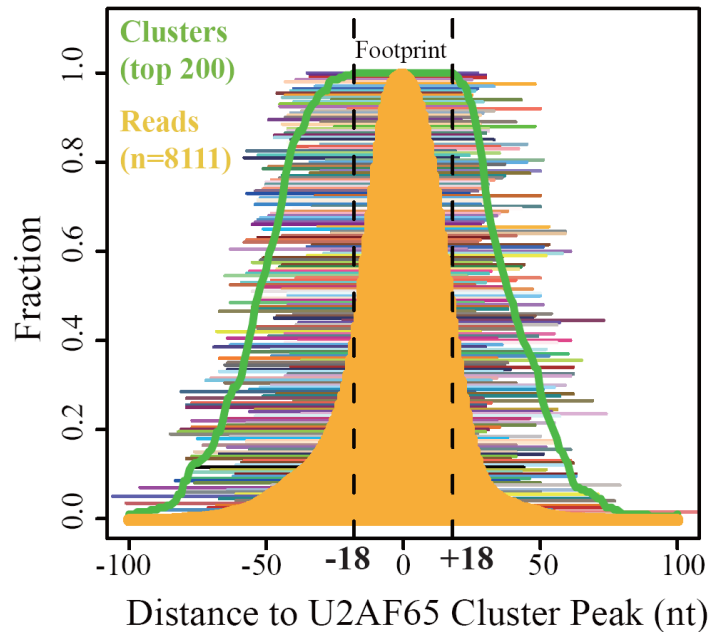


Figure 2.3.5. U2AF65 footprint on RNA. A set of high-density clusters (clusters=200; tags=8111) was used to derive the footprint. The peaks of top 200 robust clusters (peak height > 30, with single peaks) were determined, and the position of tags (brown graph) and width of individual clusters (colour lines and fraction plotted as green graph) are shown relative to the peaks (Chi et al., 2009). The minimum region of overlap of all clusters (100%) was within -18 and +18 nucleotides of cluster peaks, suggesting that the U2AF footprint on mRNA spans stringently 36 nucleotides.

Based on crosslinking-induced mutation sites (CIMS), as described earlier (Zhang et al., 2011), which displays characteristic distribution of base deletions, but not insertions or substitutions with uridine (U) being the most frequently deleted base within U2AF65 bound regions (see Figure 2.3.6).

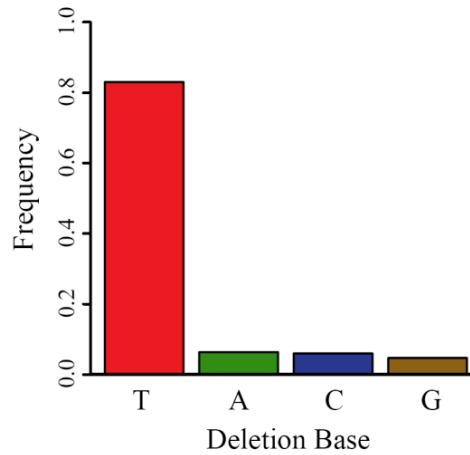


Figure 2.3.6. Preferential deletion mutation on uridine residues in CIMS.

Meta-gene analysis demonstrated prevalent U2AF65 binding at the 3' splice site of a composite pre-mRNA (see Figure 2.3.7), which is also illustrated on the SNRPA1 gene based on both mapped tags and identified CIMS (see Figure 2.3.8).

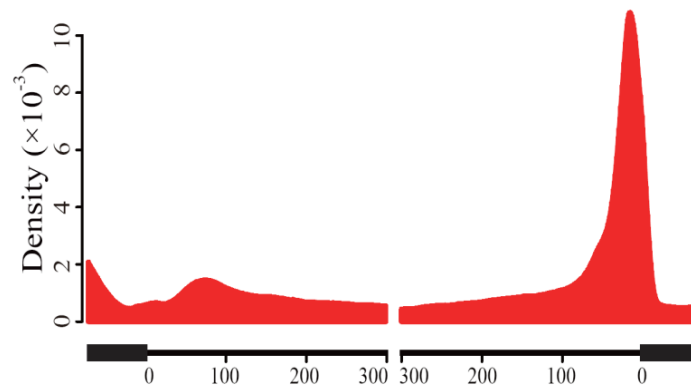


Figure 2.3.7. Meta-gene analysis of U2AF65-RNA interactions on a composite pre-mRNA.

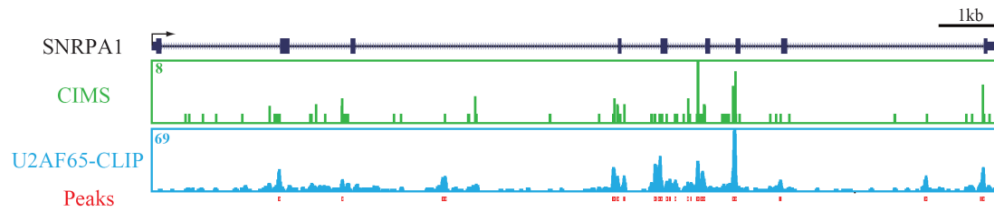


Figure 2.3.8. U2AF65 binding on a gene example (SNRPA1), showing raw tags, peaks and identified Crosslinking-induced Mutation Sites (CIMS).

These data demonstrated high fidelity mapping results for U2AF65-RNA interactions in the human genome.

2.3.2 U2AF recognition of ~88% functional 3' splice sites in the human genome

Consistent with the biochemically defined binding specificity of U2AF (Singh et al., 1995), motif analysis showed highly pyrimidine-enriched sequences on mapped U2AF65 binding sites (see Figure 2.3.9).

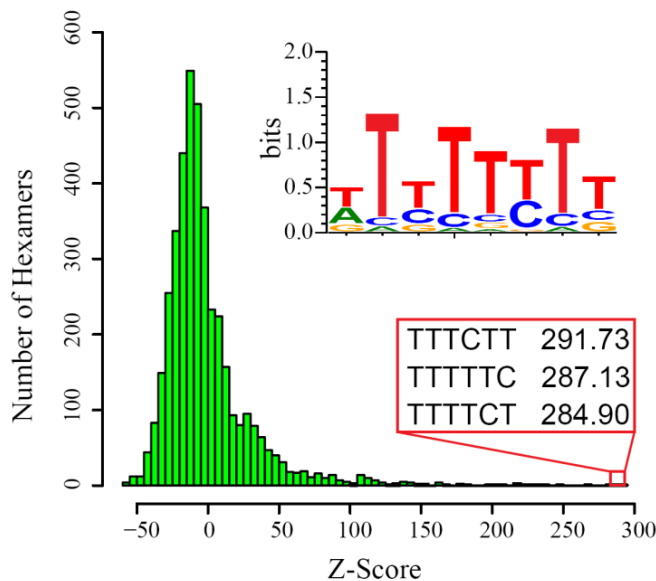


Figure 2.3.9. Enriched motifs for U2AF65 binding. Top 3 motifs were shown and top 50 motifs were used to deduce the consensus in the insert.

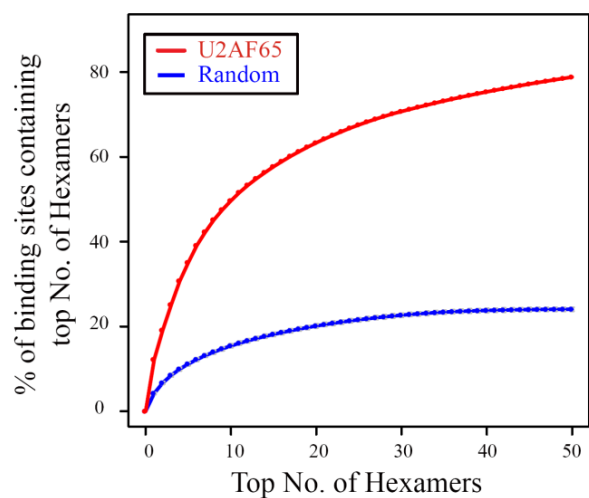


Figure 2.3.10. Percentage of U2AF65 binding sites that contain one or more top 50 motifs (red), compared with randomly selected 50 hexamers (blue).

Top 50 hexamers alone, which all consist of pyrimidines, account for 80% of all mapped U2AF65 binding sites, whereas randomly selected 50 hexamers only cover ~20% potential U2AF65 binding sites (See Figure 2.3.10). Alignment of the mapped U2AF65 binding sites according to the center of CIMS in individual tags generated a Py-tract like sequence, typical of those associated with functional 3' splice sites (see Figure 2.3.11). This high quality dataset allowed us to address two critical rules deduced from previous in vitro studies.

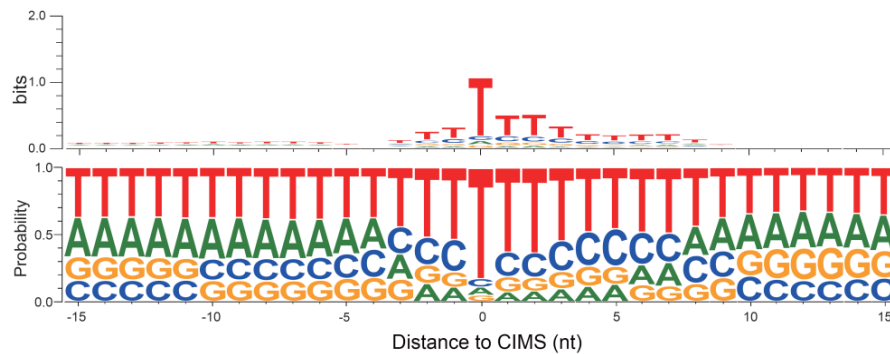


Figure 2.3.11. Nucleotide frequency centered on identified CIMS.

The first concerns the degree by which U2AF is involved in defining the functional 3' splice sites in mammalian genomes. From 12 million iCLIP tags, U2AF65 was previously found to bind 58% actively used 3' splice sites in HeLa cells (Zarnack et al., 2013). However, we noted that this simple counting method is likely to miss many U2AF-dependent 3' splice sites, especially among genes that are expressed at modest to low levels in the cell.

We therefore developed a maximal neighborhood approach to estimate the percentage of 3' splice sites that could be bound directly by U2AF65. We first sorted expressed genes according to the average tag density per annotated 3' splice site in each gene and then divided these genes into consecutive groups, each consisting of 50 genes. This allowed us to calculate the coverage of annotated 3' splice sites by U2AF65 with standard deviation in all groups. We next determined the percentage of coverage of the 3' splice sites when the tag density per 3' splice site is progressively increased. As shown in Figure 2.3.12 (blue dots), we observed that the coverage reached saturation at

~88% with increasing levels of U2AF65 binding at annotated 3' splice sites, indicating the existence of ~12% U2AF65-independent introns in the human genome.

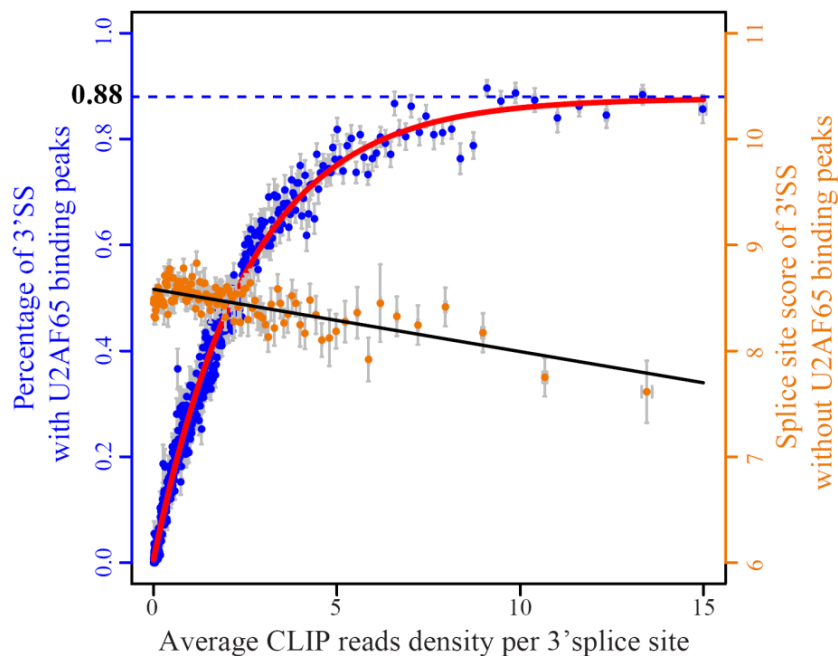


Figure 2.3.12. U2AF65 has the capacity to bind ~88% of annotated 3' splice sites in the human genome based on the maximal neighborhood analysis. Each blue dot represents averaged occupancy of group of 50 genes, which were sorted according to the averaged tag density at 3' splice sites; each orange dot shows the average of 3' splice site score among those in each group of 100 genes that exhibited no U2AF65 binding peaks.

We next asked whether those U2AF65 unbound 3' splice sites are drifted from U2AF65 binding consensus. For this purpose, we similarly sorted expressed genes according to the average tag density per 3' splice site and then group those splice sites without U2AF65 peak into consecutive groups, each consisting of a total of 50 introns. We next calculated the averaged 3' splice site score of U2AF65 unbound 3' splice sites in each group according to Yeo and Burge36. As shown in Figure 2.3.12 (orange dots), we detected progressive decrease in the averaged 3' splice site score with U2AF65 unbound introns. These data indicate that, among genes that show less efficient U2AF binding in general, the lack of U2AF binding in unoccupied introns is likely due to limited expression, but among genes that show extensive U2AF binding, the lack of

U2AF binding in the remaining introns likely results from poor consensus in their 3' splice sites. Therefore, coupled with the maximal neighborhood analysis, our data suggest that a significant fraction (~12%) of functional 3' splice sites may indeed represent U2AF-independent ones.

2.3.3 Additional U2AF binding events beyond functional 3' splice sites

The second rule concerns the ability of the U2AF heterodimer to discriminate Py-tracts with or without a flanking AG dinucleotide in mammalian genomes. In vitro binding studies suggest that U2AF efficiently binds Py-tracts followed by AG, but much less to Py-tracts without ending with an AG dinucleotide (Wu et al., 1999; Merendino et al., 1999), and such specificity appears to be enhanced by additional RNA binding factors, such as DEK and hnRNP A1 (Soares et al., 2006; Tavanetz et al., 2012). Because U2AF65 functions as a heterodimer with U2AF35 based on their tight interactions in co-IP experiments, it is likely that the mapped genomic U2AF65 binding events largely reflect the action of the U2AF65/35 heterodimer in vivo, which now affords us to directly test whether the U2AF heterodimer indeed prefer for Py tracts each followed by an AG dinucleotide in the human genome.

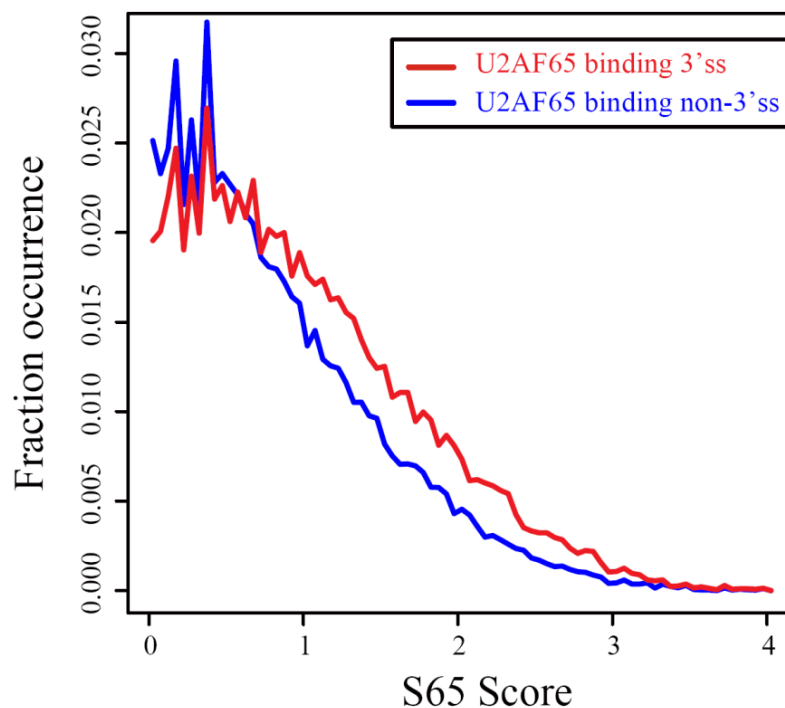


Figure 2.3.13. S65 scores of U2AF65 binding sites in 3' splice sites and non-3' splice sites.

Comparing between U2AF65 binding events on canonical 3' splice sites and other regions, we found that both U2AF65-bound 3' splice sites and non-3' splice sites exhibited a similar profile of the S65 score, a measure of U2AF65 binding affinity based on SELEX experiments (Murray et al., 2008) (see Figure 2.3.13). We next segregated U2AF65 binding events on non-3' splice sites into two classes. The first contains potential decoy exons (those with flanking sequences that resemble a 3' or 5' splice site) or pseudo exons (those with flanking potential 3' and 5' splice sites separated by a sequence up to 250nt) (Danckwardt et al., 2007), and the other has no obvious evidence for any splicing signals. We found that U2AF65 binding at functional 3' splice sites are strongly associated with a downstream AG dinucleotide; its binding near decoy and pseudo exons shows less, but still significant, link to a downstream AG; and the remaining U2AF65 binding events in other intronic locations exhibit no selective enrichment with a downstream AG dinucleotide (see Figure 2.3.14).

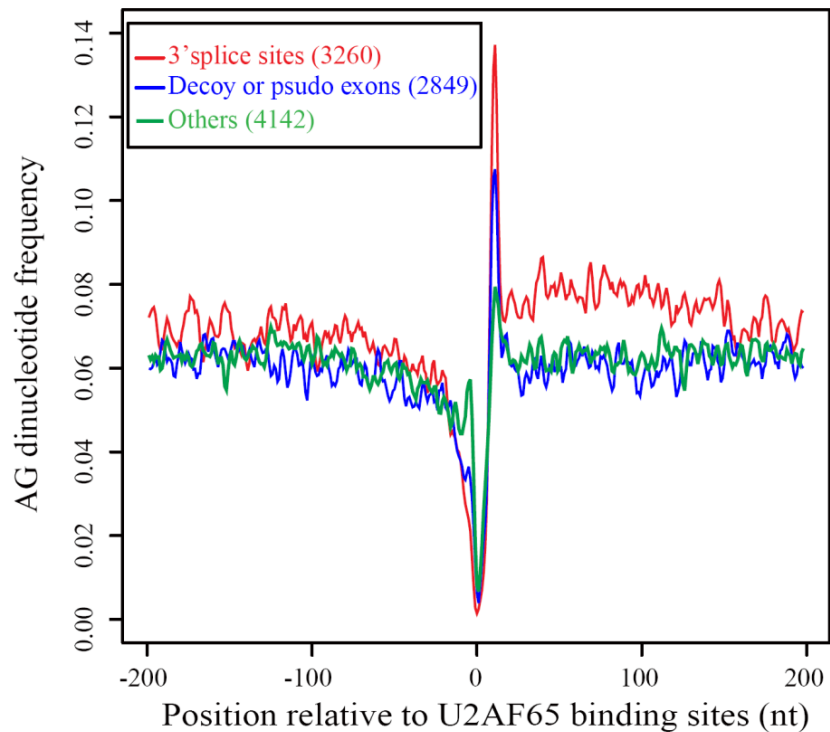


Figure 2.3.14. The frequency of the AG dinucleotide from the mapped U2AF65 binding sites on

annotated 3' splice sites (red), deduced decoy and pseudo exons (blue), or other intronic regions (green).

These data suggest that, despite the presence of other specificity enhancing factors to prevent U2AF65 from binding to other pyrimidine-rich sequences, a significant fraction of U2AF65 is still able to bind other locations in pre-mRNA besides functional 3' splice sites. These U2AF65 binding events may interfere with functional definition of adjacent bona fide 3' splice sites as a mechanism to modulate alternative splice site selection (see below) and/or reflect a role of U2AF65 in other RNA metabolism steps, such as mRNA export (Gama-Carvalho et al., 2006; Xiao et al., 2012).

2.3.4 Critical roles of U2AF in regulated splicing

U2AF65 has been implicated as a regulator of alternative splicing besides its role in constitutive splicing (Hastings et al., 2007; Pacheco et al., 2006), but it has been unclear how extensively U2AF65 is involved in regulated splicing in mammalian cells. To determine this question, we performed RNA-seq, generating 14.1 and 16.8 million uniquely mapped tags before and after knockdown of U2AF65 in HeLa cells, respectively (see Table 2.3.2).

	RNA-Seq data	
	Ctrl	Knock down U2AF65
total reads	28228751	25595461
mapped reads	14384722	17183922
mapped ratio	50.96%	67.14%
uniquely mapped reads	14119360	16834141
uniquely mapped ratio	91.16%	97.96%

Table 2.3.2. Summary information of RNA-seq data.

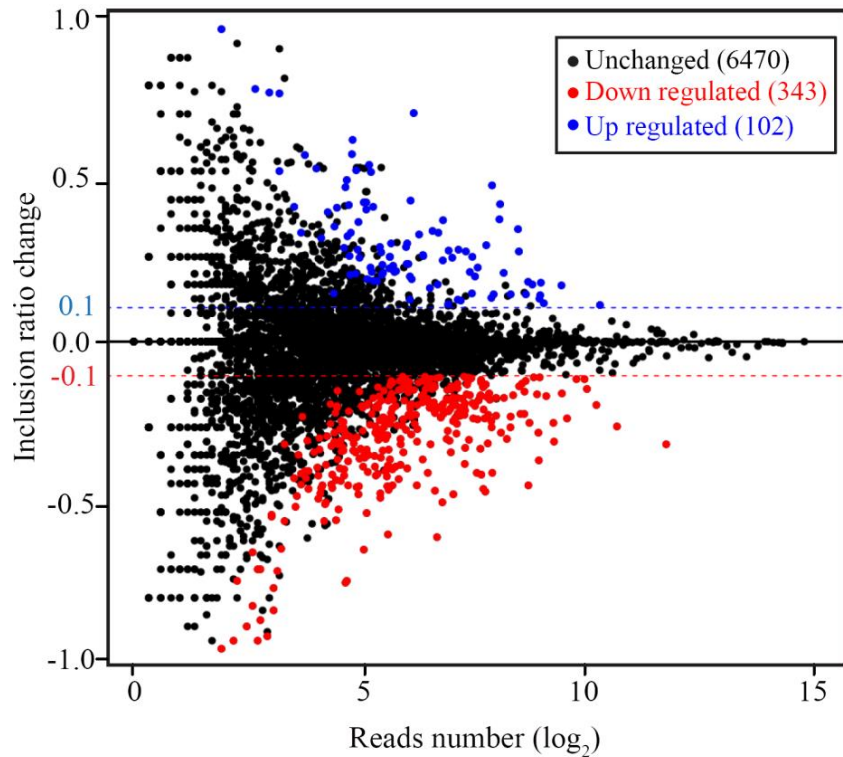


Figure 2.3.15. Altered alternative splicing events determined by RNA-seq, showing significantly induced (blue) or repressed (red) splicing events in U2AF65 knockdown cells.

We analyze the RNA-seq data to deduce altered splicing events in an unbiased manner. Taking advantage of 75nt sequences from both ends of our libraries, we generated sequence contigs that cover alternative splice junctions, which permitted calculation of the splicing ratio (Percentage of Splice In or PSI) of individual annotated cassette exons, as described (Zhou et al., 2012). The data revealed 102 and 343 (out of a total of 6915) cassette exons that showed significantly increased and decreased inclusion, respectively, in response to U2AF65 depletion (see Figure 2.3.15).

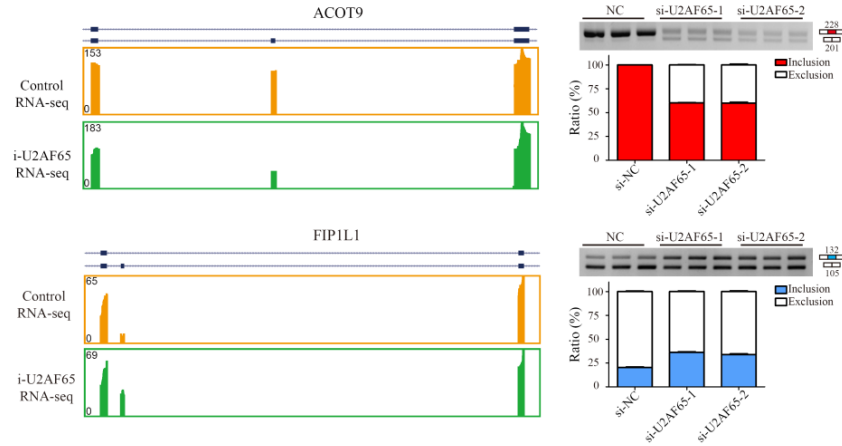


Figure 2.3.16. Splicing of two representative genes in response to U2AF65 knockdown. RNA-seq data were validated by RT-PCR in HeLa cells treated with two independent U2AF65 RNAi.

Most identified alternative splicing events are evident even from RNA-seq tags mapped on the alternative and flanking exons (see examples in Figure 2.3.16). We validated 70 randomly selected alternative splicing events by semi-quantitative RT-PCR and found that the induced exon inclusion or skipping events detected by RNA-seq were well correlated with the RT-PCR results ($R^2=0.65$, $p\text{-value}<2.2e-16$, see Figure 2.3.17).

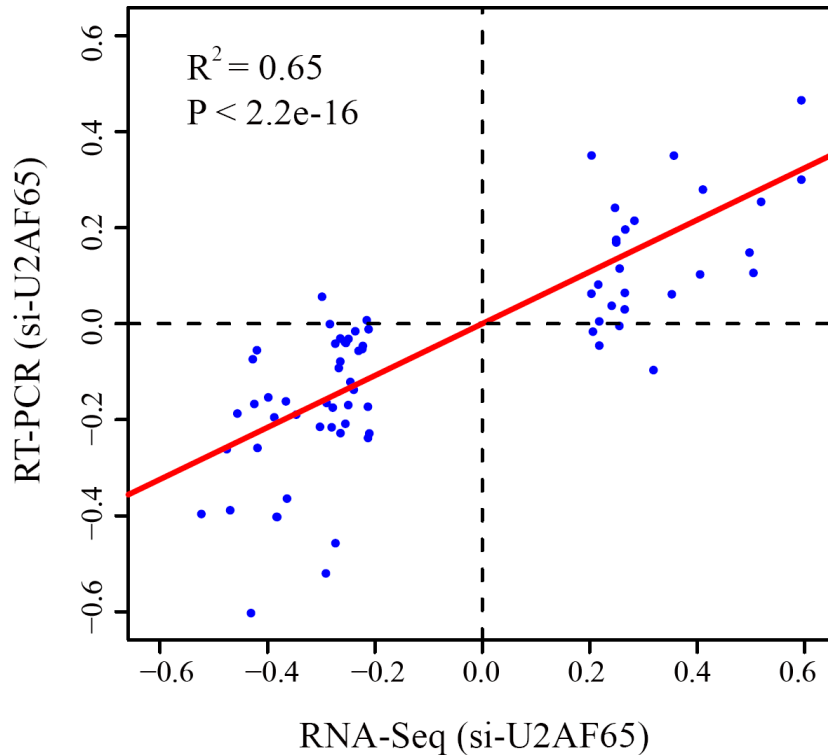


Figure 2.3.17. Comparison between the alternative splicing events detected by RNA-seq and those validated by semi-quantitative RT-PCR.

These data demonstrate that U2AF65 is extensively involved in the regulation of alternative splicing. Importantly, while 2/3 of induced events by U2AF65 RNAi showed increased exon skipping, the remaining 1/3 exhibited increased exon inclusion, raising an important mechanistic question on the positive and negative effects of this essential splicing factor on splice site selection.

2.3.5 Multiple mechanisms underlying U2AF-regulated alternative splicing

Because numerous genes were down regulated in U2AF65-depleted cells, many induced changes in alternative splicing might result from indirect effects of reduced expression of either positive or negative splicing regulators, which is expected to cause exon inclusion and skipping in about equal frequencies. However, our data clearly showed more induced exon skipping events than exon inclusion events in U2AF65-

depleted cells (Figure 2.3.15), indicating that at least a fraction of U2AF65 depletion-induced exon skipping events may result from the direct effect of U2AF65. This is consistent with levels of U2AF65 binding that are generally proportional to the levels of exon inclusion (see Figure 2.3.18), suggesting that the 3' splice site of the alternative exons is weaker in general than that of the flanking competing exons, and when U2AF65 is reduced in RNAi-treated cells, the alternative exons may be preferentially affected.

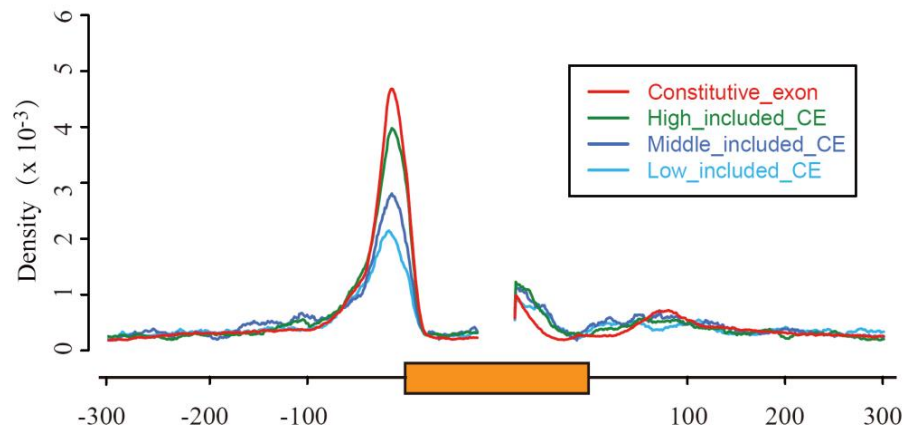


Figure 2.3.18. U2AF65 binding levels proportional to levels of exon inclusion.

While U2AF65 RNAi-induced exon skipping events could be comprehended, it remains to be determined whether some U2AF65 RNAi-induced exon inclusion events might also result from the direct effect of U2AF65. We noted many examples in which U2AF65 binds on exons, as illustrated on the *GANAB* gene (See Figure 2.3.19). This is actually consistent with a report showing the existence of many U2AF65 binding consensus in exonic regions and the inhibitory effect of exon-bound U2AF65 on exon inclusion (MacMillan et al., 1997).

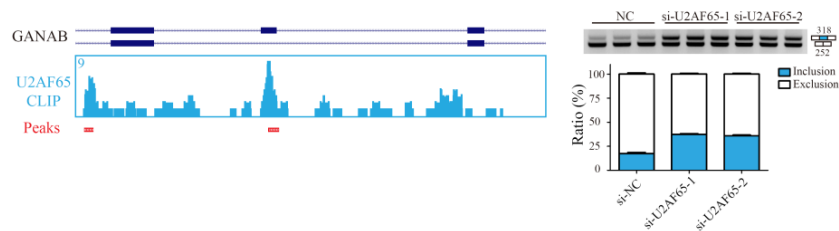


Figure 2.3.19. U2AF65 binds on exon in *GANAB* to repress exon inclusion.

The mechanism for the inhibitory role of U2AF65 via direct binding on the alternative exon, however, could not explain numerous other U2AF65 RNAi-induced exon inclusion events. To aid in mechanistic dissection, we constructed the U2AF65 RNA map based on detected exon inclusion or skipping events in response to U2AF65 RNAi (see Figure 2.3.20).

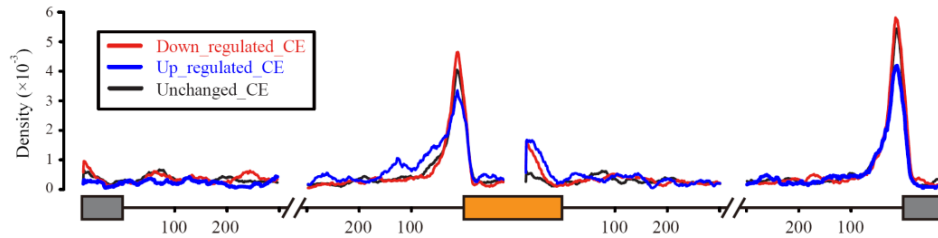


Figure 2.3.20. Normalized U2AF65 binding events on unaffected cassette exons (black), up-regulated (blue) or down-regulated (red) cassette exons in U2AF65 knockdown cells. U2AF65 binding appears higher upstream of the alternative cassette exons that were up regulated in response to U2AF65 knockdown.

However, we could not see any obvious trend for U2AF65-dependent exon inclusion or skipping, except some additional intronic binding events upstream of functional 3' splice sites associated with U2AF65-repressed alternative exons (blue line in Figure 2.3.20), comparing with the upstream of functional 3' splice site associated with the downstream exons.

It is real that the difference in U2AF65 binding in Figure 2. 3.20 are modest. This is because the size of introns varies greatly. As we displayed U2AF65 intronic binding events in a lineage fashion, the figure misses many intronic binding events that are beyond the adjacent regions from 5' and 3' splice sites.

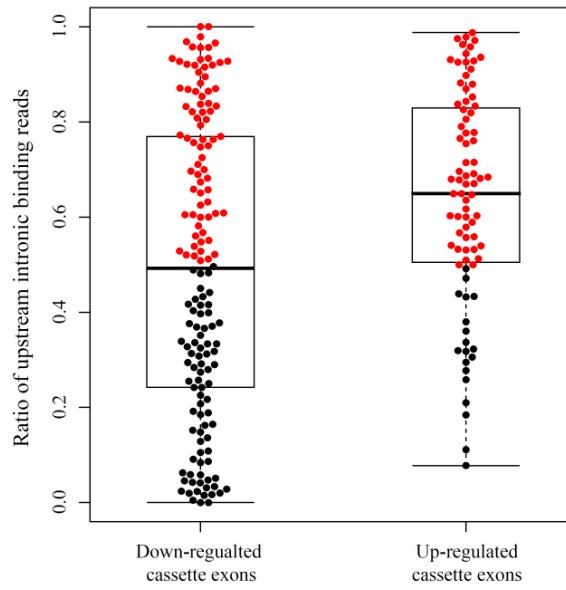


Figure 2.3.21. Ratio of upstream and downstream intronic binding events on down- and up-regulated exons

To solve this problem, we choose to keep the original Figure 2.3.20 to illustrate our points. One of the key features of U2AF-regulated alternative splicing events is elevated binding of U2AF65 in the upstream intronic region in many up-regulated cases, which is not evident with down-regulated ones. To further emphasize this point, we display the ratio of upstream and downstream intronic binding events on down- and up-regulated exons (see Figure 2.3.21).

It is significant that, among down-regulated exons, the ratio is evenly distributed between 0 and 1, indicating that the dominant regulatory mode for these events is selective weakening of U2AF binding at the alternative 3' splice site relative to the downstream 3' splice site. In contrast, we observe that most ratios are >0.5 among up-regulated exons, indicating that prevalent upstream intronic binding events interfere with the function of U2AF65 at the 3' splice site of the alternative exon, and as a result, removal of such interference induces the inclusion of the alternative exon. This is next validated by mutational analysis in the following panels, which additionally show that the same regulatory principle also holds for some strong downstream intronic binding events where they interfere with the function of U2AF65 at the 3' splice site of the

downstream exon, thus producing the opposite functional consequence.

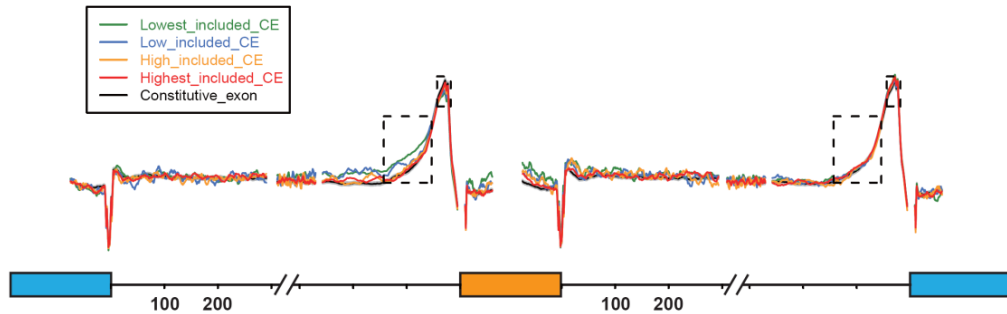


Figure 2.3.22. CU content levels proportional to levels of exon inclusion.

This is highly consistent with levels of CU content (U2AF65 binding sequence) in the upstream region of 3' splice site of cassette exon (the bigger box regions in Figure 2.3.22) that are generally inversely proportional to the levels of exon inclusion (see Figure 2.3.22), suggesting that the more CU content, or the more U2AF65 binds in the upstream region of functional 3' splice site, the less cassette exons included.

This finding raises an intriguing possibility that these additional U2AF65 binding events may interfere with normal recognition of adjacent functional 3' splice sites.

2.3.6 Polar effect of U2AF65 binding on downstream 3' splice site recognition

We chose three representative genes to perform mutational analysis on their minigenes, which could avoid potential indirect effects of U2AF65 depletion, and to compare between the effect of deletion mutations and response to U2AF RNAi.

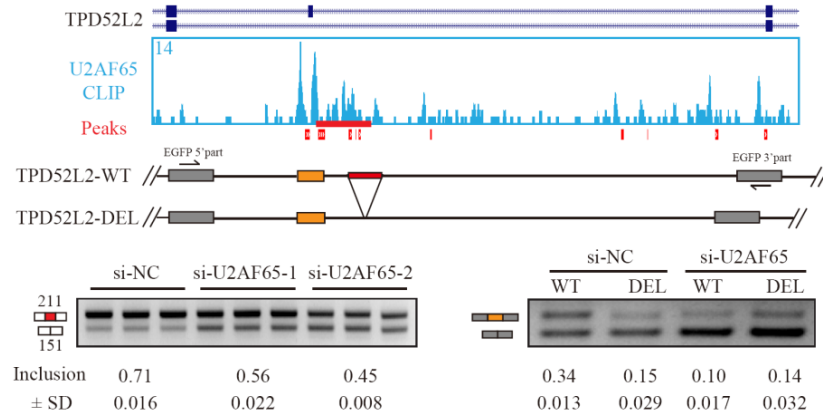


Figure 2.3.23. U2AF65 RNAi induced alternative splicing of TPD52L2. U2AF65 binds within intronic regions downstream of the alternative exon. The splicing response of these genes to U2AF65 RNAi was each analyzed by RT-PCR on the bottom.

On the TPD52L2 gene, U2AF65 binding predominantly occurred within the downstream intron, and depletion of U2AF65 caused skipping of the upstream alternative exon. Deletion of the major U2AF65 binding site near the 5' splice site of the alternative exon induced exon skipping in the same way as in U2AF65-depleted cells (see Figure 2.3.23).

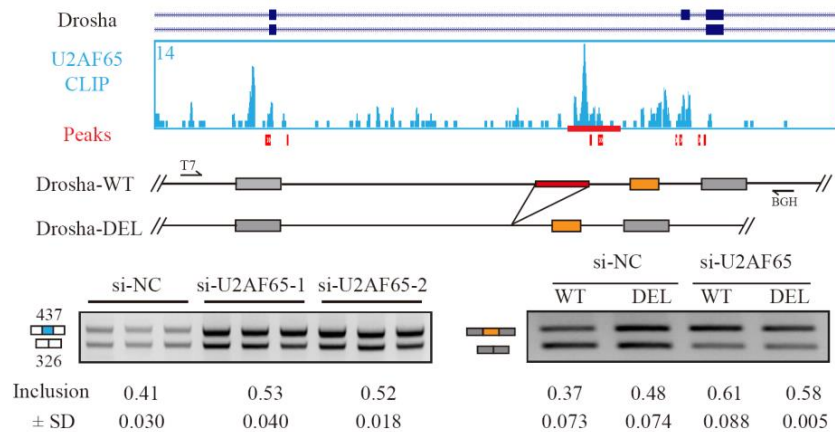


Figure 2.3.24. U2AF65 RNAi induced alternative splicing of Drosha. U2AF65 binds within intronic regions upstream of the alternative exon. The splicing response of these genes to U2AF65 RNAi was each analyzed by RT-PCR on the bottom.

On the Drosha gene, CLIP-seq detected a major U2AF65 binding event upstream

of the 3' splice site of the alternative exon and deletion of the U2AF65 binding site triggered the inclusion of the alternative exon, again similar to the U2AF65 RNAi effect (see Figure 2.3.24).

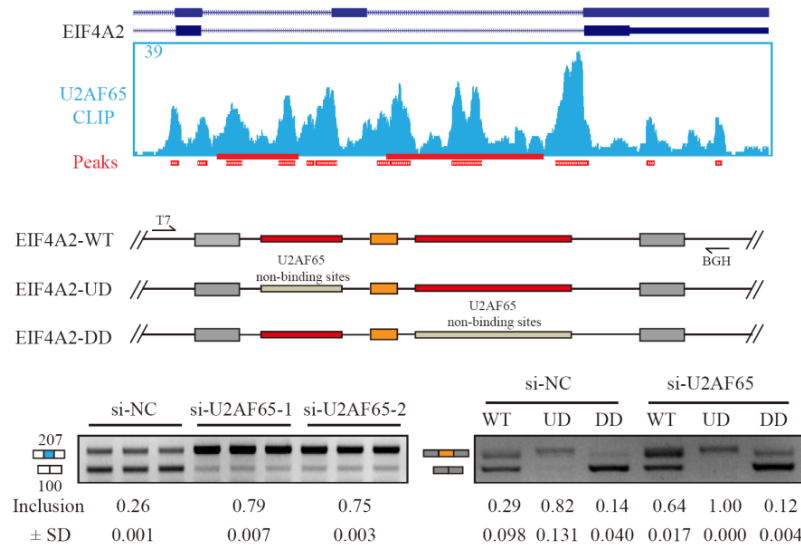


Figure 2.3.25. U2AF65 RNAi induced alternative splicing of EIF4A2. U2AF65 binds within both introns flanking the alternative exon. The splicing response of these genes to U2AF65 RNAi was each analyzed by RT-PCR on the bottom.

We next dissected the EIF4A2 minigene where U2AF65 binds extensively on both up- and downstream introns and U2AF65 depletion induced the net increase in the inclusion of the alternative exon. In this case, instead of constructing simple deletion mutants (because deletion of the U2AF binding sequence would remove most of the upstream or downstream intron), we replaced the U2AF65 binding sequences with a non-U2AF65 binding sequence of similar length. Interestingly, we detected enhanced exon inclusion when the upstream U2AF65 binding site was substituted, but enhanced exon skipping when the downstream U2AF65 binding site was replaced (see Figure 2.3.25).

Considered together, the simplest interpretation of the above results is that U2AF65 binding in intronic regions interferes with the recognition of the immediate downstream functional 3' splice site. In the case of TPD52L2, release of such inhibition

increases the competitiveness of the flanking 3' splice site, thereby suppressing the selection of the upstream 3' splice site associated with the alternative exon. This is also the case with U2AF65 binding in the downstream intron of the EIF4A2 gene. On the other hand, the removal of U2AF65 competition from the upstream intron in both Droscha and EIF4A2 genes likely increases the competitiveness of the 3' splice site of the alternative exon, allowing it to be included more efficiently in each case. When both competing events are operating in the same alternative splicing unit, a strong one would win, as in the case the EIF4A2 gene, thus generating a net effect of exon inclusion in U2AF65-depleted cells.

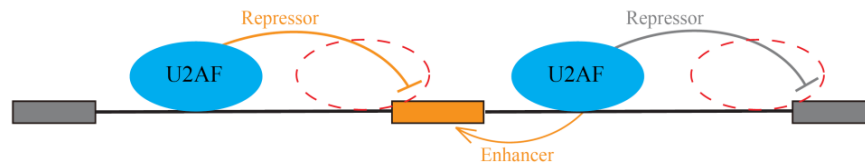


Figure 2.3.26. Proposed polar effect model for the effect of intronically bound U2AF65 to interfere with the recognition of the immediate downstream 3' splice site in regulated splicing.

Based on these findings, we propose a polar mechanism for intronic U2AF65 binding to interfere with the recognition of the downstream 3' splice site (see Figure 2.3.26).

2.3.7 Coordinated action of U2AF65 and U2AF35 in regulated splicing

It has been unclear thus far whether U2AF65 predominantly acts alone or in conjunction with U2AF35 or with other U2AF35-related molecules in the regulation of alternative splicing. Because the vast majority of U2AF65 appears to exist as the heterodimer with U2AF35 in the cell, it is likely that the U2AF65/35 heterodimer may play a dominant role in both constitutive and regulated splicing. To directly test this hypothesis, we used alternative splicing as a functional readout to compare the cellular response to U2AF65 and U2AF35 RNAi. As previously reported (Pacheco et al., 2006), U2AF35 RNAi only reduced the expression of U2AF35 while U2AF65 RNAi reduced the levels of both subunits of the U2AF heterodimer (see Figure 2.3.27).

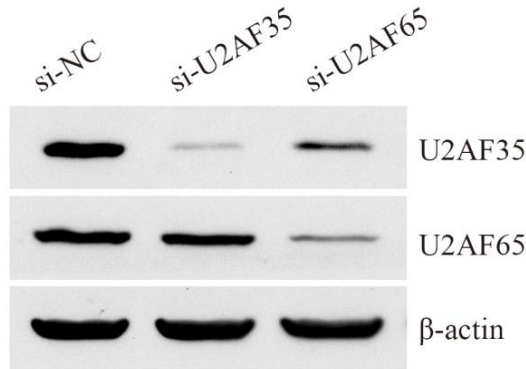


Figure 2.3.27. Western blotting analysis of RNAi-mediated U2AF65 and U2AF35 knockdown. Note reduced U2AF35 in U2AF65 RNAi-treated cells.

To determine how the reduction of U2AF35 alone or the U2AF65/35 heterodimer might affect alternative splicing from a global prospective, we employed the RASL-seq based technology we recently developed (Wei et al., 2012) to conduct a cost-effective survey of alternative splicing events in U2AF65 and U2AF35 RNAi-treated HeLa cells.

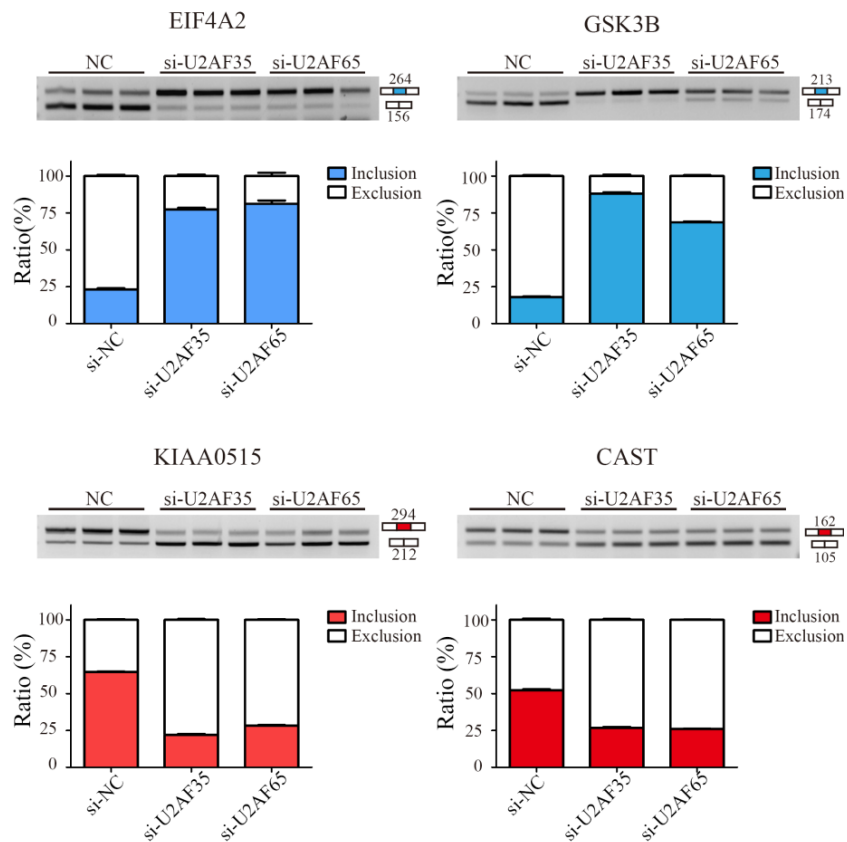


Figure 2.3.28. Splicing response of representative genes in response to RNAi against U2AF65 or U2AF35.

Using this oligonucleotide ligation-based approach, which was designed to specifically interrogate a large set of annotated splicing events (~5,000), we detected 1892 alternative splicing events in control RNAi-treated HeLa cells, among which 271 and 334 events showed significant changes ($p < 0.001$) in response to U2AF65 and U2AF35 depletion, and U2AF65 depletion respectively, which were extensively validated (see Figure 2.3.28). Significantly, nearly identical sets of alternative splicing events were induced (see Figure 2.3.29, Table 2.3.3).

RASL-Seq data		
	Knock down U2AF35	Knock down U2AF65
total detectable events	1892	
significantly changed events	334	271
co-changed events	208	
Co-changed events with same direction	206	
ratio	99%	

Table 2.3.3. Summary result of RASL-Seq data.

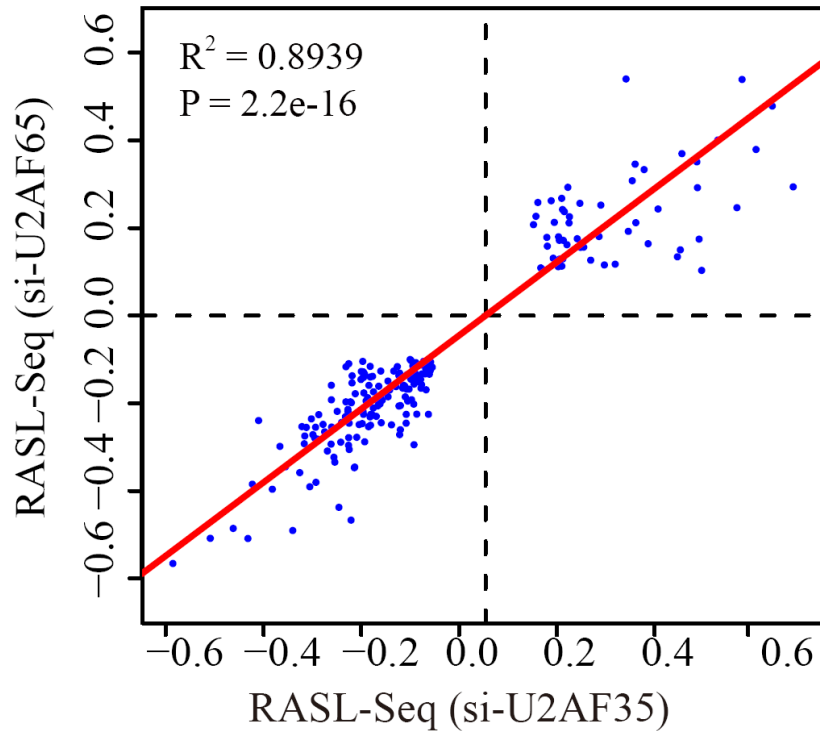


Figure 2.3.29. Global concordance of U2AF65 and U2AF35 dependent splicing revealed by RASL-seq.

While since depletion of U2AF65 also decreases the levels of U2AF35 (see Figure 2.3.27), it cannot be concluded that U2AF35 largely functions in conjunction with U2AF65 in the regulation of AS in mammalian cells. It could be that the effects seen in both experiments are due to a decreased level of U2AF35. So we should overexpress U2AF35 in cells that are subject to siRNA against U2AF65. If then, U2AF35 reach levels similar to the control, then they will be able to control effects of depleting U2AF35 and U2AF65.

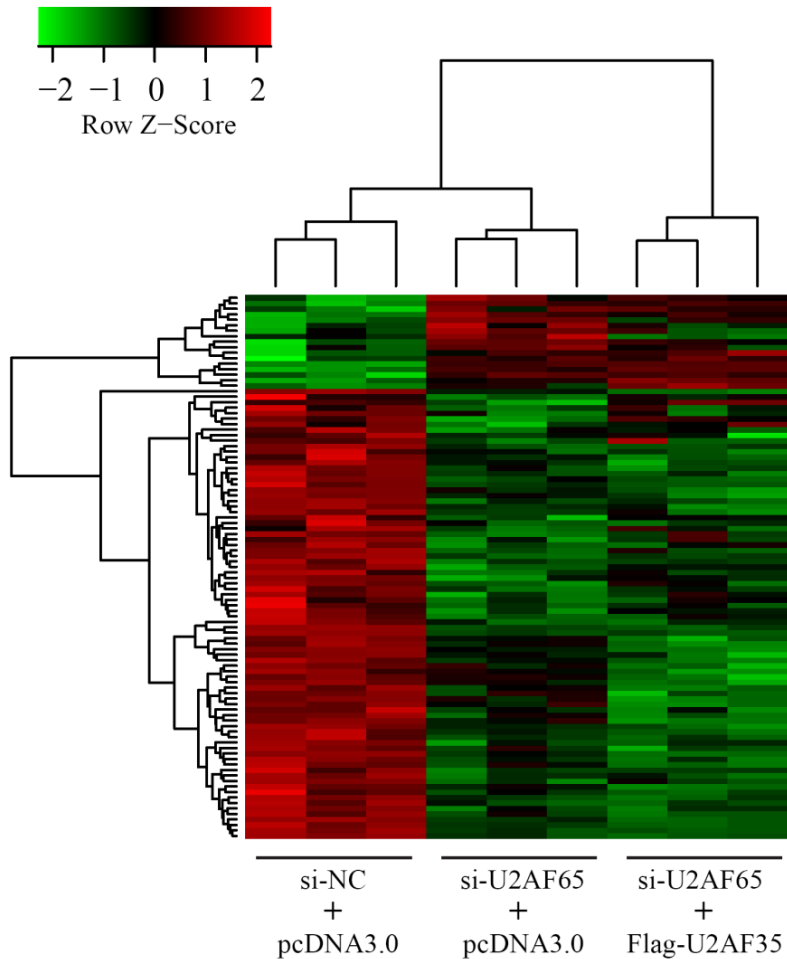


Figure 2.3.30. Heatmap of inclusion ratio of changed cassette exon induce by knocking down U2AF65 with or without exogenously expressed U2AF35.

We performed the RASL-seq experiments by knocking down U2AF65 with or without exogenously expressed U2AF35. The data show that the exogenous U2AF35 has little impact on U2AF65 depletion-induced splicing events, indicating that U2AF35 has to function in conjunction with U2AF65 in regulated splicing (see Figure 2.3.30).

These data demonstrated that U2AF35 largely functions in conjunction with U2AF65 in the regulation of alternative splicing in mammalian cells.

2.3.8 U2AF65 binding scores

Using sequences of 12 nucleotides, we should iterate $4^{12} = 16777216$ times for all the sequences in a loop for a specific constrain, and there are 48 constrains even for

the simplest type of pattern. Being limited of our computers' performance, we have only tried three kinds of patterns now. Latter, we could try to break the long target sequences into smaller ones to predict, and then join them together. In this way, we could test more complex pattern and mixed pattern of them.

The three patterns just present the weight matrix model (me1s0), the first-order Markov model (me2s0) and a simplest nonadjacent dependence model (me2s1) (see Figure 2.3.31). As shown in Figure 2.3.31, there are not too much difference among them, indicating that the adjacent and nonadjacent dependencies between nucleotides maybe not be used so much by U2AF65 to recognize it target sites. And all the patterns do not perform very well. We think that there are two reasons at least: There are many assistant factors (U2AF35, hnRNPA1) could help U2AF65 to recognize target sites, as described previously; RNA structures in the intronic regions may also affect U2AF65 binding on the target patterns.

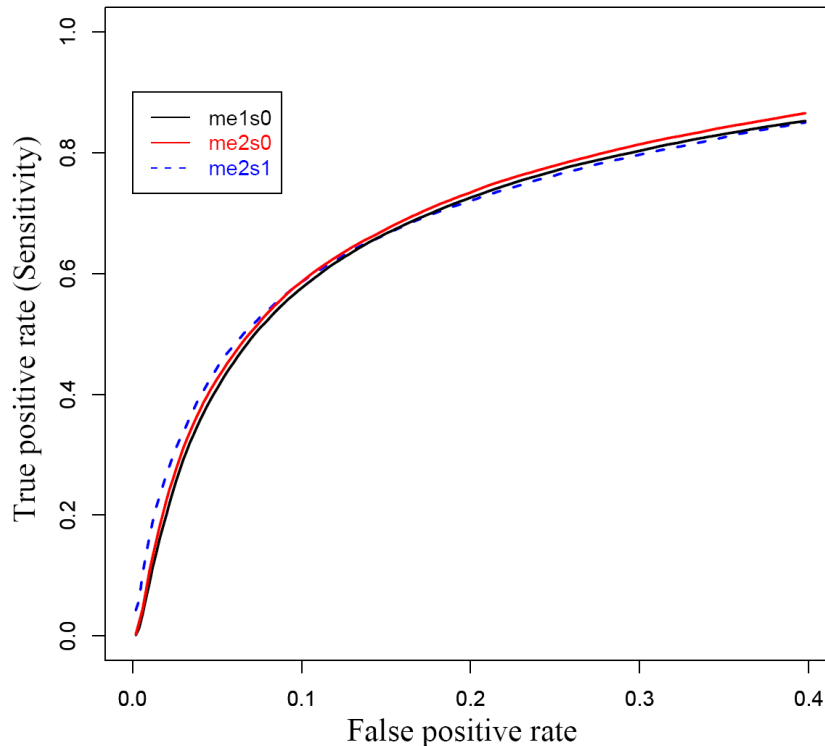


Figure 2.3.31. Receiver operating characteristic (ROC) curve of three type of constrains performing on test data sets. 'me' stands for maximum entropy model; 's' stands for skipping. For example,

'me2s1' means the constrains take the nonadjacent dependencies of two nucleotides with one random base between them, like (ANA).

While the first-order Markov model (me2s0) perform a little better than the others, we take the log-likelihood ratio of this model as the U2AF65 binding scores. Base on this score, we could try to predict the possibility that if the U2AF65 likes of dislikes binding on a specific sequence.

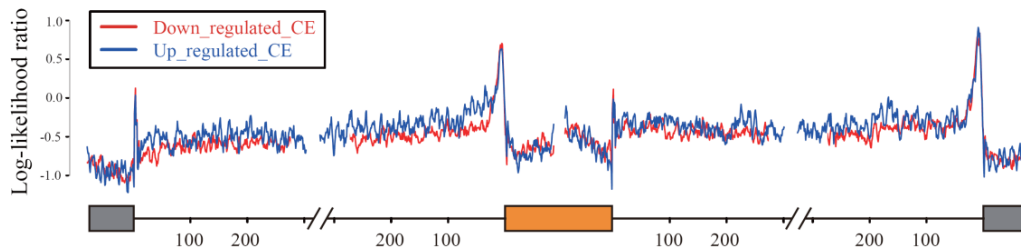


Figure 2.3.32. Normalized U2AF65 binding scores on up-regulated (blue) or down-regulated (red) cassette exons in U2AF65 knockdown cells. U2AF65 binding appears higher upstream of the alternative cassette exons that were up regulated in response to U2AF65 knockdown.

We try to use this scoring scheme to illustrate the difference of the up-regulated and down-regulated cassette exons in U2AF65 knockdown cells again. As shown in Figure 2.3.32, both the 3' splice sites have a peak, indicating binding preference. Comparing the upstream and downstream intronic region, U2AF65 binding score appears a little higher along the upstream intronic region of the alternative cassette exons for up-regulated cassette exons than down-regulated cases, but not for the downstream region.

2.4 Discussion

Our current genome-wide study demonstrates that U2AF65 plays a predominant role in functional definition of 3' splice sites and is required for efficient expression of most intron-containing genes in the human genome. Interestingly, however, our data also suggest the existence of ~12% U2AF65-independent introns because they lack evidence for U2AF65 binding and their Py tracts are considerably degenerate from the pyrimidine-rich consensus. It is important to point out that the functional requirement for U2AF is not strictly determined by the consensus, as many poor 3' splice sites could be aided in by other intronic splicing enhancer factors, such as YB1 (Shen et al., 2010). However, the existence of a fraction of U2AF-independent introns is fully consistent with the observations made in fission yeast (Sridharan et al., 2011; Sridharan et al., 2007), which begs the question of which specific splicing factors fulfill such role in defining various untypical 3' splice sites. Although several RNA binding splicing factors have structures related to U2AF65 or U2AF35 (Mollet et al., 2006), the available functional evidence suggests that most of them function in synergy with, rather than independently from, U2AF (Page-McCaw et al., 1999; Tronchere et al., 1997; Shepard et al., 2002; Han et al., 2011b). Therefore, it remains to be understood how U2AF-independent introns are recognized in mammalian genomes.

The preferential binding of U2AF65 to functional 3' splice sites over other pyrimidine-rich sequences in the genome appears to be enforced by the U2AF35 subunit. Other factors have also been suggested to provide the proofreading function of the U2AF heterodimer in the genome (Soares et al., 2006; Tavanez et al., 2012). However, our genome-wide binding data clearly show that U2AF65 can also bind to various locations that are not part of annotated 3' splice sites and these binding events do not seem to depend on a downstream AG dinucleotide. This is consistent with the proposed function of U2AF65 in promoting nuclear export of intronless transcripts in *Drosophila* (Gama-Carvalho et al., 2006) and with binding of U2AF65 on some spliced mRNAs (Xiao et al., 2012). A more recent study showed that hnRNP C is able to prevent U2AF65 from binding to many *Alu*-containing transcripts to suppress

exonization of those *Alu* elements (Zarnack et al., 2013). Therefore, U2AF binding appears to be a highly regulated process in mammalian genomes.

Besides its role in constitutive splicing, U2AF has been implicated in the regulation of alternative splicing. Our metagene analysis indicates that U2AF binding on the 3' splice site of alternative exons generally tracks the level of exon inclusion. This has been generally perceived as a predominant mechanism for U2AF-regulated splicing. However, we also found that U2AF65 exhibits other modes of binding in the human genome, one corresponding to its binding to exonic regions to interfere with the selection of nearby 3' splice site, which has been demonstrated on engineered minigenes (Lim et al., 2011). A more widespread mode of U2AF65 binding appears to occur in various intronic locations.

By mutational analysis, we found that those intronic U2AF65 binding events appear to selectively interfere with the recognition of the immediate downstream 3' splice site, and thus, the competition between the alternative and flanking constitutive splice sites dictates the splicing outcome. This splice site competition model provides a universal mechanism for the regulation of alternative splicing by both sequence-specific RNA binding proteins and core components of the splicing machinery (Zhou et al., 2012). The observed polar effect may underlie the positional effect of many other splicing regulators whose binding on the upstream intron may inhibit the inclusion of the alternative exon, whereas their interaction with the downstream intron may induce the skipping of the alternative exon (Przychodzen et al., 2013).

One of the most important advances in the field is the identification of specific mutations in multiple splicing factors, including U2AF65 and U2AF35, in specific types of myeloid leukemia. Because of the prevalence of those mutations in the disease, they are generally considered driver mutations, which actually remain to be functionally defined.

Therefore, although our current study was not carried out in a disease-relevant cell type, our findings provide critical insights into the nature of specific mutations in the

splicing regulators. The challenge ahead is to link specific molecular defects in right cell types, likely hemopoietic stem cells, to the etiology of the disease.

Chapter 3: Consistent-Pivot: A New effective Pivot Algorithms for Ranking Aggregation Problem

3.1 Introduction

With the increasing development of high throughput technologies, very high amounts of data are produced and stored in public databases to make them available to the scientific community, for example, Gene Expression Omnibus (GEO) which is a public functional high-throughput sequencing genomics data repository (Barrett et al., 2013) (see Figure 3.1.1).

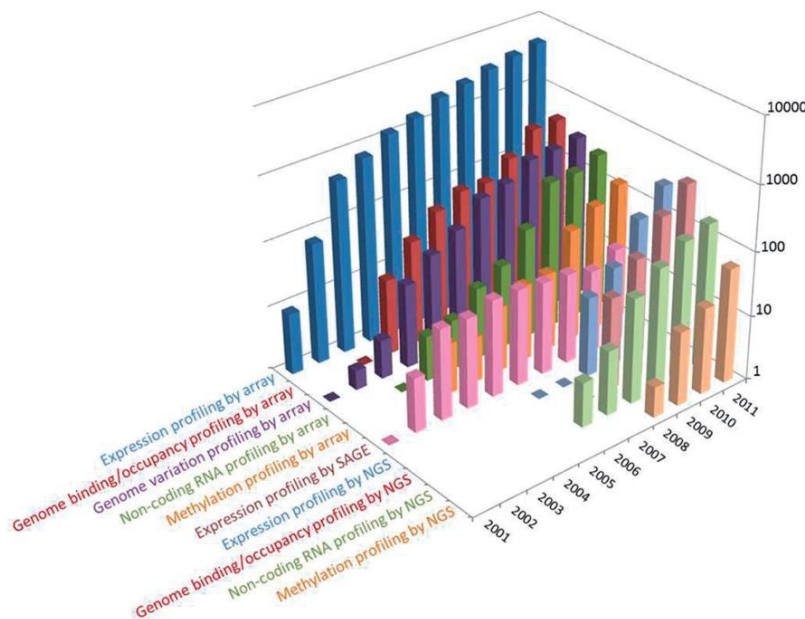


Figure 3.1.1. Distribution of the number and types of selected studies released by GEO each year since inception. Users can explore and download historical submission numbers using the ‘history’ page, as well as constructing GEO DataSet database queries for specific data types and date ranges using the ‘DataSet type’ and ‘publication date’ fields. Figure from (Barrett et al., 2013)

From the biological Big Data, vast amounts of genes lists of expression, regulation, interaction, correlation could be extracted from the data mining results, such as cell expressed microRNAs, gene regulated genes, protein-protein interaction, disease related genes, or just gene association from text mining (Metzker, 2010). Facing these kinds of lists, it is very difficult to exploit them if they are not ranked. However, rankings of biological data on a same query are always very different between different processing methods, algorithms or datasets, especially for biological data mostly with noise, fuzziness, biases and errors (Brusic et al., 1998). Based on all these issues, how to get a convincing ranking result from biological data becomes an important task in post-genome era.

Instead of developing new ranking methods, Cohen-Boulakia and her colleagues proposed to generate a consensus ranking to highlight the common points of a set of rankings while minimizing their disagreements to combat the noise and error for biological data (Cohen-Boulakia et al., 2011). This idea had already been used for combining results of microarray data (DeConde et al., 2006), microRNA targets prediction algorithms (Sengupta et al., 2013), Comparison ligand-binding site prediction methods (Gao et al., 2012), and so on.

There has been also a lot of interest in this problem in the computer science community in recent years which arises when building meta-search engines for Web search, where one wants to combine the rankings obtained by different algorithms into a representative ranking. For example, Dwork combines the rankings of individual search engines to get more robust rankings that are not sensitive to the various shortcomings and biases of individual search engines (for instance, “paid placement” and “paid inclusion” among search engines) (Dwork et al., 2001).

The process of generating a consensus ranking is based on the concept of ranking aggregation, originating in social choice theory, machine learning, and theoretical computer science (Ali et al., 2012), defined on rankings: Given m rankings of n elements and a distance function, the ranking aggregation problem is to find a ranking of all the elements that is the closest of the m given rankings.

It could be easily thought of a kind of a ranking aggregation method, where the order of each element is determined by taking simple average of positions of it from different rankings. This method was firstly proposed by Borda as a voting system for elections in the late eighteenth century (Young, 1974). Condorcet proposed a more reasonable method of pairwise majority voting known as Condorcet's criterion, which permits A to be ranked higher than B if the majority vote for A over B in pairwise comparison, even if the average of positions of A is after B (De Grazia, 1953).

Obeying to extended Condorcet criterion, Kemeny proposed the Kemeny optimal aggregation for determining the best aggregate ranking based on the Kendall-tau distance which counts the number of pairwise disagreements between orderings of elements (Kemeny et al., 1962).

However, Kemeny optimal aggregation is unfortunately a computational challenge, because the problem is NP-hard even for only four rankings (Dwork et al., 2001; Blin et al., 2011). Since the problem is important across a variety of fields, many researchers across these fields have converged on finding good, practical algorithms for its solution. There are formulations that lead to exact algorithms, of course without polynomial running time guarantees. There are also a large number of heuristic and approximation algorithms.

Among these, a group of algorithms are thought to be very prospective, named pivot algorithms (Ailon et al., 2008; Van Zuylen et al., 2009). In common, they recursively generate a solution by choosing an elements as pivot and ordering all the other elements with respect to the pivot according to some criterion. It divides the problem into smaller ones and conquers separately, and uses the transitive property (see below) which is right in most situations, especially for the rankings with high agreement. So the pivot algorithms are always fast in time and not bad in accuracy.

In this chapter, we propose a new variant of pivot algorithms named as Consistent-Pivot. It uses a new strategy of pivot selection and other elements assignment which

performs much better both on computation time and accuracy than previous pivot algorithms.

3.2 Notations

In this section, we introduce the definition of ranking and the distance used to compare two rankings, then we provide the general statement of the problem of Kemeny optimal aggregation with ties under generalized Kendall-tau distance.

3.2.1 Ranking with ties

Following the definition of Fagin and his colleagues, given a universe set U , a ranking with ties (or bucket order) of a subset $S \subseteq U$, r is a transitive binary relation \triangleleft represented as set of non-empty buckets B_1, \dots, B_k that form a disjoint partition of the elements of S , such that $x \triangleleft y$ if and only if there are i, j with $i < j$ such that $x \in B_i$ and $y \in B_j$ (Fagin, 2004). We may assume without loss of generality that a ranking with ties on $[n]$ is defined as $r = [B_1, \dots, B_k]$, and let $r(x) = i$ if $x \in B_i$ which denotes the rank of x .

If r contains all the elements in U , then it is said to be a full ranking. There are situations where full rankings are not possible. For instance, the ranking result of target genes of a miRNA from a prediction tool usually cannot include all the targets. Such rankings that rank only some of the elements in U are called partial rankings.

3.2.2 Unifying a set of partial rankings

Aiming to penalize the fact that one element is considered in a ranking but not in another one, Cohen-Boulakia and her colleagues present a unifying preprocess for sets of partial rankings to append the set of elements belonging to the other rankings to the end in a same bucket.

Example 1 For instance, let us consider three different ranking methods which outputs are the following:

$$\begin{aligned}
r_1 &= [\{1\}, \{7\}, \{2\}, \{3\}] \\
r_2 &= [\{2, 4, 5\}, \{7\}, \{3\}] \\
r_3 &= [\{1, 2, 3\}, \{4, 5\}, \{6, 7\}]
\end{aligned}$$

Here we have $U = \{1, 2, 3, \dots, 7\}$, $U \setminus r_1 = \{4, 5, 6\}$, $U \setminus r_2 = \{1, 6\}$ and $U \setminus r_3 = \emptyset$.

The rankings processed using the unifying preprocess are then the followings:

$$\begin{aligned}
r_1^i &= [\{1\}, \{7\}, \{2\}, \{3\}, \{4, 5, 6\}] \\
r_2^i &= [\{2, 4, 5\}, \{7\}, \{3\}, \{1, 6\}] \\
r_3^i &= [\{1, 2, 3\}, \{4, 5\}, \{6, 7\}]
\end{aligned}$$

This is a normalized method to facilitate the comparison between the rankings and the consensus ranking, especially for comparing the performance of the different ranking methods. In the remainder of this chapter, the unifying preprocess is applied before running the ranking aggregation algorithm.

3.2.3 Distance measures

How do we define a distance between two full rankings with respect to a set S ? In the last century, this problem has been studied and defined from a mathematical perspective (Kendall, 1938).

3.2.3.1 The Spearman footrule distance

For all elements $i \in S$, the Spearman footrule distance is the sum of the absolute difference between the rank level of i according to the two rankings. Formally, given two full rankings r_1 and r_2 , the distance is given by:

$$F(r_1, r_2) = \sum_{i=1}^{|S|} |r_1[i] - r_2[i]|$$

So if based on the Spearman footrule distance, the consensus ranking of m rankings with smallest distance is just the median value of the set of positions of every element in the m rankings, because only in this way, the footrule distance is the smallest (Dwork et al., 2007).

3.2.3.2 Kendall-tau distance

A good dissimilarity measure for comparing two rankings without ties is the Kendall-tau distance which counts the number of pairwise disagreements between positions of elements in these rankings (Kendall, 1938). The larger the distance, the more dissimilar the two rankings are. Kendall-tau distance is also called bubble-sort distance since it is equivalent to the number of swaps that the bubble sort algorithm would make to place one ranking in the same order as the other ranking.

A strict ranking without ties, or permutation, r is a bijection of $[n] = \{1, 2, \dots, n\}$ on to itself. It represents a strict total order of the elements of $[n]$. The Kendall-tau distance, denoted K , counts the number of pairwise disagreements between two permutations. For permutations r_1 and r_2 of $[n]$, it is defined as:

$$K(r_1, r_2) = \#\{(i, j) : i < j \text{ and } [(r_1[i] < r_1[j] \text{ and } r_2[i] > r_2[j]) \text{ or } (r_1[i] > r_1[j] \text{ and } r_2[i] < r_2[j])]\}$$

where $r[i]$ denotes the position of integer i in permutation r and $\#S$ the cardinality of set S . For example, if

$$r_1 = [\{1\}, \{2\}, \{3\}, \{4\}],$$

$$r_2 = [\{2\}, \{3\}, \{1\}, \{4\}],$$

then $K(r_1, r_2) = 2$ since elements 1 and 2 appear in different orders in the two rankings as do elements 1 and 3, but not others.

3.2.3.3 Generalized Kendall-tau distance for rankings with ties

Following the definition of Fagin et al., the generalized Kendall-tau distance, denoted $K^{(p)}$ (or simply K , when parameter $p = 1$), is defined according to a parameter p , $0 < p \leq 1$:

$$\begin{aligned}
K^{(p)}(r_1, r_2) = & \#\{(i, j) : i < j \text{ and } [(r_1[i] < r_1[j] \text{ and } r_2[i] > r_2[j]) \text{ or} \\
& (r_1[i] > r_1[j] \text{ and } r_2[i] < r_2[j])]\} \\
& + p \times \#\{(i, j) : i < j \text{ and } [(r_1[i] = r_1[j] \text{ and } r_2[i] \neq r_2[j]) \text{ or} \\
& (r_1[i] \neq r_1[j] \text{ and } r_2[i] = r_2[j])]\}
\end{aligned}$$

In other words, the generalized Kendall-tau distance considers the number of disagreements between two rankings with ties: a disagreement can be either two elements that are in different buckets in each ranking, where the order of the buckets disagree, and each such disagreement counts for 1 in the distance; or two elements that are in the same bucket in one ranking and in different buckets in the other, and each such disagreement counts for p , $0 < p \leq 1$. For example, if

$$r_1 = [\{1\}, \{2, 3, 4\}]$$

$$r_2 = [\{2, 3\}, \{1, 4\}],$$

then $K(r_1, r_2) = 2 + 3p$ since two pairs of elements 1 and 2, 1 and 3 appear in different orders in the two rankings, and three pair of elements 1 and 4, 2 and 4, 3 and 4 appear in different buckets in one ranking while in a same bucket in the other ranking.

3.2.4 Kemeny optimal aggregations

Based on the definition of Kendall-tau distance, Kemeny proposed a precise criterion for determining the “best” aggregate ranking (Kemeny and James, 1962). Given n elements and m rankings of the elements, a Kemeny optimal ranking of the elements is a ranking r^* that minimizes the sum of distances, $\sum_{i=1}^m K(r^*, r_i)$. In other words a Kemeny optimal ranking minimizes the number of pairwise disagreements with the given m rankings, corresponding to the geometric median of the inputs (Farah and Vanderpooten, 2007).

More formally, let $Rank_n$ be the set of all possible rankings with ties over $[n]$. Given any subset $R \subseteq Rank_n$ and a ranking r , we define

$$K^{(p)}(r, R) = \sum_{r_i \in R} K^{(p)}(r, r_i)$$

A Kemeny optimal ranking of a set of rankings with ties $R \subseteq \text{Rank}_n$ under the generalized Kendall-tau distance is a ranking with ties r^* such as

$$K^{(p)}(r^*, R) \leq K^{(p)}(r, R), \text{ for all } r \in \text{Rank}_n$$

Kemeny optimal aggregations have maximum likelihood interpretation. Suppose there is an underlying “correct” ordering r^* of S , and each order, $r_1, r_2 \dots r_i$, is obtained from r^* by swapping two elements with some probability less than $1/2$. Thus, the (r_i) s are “noisy” versions of r^* . A Kemeny optimal aggregation of $r_1, r_2 \dots r_i$, is one that is maximally likely to have produced the (r_i) s, so it is just r^* . Viewed in this way, Kemeny optimal aggregation has the property of eliminating noise from various different ranking schemes (Dwork et al., 2007).

However finding a Kemeny optimal ranking is NP-hard and remains NP-hard even when there are only four input rankings to aggregate (Dwork et al., 2001; Blin et al., 2011). This motivates the problem of finding a ranking that approximately minimizes the number of disagreements with the given input rankings.

3.3 Previous algorithms

As for the Kemeny optimal aggregation problem, Conitzer et al have provided a integer linear programming scheme for treating strict rankings (Conitzer et al., 2006) and Blin expands it generally for rankings with ties (Brancotte et al., in preparation). However, of course solving the integer linear programming problem is also NP-hard.

Another exact algorithm was proposed by Meila et al. It is a branch and bound algorithm (B&B). Each node in the search tree corresponds to a prefix $\sigma = [x_1, x_2, \dots, x_j]$ of r^* , so that level j in the tree contains all possible prefixes of length j ; branching is on the item to be added in rank $j+1$ which is one of the other elements. The cost and cost-to-go at a node are computed for bounding. A brute force search tree has $n!$ paths if there are no ties, while if the lower bound of some nodes A is greater than the upper bound of some other nodes B , branch and bound algorithm could safely discard A from the search, what is called pruning. However in bad cases, as aggregation of strong disagreement rankings, pruning can not always be effective. So, branch and bound algorithm, limiting the available memory leads to a family of approximate algorithms in which memory and runtime can be traded off for accuracy.

So, many heuristic and approximate algorithms were developed.

3.3.1 Some heuristics and approximation algorithms

Heuristics and approximation algorithms are techniques designed for solving a problem more quickly when classic methods are too slow, or when classic methods fail to find any exact solution, especially for NP-hard problems. However, more than heuristics algorithms, approximation algorithms want provable solution quality and provable run-time bounds. For example, a ρ -approximation algorithm A is defined to be an algorithm for which it is proven that the result of the approximation algorithm $A(x)$ will not be more (or less, depending on the situation) than a factor ρ times the

optimum solution (OPT).

$$\begin{cases} OPT \leq A(x) \leq \rho OPT, & \text{if } \rho > 1; \\ OPT \geq A(x) \geq \rho OPT, & \text{if } \rho < 1; \end{cases}$$

The factor ρ is called the constant ratio approximation factor.

3.3.1.1 Borda count

As described before, Borda count comes from the social choice theory. It is “positional” method, which sorts items in descending order according to their average position across all the input rankings (Borda, 1781).

It aims at finding the winner of a pole by taking into consideration the preferences between candidates each voter has by letting them rank all the candidates, which form R a set of rankings. The principle of the algorithm is simple it assigns to each element x a Borda score $Borda(x)$ and sorts the elements by this score. It runs in time

$O(nm)$. The score is computed as follows: $Borda(x) = \sum_{r_i \in R} r_i(x)$ where $r_i(x)$ denote

as the rank of element x in ranking r_i , as defined before.

Obviously, this is a heuristic algorithm, which is not developed for solving the median problem. However, it could give a good solution very quickly.

3.3.1.2 MEDRank

MEDRank was designed for a database environment where, in order to quickly provide an answer, one needs to have as few accesses as possible to each record of each ranking (Fagin et al., 2003).

In order to build the consensus, all rankings of R are read in parallel, element by element. Having m rankings and a threshold tr , $0 < tr \leq 1$, as soon as an element has been read in $tr \times m$ rankings, it is added at the end of the consensus in a new bucket. Obviously, the algorithm runs also in $O(nm)$.

In the study of Fagin and colleagues', the default threshold considered by the authors is $tr = 0.5$. In this way, the algorithm is just sorting the median value of the set of positions of every element in the rankings. As described above, so this is just the optimal solution based on the Spearman footrule distance. It is known that:

$$K(r_1, r_2) \leq F(r_1, r_2) \leq 2K(r_1, r_2)$$

So it is proven that it is a 2-approximation algorithm (Fagin et al., 2003).

3.3.1.3 FaginLarge and FaginSmall

This Fagin et al.'s algorithm is a kind of improvement of the MEDRank, based on the intuition that if two items i and j have very close median ranks, items i and j should be put into the same bucket in the output ranking (Fagin, 2004). So it is also called the median aggregation algorithm. It starts from the ordering result of median rank of elements, then groups elements with close median ranks into same bucket to minimize the sum of all the buckets cost based on dynamic programming.

In detail, suppose a bucket B in the final result ranking r , contains items starting from the i -th position to the j -th position in the MEDRank result. Then the bucket cost c associated with this bucket is defined as follows:

$$c(i, j) = \sum_{l=i}^j \left| Med(l) - \frac{i+j}{2} \right|$$

Where $Med(l)$ denotes the median rank of item l and the term $(i+j)/2$ represents the "average position" of the bucket in the output bucket order.

At each step of the dynamic programming the solution is built from the best of the sub-solutions. The variant FaginLarge chooses the first best sub-solution encountered while FaginSmall uses the last one. Their names come from that experimentally it was noticed that FaginSmall tends to do smaller bucket than FaginLarge (Brancotte et al., in preparation). They run in time $O(nm + n^2)$.

It has been proven that this algorithm is a constant factor approximation both full rankings and partial rankings. For full rankings, the median aggregation algorithm gives a near-optimal full ranking, with an approximation factor of two (Fagin, 2004).

3.3.1.4 BioConsert

BioConsert was proposed by Cohen-Boulakia and her colleagues. It works by iteratively trying to move a element to another bucket or a new bucket from an input ranking to reduce the sum of Kendall-tau distance which improves the input ranking step by step. If none of the elements are changed from their buckets, then the algorithm terminates (see Algorithm 1) (Cohen-Boulakia et al., 2011).

Algorithm 1: BioConsert (R_{start}, \mathcal{R})

Data: a set of elements E , a set \mathcal{R} of rankings with ties (which contain at least the elements of E)

Result: The best consensus found i.e. the ranking r aiming to minimize $K(r, \mathcal{R})$

```

begin
   $n \leftarrow \text{domain}(R_{start})$ 
   $k \leftarrow \text{number of buckets of } R_{start}$ 
   $bool \leftarrow 0$  (will be changed to 1 if there is no more possible "good"
  operation)
   $change \leftarrow 0$  (will tell us if some operations were made)
  while  $bool \neq 1$  do
    for  $i$  from 1 to  $n$  do
      for  $j$  from 1 to  $k$  do
        if  $\text{changeBucket}(i, j)$  is a good operation then
           $R_{start} \leftarrow \text{changeBucket}(i, j)(R_{start})$ 
           $change \leftarrow change + 1$ 
        end if
      end for
      for  $j$  from 1 to  $k + 1$  do
        if  $\text{addBucket}(i, j)$  is a good operation then
           $R_{start} \leftarrow \text{addBucket}(i, j)(R_{start})$ 
           $change \leftarrow change + 1$ 
        end if
      end for
    end for
    if  $change = 0$  then
       $bool \leftarrow 1$ 
    end if
  end while
  return  $R_{start}$ 
end

```

Algorithm 1. BioConsert

In contrast to the two previous one, this heuristic is an anytime algorithm, as the

input ranking is iteratively improved and interrupting the algorithm at any time will return a proper result. This heuristic can be implemented with a time complexity of $O(n^3m)$. BioConsert is a kind of local search algorithm. At each step, the BioConsert algorithm is only looking for a better neighbor. So it would fall in to a local best solution, which can be the global best one sometimes.

3.3.2 Other algorithms

There are some other algorithms for the ranking aggregation problem. Dwork et al. introduced a Markov chain based algorithm (Dwork et al., 2001). Qin and colleagues developed a possibility based algorithm (Qin et al., 2010). In addition, the attempts of combinations of several algorithm to give a better result were also reported (Ailon et al., 2008; Schalekamp and van Zuylen, 2009; Ali and Marina, 2012). For example, the combination of KwikSort and Pick-A-Perm could get a $\frac{11}{7}$ -factor approximation algorithm, which is a little better than KwikSort algorithm (2-factor approximation algorithm).

3.3.3 Pivot Algorithms

Previous pivot algorithms are all published for rankings without ties, but they all could be expanded to the rankings with ties. Besides the two relationships for two elements ($i \triangleleft j$, i is before j ; $i \triangleright j$, i is after j), rankings with ties allow elements in a same level. So, it is a little more complex for rankings with ties. Here for simple description, we follow the same situations described in the papers before for the previous pivot algorithms.

3.3.3.1 Transitive property and conflicts

We define the weight that element i is before element j as w_{ij} , which is how many times the element i is before element j in the m rankings. So if $w_{ij} > w_{ji}$, we would say that the situation where element i is before element j ($i \triangleleft j$) is

dominant.

We have stated that sets of rankings usually have transitive property for elements. It means that if $i \triangleleft j$ and $j \triangleleft k$ are dominant for the set of rankings, we could usually see that $i \triangleleft k$ in most time (or, $i \triangleleft j \triangleleft k$), especially for the rankings with high agreement. Let us illustrate this property in an example, for the three rankings below:

$$r_1 = [\{1\}, \{3\}, \{4\}, \{2\}];$$

$$r_2 = [\{4\}, \{2\}, \{3\}, \{1\}];$$

$$r_3 = [\{1\}, \{2\}, \{3\}, \{4\}].$$

Here we try to illustrate the positional relationship of all the elements in a weighted directed graph (see Figure 3.3.1). The relationship of “before” is plotted on the upside, and “after” is plotted on the underside. In this weighted directed graph, all the thicker lines have a weight of 2, while the thinner lines have a weight of 1. As shown in the figure, element 1 is before element 2 in two rankings (r_1 and r_3), so there is a thicker line (weight of 2 in this figure) linking the element 1 to the element 2. At the same time, element 1 is after element 2 in the ranking r_2 , so there is also a thinner line (weight of 1 in this figure) linking the element 2 to the element 1. Here it is the dominant positional relationship between the two elements that element 1 is before element 2 ($1 \triangleleft 2$)

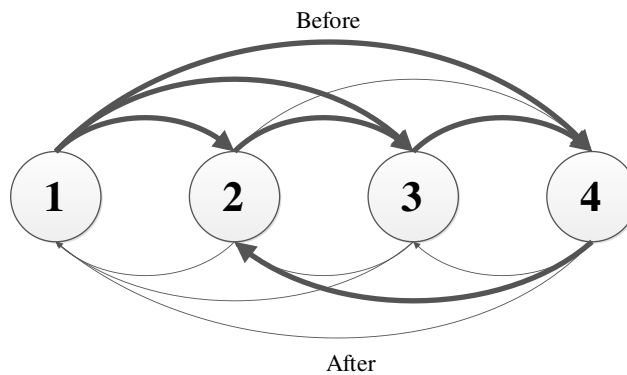


Figure 3.3.1. A weighted digraph to describe the positional relationship of all the elements. The relationship of “before” is plotted on the upside, and “after” is plotted on the underside. In this weighted digraph, all the thicker lines have a weight of 2, while the thinner lines have a weight of

1.

For convenience, we remove the minor directed edges to only keep the dominant relationship between two elements (see Figure 3.3.2).

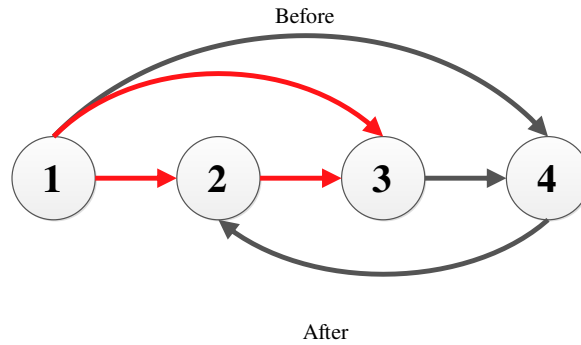


Figure 3.3.2. A weighted directed graph to describe the positional relationship of all the elements with only the dominant relationships. The red lines show the transitive property for elements 1, 2 and 3 ($1 < 2 < 3$).

As shown in Figure 3.3.2, the transitive property is that element 1 is dominantly before element 2 ($1 < 2$), and element 2 is dominantly before element 3 ($2 < 3$), so we usually could see that 1 is also dominant before 3 ($1 < 3$ or $1 < 2 < 3$). It is the same for element 1, 3 and 4 ($1 < 3 < 4$), element 1, 4 and 2 ($1 < 4 < 2$).

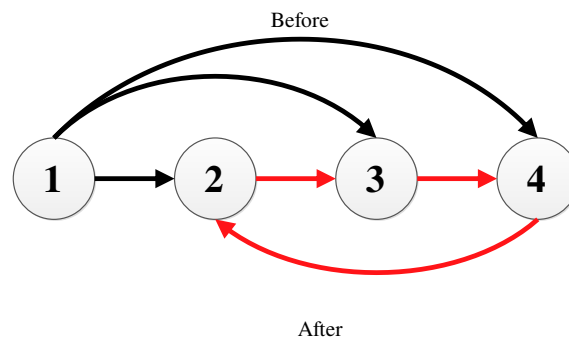


Figure 3.3.3. A weighted directed graph to describe the positional relationship of all the elements with only the dominant relationships. The red lines show a conflict for element 2, 3 and 4, forming a directed cycle.

But it is clear that the transitive property is not true for element 2, 3 and 4 (see

Figure 3.3.3). element 2 is before 3 ($2 \triangleleft 3$), and element 3 is before 4 ($3 \triangleleft 4$). While we could not see that element 2 is before element 4, but it is just the opposite that element 2 is after element 4. In this way, they form a directed cycle. We also call it a conflict in the set of rankings, because it could not simultaneously be satisfied in a linear ordering.

Ranking aggregation is just aiming to set up a compatible positional relationship (or a linear ordering) by removing a set of conflicting edges with a sum of smallest weight. It is worth mentioning that this is just the definition of the minimum feedback arc set problem. And in fact it has been stated that the problem of Kemeny optimal aggregation of rankings can be cast as a special case of the minimum feedback arc set problem (Ailon et al., 2008). It is easy for this example that we could get three different results by removing any edge in the directed cycle, because they are all same weighted (see Figure 3.3.4).

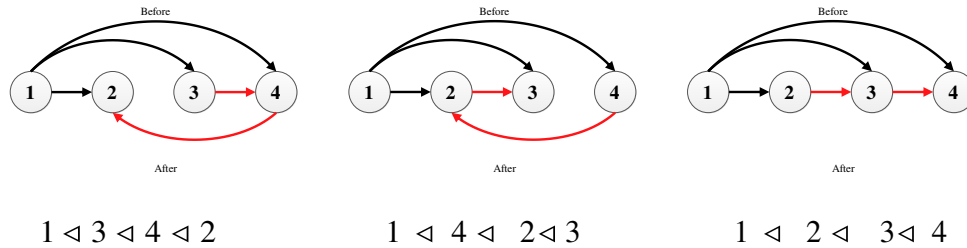


Figure 3.3.4. The three types of answers for the problem are all right.

3.3.3.2 KwikSort

Based on the transitive property of the elements in rankings, Ailon, Charikar and Newman developed a 2-factor approximation algorithm for rankings without ties, KwikSort. It was named KwikSort, mainly because the algorithm looks like a type of sorting algorithm, Quicksort. It was defined for the feedback arc set problem (Ailon et al., 2008). Here we describe it for the ranking aggregation problem without ties.

Let $G = (V, W)$ be a directed graph of a set of rankings, where V indicates all the elements, and W is the weight table between any two elements (w_{ij} and w_{ji}). The

algorithm recursively generates a solution by choosing a random element as “pivot” and ordering all other elements with respect to the pivot element (see Algorithm 2). In this way, the positional relationship between elements in the sets of both sides of the pivot do not need to be taken into account: all the elements on the left side are before all the element on the right side.

Algorithm 2: KwikSort($G = (V, W)$)

```

begin
  if  $V = \emptyset$  then
    | return empty-list
  else
    |  $V_L \leftarrow \emptyset$ 
    |  $V_R \leftarrow \emptyset$ 
    | Pick random pivot  $i \in V$ 
    | for all vertices  $j \in V \setminus \{i\}$  do
    |   | if  $w_{ij} \geq w_{ji}$  then
    |   |   | Add  $j$  to  $V_R$  (place  $j$  on right side).
    |   |   else
    |   |   | Add  $j$  to  $V_L$  (place  $j$  on left side).
    |   |   end if
    |   end for
    end if
  Let  $G_L = (V_L, W_L)$  be directed weighted graph induced by  $V_L$ .
  Let  $G_R = (V_R, W_R)$  be directed weighted graph induced by  $V_R$ .
  return KwikSort( $G_L = (V_L, W_L)$ ),  $\{i\}$ , KwikSort( $G_R = (V_R, W_R)$ )
end

```

Algorithm 2. KwikSort

The advantage of this algorithm is that it is very fast. The weight table could be calculated with a time complexity of $O(n^2m)$. We note that the weight table only need to be calculated once and the same table can be used in all recursive calls. And even in the worst situation, it makes $O(n^2)$ comparisons. In addition, the accuracy of this algorithm is not very bad, especially for the rankings with high consistence. It has been proven that this algorithm is a 2-factor approximation algorithm for rankings without ties (Ailon et al., 2008).

In fact, the KwikSort algorithm uses the transitive property which is usually true for elements, but not takes the conflicts in rankings into account. So some more algorithms were developed to try to solve this problem, by changing the assignment method or pivot picking method.

3.3.3.3 LP-KwikSort

As described above, the integer linear programming (ILP) for ranking aggregation problem is also NP-hard. But as we know, the linear programming (LP) relaxation without integrality constraint can be solved in polynomial time (Khachiyan, 1980). Based on the pivot and the linear programming scheme, Ailon and colleagues proposed another algorithm, LP-KwikSort (see Algorithm 4).

Here we define the solution of the following linear programming as P , where p_{ij} indicate the probability that element i is before element j .

$$\begin{aligned} \text{minimize } Z &= \sum_{i \in V, j \in V \setminus \{i\}} (p_{ij} * w_{ji} + p_{ji} * w_{ij}) \\ \text{s.t. for } \forall i, j, k &\left\{ \begin{array}{l} 0 \leq p_{ij} \leq 1 \\ p_{ij} + p_{ji} = 1 \\ p_{ij} + p_{jk} \geq p_{ki} \end{array} \right. \end{aligned}$$

Algorithm 3: LP-KwikSort($G = (V, P)$)

```

begin
  if  $V = \emptyset$  then
    | return empty-list
  else
     $V_L \leftarrow \emptyset$ 
     $V_R \leftarrow \emptyset$ 
    Pick random pivot  $i \in V$ 
    for all vertices  $j \in V \setminus \{i\}$  do
      if  $p_{ij} \geq p_{ji}$  then
        | Add  $j$  to  $V_R$  (place  $j$  on right side).
      else
        | Add  $j$  to  $V_L$  (place  $j$  on left side).
      end if
    end for
  end if
  Let  $G_L = (V_L, P_L)$  be directed weighted graph induced by  $V_L$ .
  Let  $G_R = (V_R, P_R)$  be directed weighted graph induced by  $V_R$ .
  return LP-KwikSort( $G_L = (V_L, P_L)$ ),  $\{i\}$ ,
  LP-KwikSort( $G_R = (V_R, P_R)$ )
end

```

Algorithm 3. LP-KwikSort

The main idea of the algorithm is changing the assignment of the other elements in such a way that, after we choose a pivot j , we should use the LP solution value (p_{ij}

and p_{ji}) to decide where to put all the other elements, instead of deciding greedily.

Ailon and colleagues proved that this algorithm is a $\frac{4}{3}$ -approximation algorithm for rankings without ties, which is better than KwikSort algorithm (Ailon et al., 2008). Based on the same scheme, Ailon introduced a $\frac{3}{2}$ -approximation algorithm for partial rankings (Ailon, 2010).

3.3.3.4 DerandLP-Pivot

Another modified pivot algorithm called DerandLP-Pivot, was proposed by Van Zuylen and colleagues (Van Zuylen et al., 2009). It is a deterministic pivot algorithm, instead of randomly picking pivot. And this algorithm directly faces up the conflicts in rankings.

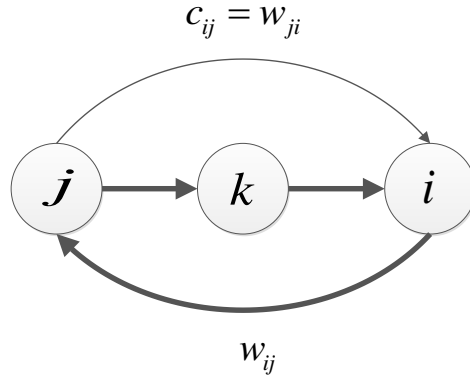


Figure 3.3.5. A schematic figure of conflict between elements for picking k as the pivot.

For a pivot k , let $T_k(G)$ be the set of combination of two elements with conflicts. $T_k(G) = \{(i, j) \mid \exists k, j \triangleleft k, k \triangleleft i, i \triangleleft j\}$. They define a *budget* for element i and element j as $c_{ij} = \min(w_{ij}, w_{ji})$. As shown in Figure 3.3.5, for a pivot k and a conflict between i and j , w_{ij} is the cost for picking k as the pivot for this conflict, and c_{ij} is just the earning of picking k as the pivot for this conflict.

So in every recursive call, we choose the pivot k that minimizes the cost-earning ratio:

$$Pivot(k) = \frac{\sum_{(i,j) \in T_k(G)} w_{ij}}{\sum_{(i,j) \in T_k(G)} c_{ij}}.$$

In this way, the choice of k costs as little as possible, and earns as much as possible.

In addition, this algorithm also improves the method of assignment of all the other elements based on the solution of linear programming without integrality constraint (see Algorithm 5). It also involves comparing of a type of cost-earning ratios of placing the element on the left sides or right sides:

$$Ratio(i \in V_L) = \frac{\mathbb{E}[W_k(V) | V_L \cup \{i\}, V_R]}{\mathbb{E}[C_k(V) | V_L \cup \{i\}, V_R]}$$

$$Ratio(i \in V_R) = \frac{\mathbb{E}[W_k(V) | V_L, V_R \cup \{i\}]}{\mathbb{E}[C_k(V) | V_L, V_R \cup \{i\}]}$$

Where

$$\mathbb{E}[W_k(V) | V_L, V_R] = \sum_{i \in V_L} w_{ki} + \sum_{i \in V_R} w_{ik} + \sum_{i \in V \setminus \{k\}} (p_{ik} w_{ki} + p_{ki} w_{ik}) + \mathbb{E}\left[\sum_{(i,j) \in T_k(V)} w_{ij} | V_L, V_R \right]$$

$$\mathbb{E}[C_k(V) | V_L, V_R] = \sum_{i \in V \setminus \{k\}} c_{ik} + \mathbb{E}\left[\sum_{(i,j) \in T_k(V)} c_{ij} | V_L, V_R \right]$$

And

$$\mathbb{E}\left[\sum_{(i,j) \in T_k(V)} w_{ij} | V_L, V_R \right] = \sum_{j \in V_L, i \in V_R} w_{ij} + \sum_{\{i,j\} \subseteq V \setminus \{k\}} (p_{ji} w_{ij} + p_{ij} w_{ji}) + \sum_{j \in V \setminus \{k\}, i \in V_R} p_{jk} w_{ij} + \sum_{i \in V \setminus \{k\}, j \in V_L} p_{ki} w_{ij}$$

$$\mathbb{E}\left[\sum_{(i,j) \in T_k(V)} c_{ij} | V_L, V_R \right] = \sum_{j \in V_L, i \in V_R} c_{ij} + \sum_{\{i,j\} \subseteq V \setminus \{k\}} (p_{ji} c_{ij} + p_{ij} c_{ji}) + \sum_{j \in V \setminus \{k\}, i \in V_R} p_{jk} c_{ij} + \sum_{i \in V \setminus \{k\}, j \in V_L} p_{ki} c_{ij}$$

Algorithm 4: DerandLP-Pivot($G = (V, W, P)$)

```
begin
  if  $V = \emptyset$  then
    | return empty-list
  else
     $V_L \leftarrow \emptyset$ 
     $V_R \leftarrow \emptyset$ 
    Pick  $k \in V$  minimizing  $Pivot(k)$ 
    for all vertices  $i \in V \setminus \{k\}$  do
      if  $Ratio(i \in V_L) \leq Ratio(i \in V_R)$  then
        | Add  $j$  to  $V_L$  (place  $j$  on left side).
      else
        | Add  $j$  to  $V_R$  (place  $j$  on right side).
      end if
    end for
  end if
  Let  $G_L = (V_L, W_L, P_L)$  be directed weighted graph induced by  $V_L$ .
  Let  $G_R = (V_R, W_R, P_R)$  be directed weighted graph induced by  $V_R$ .
  return DerandLP-Pivot( $G_L$ ),  $\{i\}$ , DerandLP-Pivot( $G_R$ )
end
```

Algorithm 4. DerandLP-Pivot

Compared to Ailon et al.'s KwikSort algorithm, the running time of DerandLP-Pivot is approximately a factor of n slower, because the pivot picking method should be implemented in $O(n^3)$ time (Van Zuylen et al., 2009).

3.4 Methods

3.4.1 Consistent-Pivot algorithm

Here we propose a new pivot algorithm, called Consistent-Pivot. It is based on a novel method of pivot picking and assignment of all the other elements. We think that this algorithm is more suitable for the transitive property of the data of ranking aggregation problem.

In this part, we introduce this algorithm for rankings with ties. Besides the two positional relationships for two elements ($i \triangleleft j$, i is before j ; $i \triangleright j$, i is after j), rankings with ties allow elements in a same level ($i \triangleq j$). In addition, there are three types of weight between two elements, w_{ij} (for i is before j), w_{ji} (for i is after j) and $w_{i\triangleq j}$ (i is the same as j). For ranking aggregation problem, we usually want to choose the positional relationship with highest weight. We define the earning of this kind of choosing as:

$$earning(i, j) = \max(w_{ij}, w_{ji}, w_{i\triangleq j})$$

And accordingly, the cost of this kind of choosing is

$$cost(i, j) = \begin{cases} w_{ji} + w_{i\triangleq j}, & (\text{if } i \triangleleft j) \\ w_{ij} + w_{i\triangleq j}, & (\text{if } i \triangleright j) \\ w_{ij} + w_{ji}, & (\text{if } i \triangleq j) \end{cases}$$

This is the minimum cost for every two elements without taking the relationships with the other elements into account. This value reflects the consistency of the positional relationship between the two elements in the rankings. The smaller the value is, the more agreement for the two elements in the set rankings shows. If $cost(i, j) = 0$, it means that the relationships for the two elements in all the rankings are all the same, without disagreement.

In what follows, we define a consistent score for element i as the sum of the costs between the element and all the other elements:

$$Consistent(i) = \sum_{j \in V \setminus \{i\}} cost(i, j)$$

This score reflect the positional certainty of the element in the rankings. The element with smaller consistent score is more stable. As a well-known landmark in a city for the other buildings, the positional relationships are clear, the element with the smallest consistent score could also be a marker to position all the other elements.

With the intuition above, we propose that the element with the smallest consistent score should be picked as the pivot.

For example, here are four rankings of 15 elements:

$$\begin{aligned} r_1 &= [\{7\}, \{3, 2\}, \{31, 41, 4, 5, 1\}, \{8\}, \{27, 43\}, \{42\}, \{40\}, \{6\}, \{17\}]; \\ r_2 &= [\{7\}, \{31, 41, 4, 5, 1, 3, 2\}, \{8\}, \{6, 17\}, \{27, 40, 42, 43\}]; \\ r_3 &= [\{7\}, \{31, 41, 4, 5, 1, 2\}, \{3\}, \{27\}, \{8\}, \{42, 6, 43\}, \{40\}, \{17\}]; \\ r_4 &= [\{7\}, \{3, 2\}, \{31, 41, 4, 5, 1\}, \{8\}, \{6\}, \{17, 27, 40, 43\}, \{42\}]. \end{aligned}$$

In the first recursive cycle, element 7 is picked as the pivot ($Consistent(7) = 0$). It is worth noting that in the second recursive cycle, element 8 is picked as the pivot ($Consistent(8) = 1$). Based on the element 8, all the other elements can be easily assigned into the two sides. And in fact, the two groups of elements beside the element 8 really have little interaction between groups, but have complex positional relationship in the groups.

Continuing to use the principle, we assign all the other elements not randomly but in an order of the consistent score from small to large. As for the method of assignment of all the other elements, we do not directly use the positional relationship between the element and the pivot, instead of using a cost function that the position with the smallest cost is chosen (see Algorithm 5).

Algorithm 5: Consistent-Pivot(V, W, X)

```

begin
  if  $V = \emptyset$  then
    return empty-list
  else
     $V_L \leftarrow \emptyset$ 
     $V_S \leftarrow \emptyset$ 
     $V_R \leftarrow \emptyset$ 
    Sort elements  $i$  in  $V$  by the  $Consistent(i)$  value
    Pick  $k \in V$  with the minimum  $Consistent(k)$  score
    for  $i \in V \setminus \{k\}$  (in the order of  $Consistent(i)$  from small to large)
    do
      if  $Cost(i|same) \leq Cost(i|before)$  and
          $Cost(i|same) \leq Cost(i|after)$  then
        Add  $i$  to  $V_S$  (place  $i$  in the same set).
      else if  $Cost(i|before) \leq Cost(i|after)$  then
        Add  $i$  to  $V_L$  (place  $i$  on the left side).
      else
        Add  $i$  to  $V_R$  (place  $i$  on the right side).
      end if
    end for
  end if
  Let  $G_L = (V_L, W_L, X_L)$  be directed weighted graph induced by  $V_L$ .
  Let  $G_R = (V_R, W_R, X_R)$  be directed weighted graph induced by  $V_R$ .
  return Consistent-Pivot( $G_L$ ),  $\{V_S\}$ , Consistent-Pivot( $G_R$ )
end

```

Algorithm 5. Consistent-Pivot

For a given pivot k , the costs of element i to be placed before, after or the same as the pivot are defined as:

$$\begin{aligned}
 Cost(i|before) = & \sum_{j \in V_L} cost(i, j) + \sum_{j \in V_S} (w_{ji} + w_{i\hat{=}j}) + \sum_{j \in V_R} (w_{ji} + w_{i\hat{=}j}) + \\
 & \sum_{j \in V \setminus \{i\}} \min(cost(i, j)|_{x_{jk}=1}, (w_{ji} + w_{i\hat{=}j})|_{x_{j\hat{=}k}=1}, (w_{ji} + w_{i\hat{=}j})|_{x_{kj}=1});
 \end{aligned}$$

$$\begin{aligned}
 Cost(i|same) = & \sum_{j \in V_L} (w_{ij} + w_{i\hat{=}j}) + \sum_{j \in V_S} (w_{ji} + w_{ij}) + \sum_{j \in V_R} (w_{ji} + w_{i\hat{=}j}) + \\
 & \sum_{j \in V \setminus \{i\}} \min((w_{ij} + w_{i\hat{=}j})|_{x_{jk}=1}, (w_{ji} + w_{ij})|_{x_{j\hat{=}k}=1}, (w_{ji} + w_{i\hat{=}j})|_{x_{kj}=1});
 \end{aligned}$$

$$\begin{aligned}
 Cost(i|after) = & \sum_{j \in V_L} (w_{ij} + w_{i\hat{=}j}) + \sum_{j \in V_S} (w_{ij} + w_{i\hat{=}j}) + \sum_{j \in V_R} cost(i, j) + \\
 & \sum_{j \in V \setminus \{i\}} \min((w_{ij} + w_{i\hat{=}j})|_{x_{jk}=1}, (w_{ij} + w_{i\hat{=}j})|_{x_{j\hat{=}k}=1}, cost(i, j)|_{x_{kj}=1}).
 \end{aligned}$$

Where $x_{jk}=1$, $x_{kj}=1$ and $x_{j\hat{=}k}=1$ are the best positional result for the element in the unassigned set V and the pivot k . Sometimes, there are two or three best

positional relationships between the element and pivot. In this situation, the cost function should take the minimum value among them.

Both the weight table (W) and best positional relationships table (X) between any two elements can be simultaneously calculated in a time of $O(n^2m)$. The processes of sorting of the elements, picking a pivot and assignment of all the others are much quicker. So the time complexity of this algorithm is $O(n^2m)$, the same as KwikSort, and faster than DerandLP-Pivot.

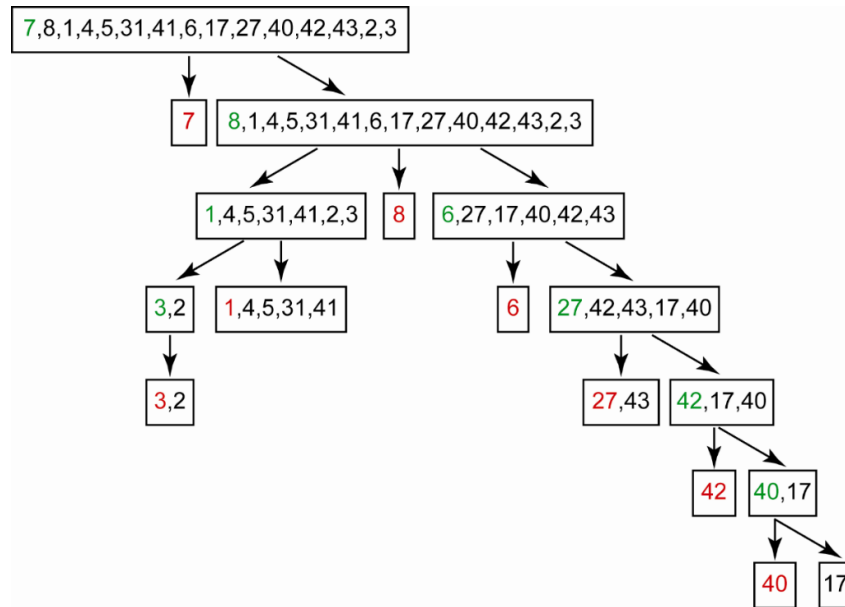


Figure 3.4.1. A tree structure of implementation of the Consistent-Pivot algorithm on the example. The elements are all sorted with the green one in the front which is selected as the pivot (in red) in the next recursive cycle.

The algorithm is implemented in a ternary tree structure. Figure 3.4.1 shows the structure of the result of the real example given above in this section.

3.4.2 Experiments on the algorithms

In the work of Cohen-Boulakia and colleagues, the BioConsert algorithm performs much better than Fagin et al.'s algorithm and the two pivot algorithms of Ailon et al. in accuracy (Cohen-Boulakia et al., 2011). In addition, Brancotte et al. shows that the

BioConsert algorithm is the best one in most cases (Brancotte et al., in preparation). So, in this section, we focus on the comparison of the results of the Consistent-Pivot algorithm with all the previous pivot algorithms and the BioConsert algorithm.

The experiments have been conducted on a personal computer with an Intel Core 2 Duo CPU, 2 GB memory and Fedora 11 system. We used the GLPK 4.45 (GNU Linear Programming Kit) package to solve large-scale linear programming problems (Makhorin, 2008). All the Algorithms were coded in C.

3.4.2.1 Experiment Settings

To measure the accuracy of the algorithms, we should set a standard. But without the best aggregation result, it is difficult to value a relative accuracy for different data sets. Based on the definition of consistent score, we propose a strict lower bound (*IdealDis*) of the best Kendall-tau distance between the Kemeny optimal ranking r^* and the set of rankings R :

$$IdealDis = \frac{1}{2} \sum_{i \in V} Consistent(i)$$

$$IdealDis \leq K^{(p)}(r^*, R)$$

Where $\sum_{i \in V} Consistent(i)$ is the sum of the consistent scores of all the elements, which is also twice the sum of the minimum cost for every two elements.

The *IdealDis* can be calculated easily. It is just the Kemeny distance between the Kemeny optimal ranking (r^*) with the sets of rankings (R), if and only if there is no conflict (or directed cycles) between elements:

$$K^{(p)}(r^*, R) = IdealDis$$

Based on the lower bound of the best result, we define a normalized gap function to measure the performance in accuracy:

$$Gap = \frac{K^{(p)}(r_{result}, R) - IdealDis}{IdealDis}$$

It is a relative value to the ideal distance. Clearly, the more the gap is, the less the accuracy shows.

3.4.2.2 Data sets

We firstly test the performance on real biological data (Cohen-Boulakia et al., 2011). It is query results from four ranking methods of rankings for genes known to be possibly associated with some kinds of diseases: Breast cancer, Prostate cancer, Neuroblastoma, Bladder cancer, Retinoblastoma, Attention Deficit Hyperactivity Disorder (ADHD), and Long QT syndrome (LQT) (see Table 3.4.1).

Query	number of elements	<i>IdealDis</i>
ADHD_reduced	15	48
LQT	35	350
Retinoblastoma_reduced	37	653
ADHD	45	670
Bladdercancer_reduced	115	3881
Prostatecancer_reduced	218	26313
Bladdercancer	308	38159
Breastcancer_reduced	386	78892
Retinoblastom	402	75032
Neuroblastoma_reduced	431	56536

Table 3.4.1. The real biological data set. The 10 sets of rankings used in the work of Cohen-Boulakia et al. are all listed. The number of elements and *IdealDis* are shown.

We also did the experiment on the WebSearch dataset, which was widely used in comparison of various algorithms for ranking aggregation (Dwork et al., 2001; Schalekamp and van Zuylen, 2009; Ali et al., 2012). It is extracted from search results of queries for 37 keywords from four search engines.

To systematically compare the algorithms, we also use a group of synthetic data

sets. We generated dataset of $m=4$, $n \in \{4 \dots 20\}$ and $n \in [20; 100]$ stepping 10 by 10 and then $n \in [200; 1000]$ stepping 100. We generate 500 datasets for each n , which gives a total of 15000 datasets. They were produced by putting n elements randomly into n buckets independently, and then sorting them by the bucket order.

3.5 Results

3.5.1 Results on real biological data

Query	<i>IdealDis</i>	CP	BC	KS	LK	DLP
ADHD_reduced	48	48	48	55	48	48
LQT	350	352	352	392	352	352
Retinoblastoma_reduced	653	653	653	653	653	653
ADHD	670	682	682	747	682	682
Bladdercancer_reduced	3881	3881	3881	3899	-	-
Prostatecancer_reduced	26313	26388	26386	27676	-	-
Bladdercancer	38159	38159	38159	38245	-	-
Breastcancer_reduced	78892	79023	79057	80089	-	-
Retinoblastom	75032	75456	75073	75111	-	-
Neuroblastoma_reduced	56536	56859	57192	58709	-	-

Table 3.5.1. Results on real biological data with ($p = 1$). “CP” stands for the Consistent-Pivot algorithm; “BC” stands for BioConsert; “KS” stands for KwikSort; “LK” stands for LP-KwikSort; “DLP” stands for DerandLP-Pivot.

As shown in Table 3.5.1, The Consistent-Pivot algorithm performs as well as the BioConsert algorithm, with two results better than the BioConsert algorithm (in red), and two worse results (in blue). As for the three previous pivot algorithms, the KwikSort algorithm is fast, but it is mostly worse than the Consistent-Pivot algorithm in accuracy; In another way, both the LP-KwikSort algorithm and the DerandLP-Pivot algorithm cannot finish running all the rest 6 datasets ($n > 100$) in one hour, so we stopped the programs and cannot get the results.

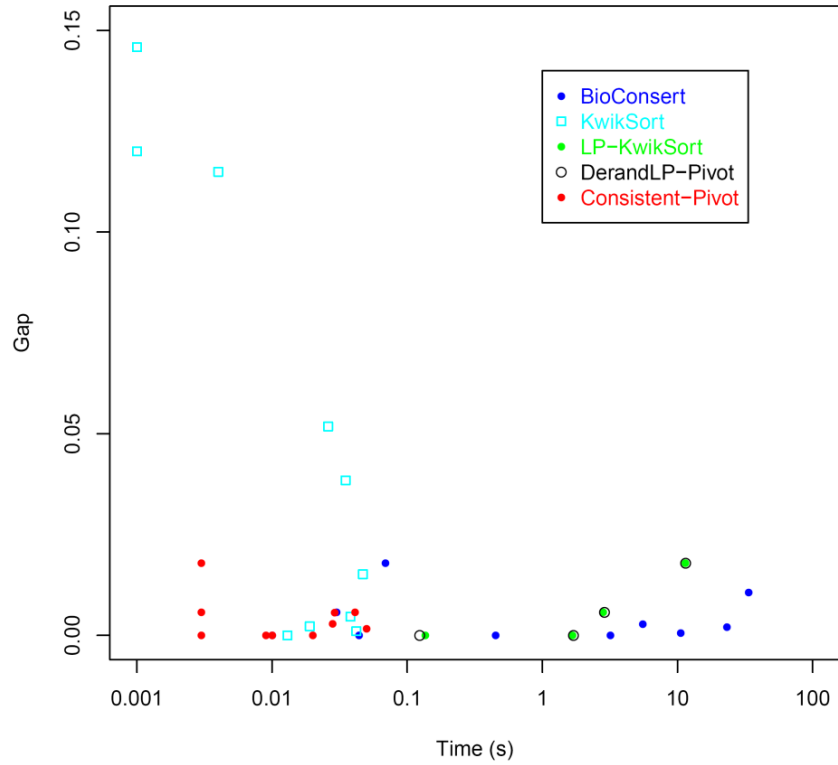


Figure 3.5.1. Gap and running time on real biological data with ($p = 1$).

The normalized gap and running time are also shown in the Figure 3.5.1. Clearly, with the similar performance in accuracy, the running time of the Consistent-Pivot algorithm is much less than the BioConsert algorithm. The result is nearly the same for $p = 0.5$, which gives a less weight of disagreement for two elements that are in the same bucket in one ranking and in different buckets in another ranking (see Figure 3.5.2).

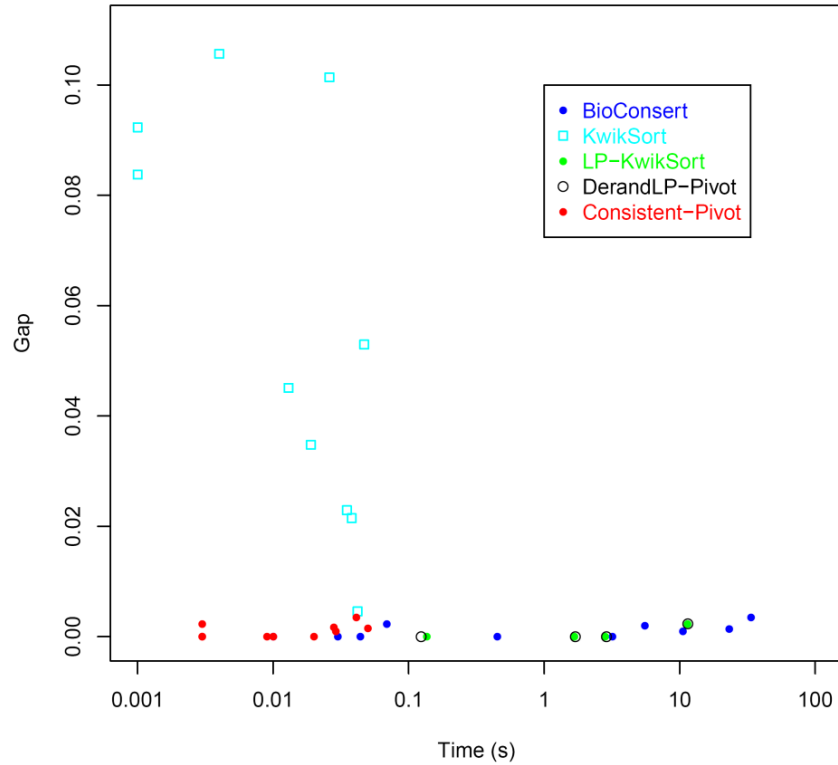


Figure 3.5.2. Results of gap and running time on real biological data with ($p = 0.5$)

3.5.2 Results on WebSearch data

To value the performance of the two pivot algorithms based on linear programming, we firstly generate a dataset with less elements for all the 37 queries. The average number of elements per query is 36.2, with a standard deviation of 4.4 ($n = 36.2 \pm 4.4$).

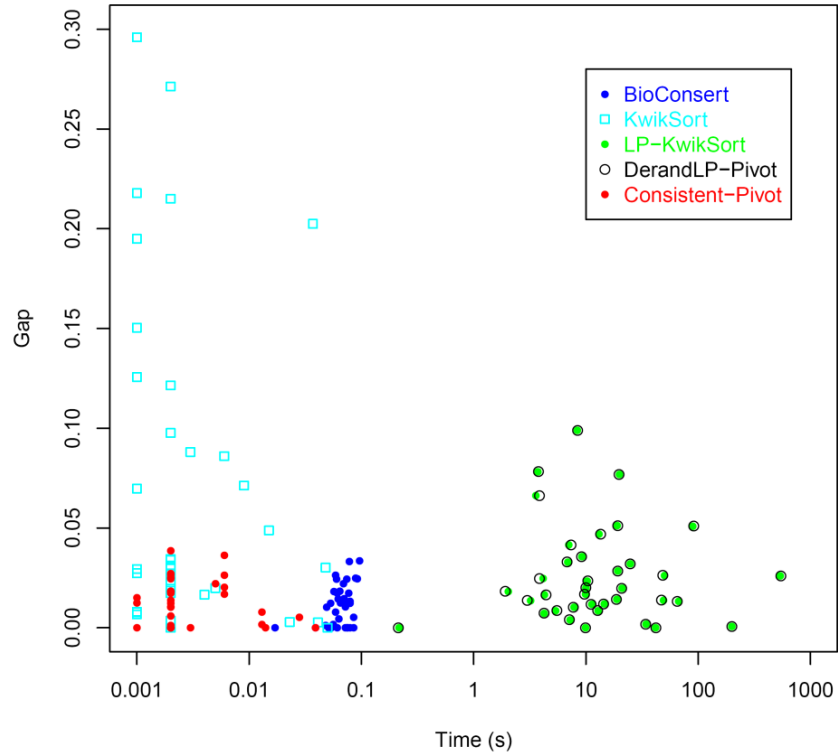


Figure 3.5.3. Results of gap and running time on the Web Search data with less elements ($n = 36.2 \pm 4.4$).

As shown in the Figure 3.5.3, the KwikSort algorithm is fast, with bigger gaps than the other algorithms. The LP-KwikSort and DerandLP-Pivot algorithms are very similar in accuracy and running time. It mainly because that both the result and running time of them largely depend on the solving of the linear programming problem. They are better than the KwikSort algorithm in accuracy, but much slower than all the other algorithms, mainly because of the solving of the linear programming problem. The Consistent-Pivot algorithm perform as well as the BioConsert algorithm in accuracy, but it is faster in running time.

The conclusions above are the same for a dataset with more elements (see Figure 3.5.4). The average number of results per query (n) is 73, with a standard deviation of 12.6. The two pivot algorithms based on LP are too slow to finish running out a result for this dataset.

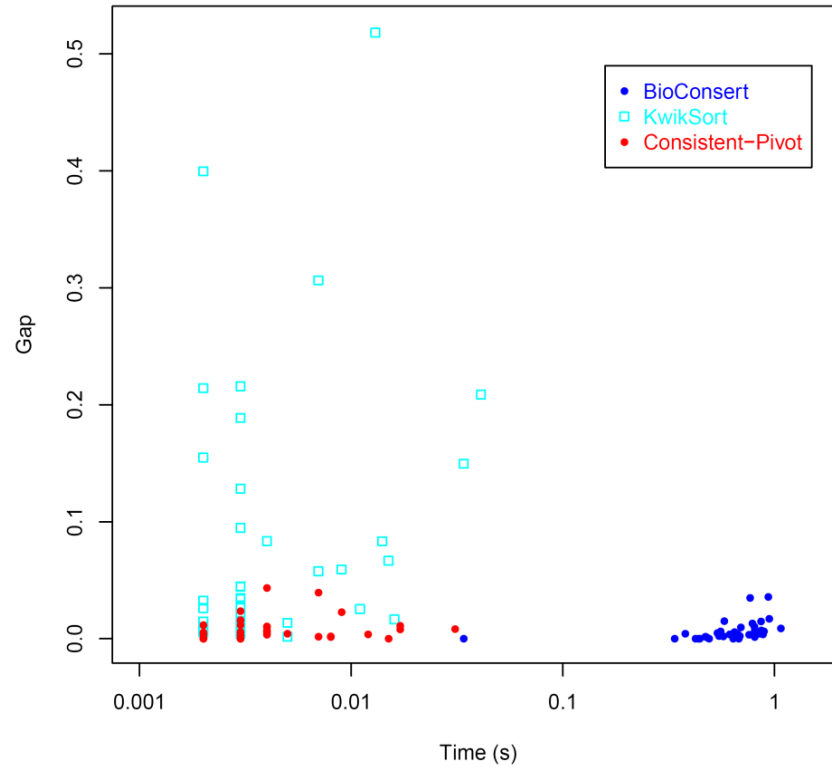


Figure 3.5.4. Results of gap and running time on the Web Search data with more elements ($n = 73 \pm 12.6$).

3.5.3 Results on synthetic data

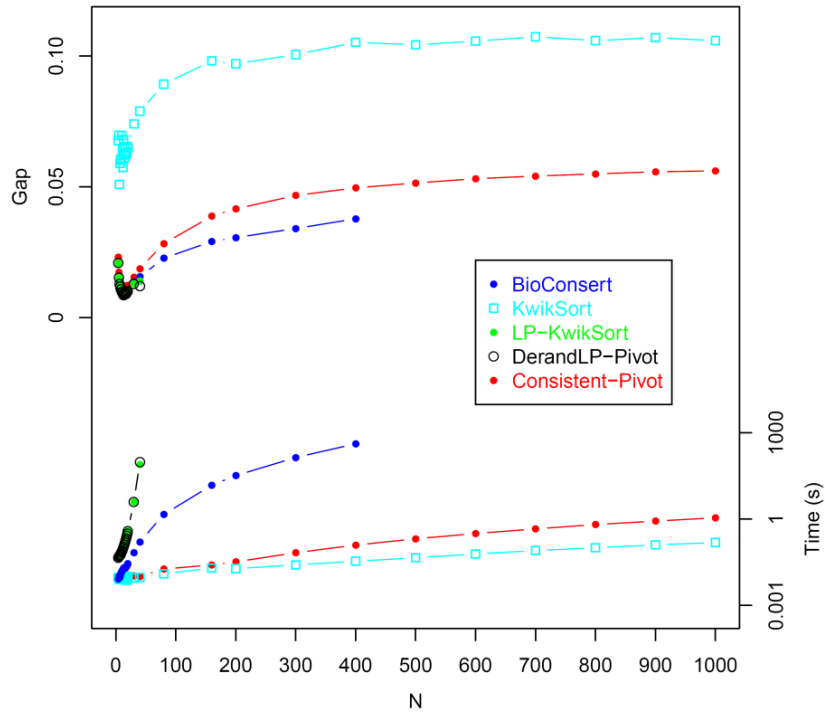


Figure 3.5.5. Result of gap and running time on the synthetic data.

As shown in Figure 3.5.5, the running time of the LP-KwikSort, DerandLP-Pivot and BioConsert algorithm grows rapidly. So we just run the two pivot algorithm based on LP for datasets with $n \leq 40$, and run the BioConsert algorithm for datasets with $n \leq 400$. Comparatively, the Consistent-Pivot and KwikSort algorithm are much faster, and even for $n=1000$, they could finish running in 1 second.

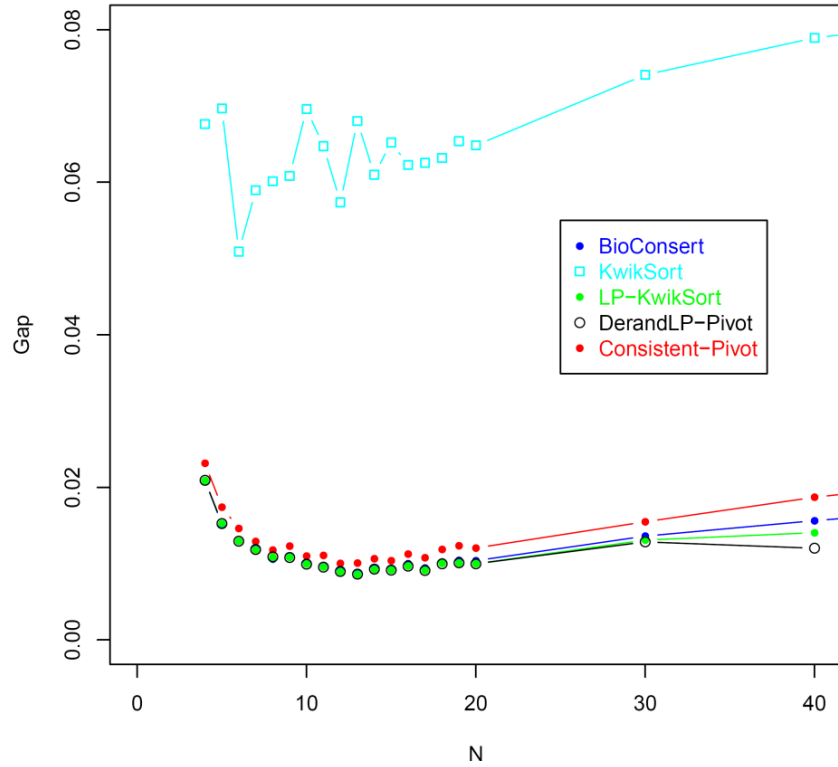


Figure 3.5.6. Enlarged figure of the result of gap on the synthetic data for the number of elements range from 4 to 40.

As for the accuracy, the DerandLP-Pivot algorithm perform best for the synthetic data with elements from 4 to 40 (see the enlarged figure in Figure 3.5.6), followed by the LP-KwikSort algorithm. The KwikSort algorithm is much worse than all the other algorithms.

It is worth noting that the BioConsert algorithms perform significantly better than the Consistent-Pivot algorithm for this synthetic data, which is not the same as the result from both the real data. However the Consistent-Pivot algorithm perform not too bad, with less than 6% relative distance to the *IdealDis* even for datasets $n=1000$.

We think it is mainly because of the synthetic datasets which are produced randomly without agreement information between the four rankings. It is not the same as the real data that have much transitive property in the rankings.

3.6 Discussion

In summary, the Consistent-Pivot algorithm is an efficient algorithm for real data both in accuracy and running time. It is much faster than the BioConsert, LP-KwikSort, DerandLP-Pivot algorithms, and performs almost as well as the BioConsert for real data.

However, there is still a lot of work to do for this project. The experiments on the algorithms are not sufficient. We could test them systematically on more real data and synthetic data, to study how the agreement in rankings affects the performance of the Consistent-Pivot algorithm. And we would try to find an improvement of the Consistent-Pivot algorithm to deal with the datasets with not so much agreement in rankings.

All the algorithms have advantages with shortcomings. The thinking of combination of several algorithms to get better performance is a good idea (Schalekamp and van Zuylen, 2009). The Consistent-Pivot followed by the better search of the BioConsert algorithm in a local range, maybe a good combined algorithm for the ranking aggregation problem.

Reference

1. Crick, F. (1970). Central dogma of molecular biology. *Nature*, 227(5258), 561-563.
2. Roy, S. W., & Gilbert, W. (2006). The evolution of spliceosomal introns: patterns, puzzles and progress. *Nature Reviews Genetics*, 7(3), 211-221.
3. Dietz, H. C., & Kendzior, R. J. (1994). Maintenance of an open reading frame as an additional level of scrutiny during splice site selection. *Nature genetics*, 8(2), 183-188.
4. Will, C. L., & Lührmann, R. (2011). Spliceosome structure and function. *Cold Spring Harbor perspectives in biology*, 3(7), a003707.
5. Yeo, G., & Burge, C. B. (2004). Maximum entropy modeling of short sequence motifs with applications to RNA splicing signals. *Journal of Computational Biology*, 11(2-3), 377-394.
6. Desmet, F. O., Hamroun, D., Lalande, M., Collod-Bérout, G., Claustres, M., & Bérout, C. (2009). Human Splicing Finder: an online bioinformatics tool to predict splicing signals. *Nucleic acids research*, 37(9), e67-e67.
7. Pertea, M., Lin, X., & Salzberg, S. L. (2001). GeneSplicer: a new computational method for splice site prediction. *Nucleic acids research*, 29(5), 1185-1190.
8. Brunak, S., Engelbrecht, J., & Knudsen, S. (1991). Prediction of human mRNA donor and acceptor sites from the DNA sequence. *Journal of molecular biology*, 220(1), 49-65.
9. Reese, M. G., Eeckman, F. H., Kulp, D., & Haussler, D. (1997). Improved splice site detection in Genie. *Journal of computational biology*, 4(3), 311-323.
10. Levine, A., & Durbin, R. (2001). A computational scan for U12-dependent introns in the human genome sequence. *Nucleic acids research*, 29(19), 4006-4013.
11. Alekseyenko, A. V., Kim, N., & Lee, C. J. (2007). Global analysis of exon creation versus loss and the role of alternative splicing in 17 vertebrate genomes. *Rna*, 13(5), 661-670.
12. Sugnet, C. W., Kent, W. J., Ares, M., & Haussler, D. (2004). Transcriptome and genome conservation of alternative splicing events in humans and mice. *In Pacific Symposium on*

Biocomputing (Vol. 9, pp. 66-77).

13. Kim, E., Goren, A., & Ast, G. (2008). Alternative splicing: current perspectives. *Bioessays*, 30(1), 38-47.
14. Black, D. L. (2003). Mechanisms of alternative pre-messenger RNA splicing. *Annual review of biochemistry*, 72(1), 291-336.
15. Keren, H., Lev-Maor, G., & Ast, G. (2010). Alternative splicing and evolution: diversification, exon definition and function. *Nature Reviews Genetics*, 11(5), 345-355.
16. Nilsen, T. W., & Graveley, B. R. (2010). Expansion of the eukaryotic proteome by alternative splicing. *Nature*, 463(7280), 457-463.
17. Pan, Q., Shai, O., Lee, L. J., Frey, B. J., & Blencowe, B. J. (2008). Deep surveying of alternative splicing complexity in the human transcriptome by high-throughput sequencing. *Nature genetics*, 40(12), 1413-1415.
18. Chen, M., & Manley, J. L. (2009). Mechanisms of alternative splicing regulation: insights from molecular and genomics approaches. *Nature Reviews Molecular Cell Biology*, 10(11), 741-754.
19. Lim, K. H., Ferraris, L., Filloux, M. E., Raphael, B. J., & Fairbrother, W. G. (2011). Using positional distribution to identify splicing elements and predict pre-mRNA processing defects in human genes. *Proceedings of the National Academy of Sciences*, 108(27), 11093-11098.
20. Irimia, M., & Blencowe, B. J. (2012). Alternative splicing: decoding an expansive regulatory layer. *Current opinion in cell biology*, 24(3), 323-332.
21. Matlin, A. J., Clark, F., & Smith, C. W. (2005). Understanding alternative splicing: towards a cellular code. *Nature Reviews Molecular Cell Biology*, 6(5), 386-398.
22. Wang, Z., & Burge, C. B. (2008). Splicing regulation: from a parts list of regulatory elements to an integrated splicing code. *Rna*, 14(5), 802-813.
23. Warf, M. B., & Berglund, J. A. (2010). Role of RNA structure in regulating pre-mRNA splicing. *Trends in biochemical sciences*, 35(3), 169-178.
24. Reid, D. C., Chang, B. L., Gunderson, S. I., Alpert, L., Thompson, W. A., & Fairbrother, W. G.

- (2009). Next-generation SELEX identifies sequence and structural determinants of splicing factor binding in human pre-mRNA sequence. *RNA*, 15(12), 2385-2397.
25. David, C. J., & Manley, J. L. (2008). The search for alternative splicing regulators: new approaches offer a path to a splicing code. *Genes & development*, 22(3), 279-285.
 26. Barash, Y., Calarco, J. A., Gao, W., Pan, Q., Wang, X., Shai, O., ... & Frey, B. J. (2010). Deciphering the splicing code. *Nature*, 465(7294), 53-59.
 27. López-Bigas, N., Audit, B., Ouzounis, C., Parra, G., & Guigó, R. (2005). Are splicing mutations the most frequent cause of hereditary disease?. *FEBS letters*, 579(9), 1900-1903.
 28. Ward, A. J., & Cooper, T. A. (2010). The pathobiology of splicing. *The Journal of pathology*, 220(2), 152-163.
 29. Fackenthal, J. D., & Godley, L. A. (2008). Aberrant RNA splicing and its functional consequences in cancer cells. *Disease models & mechanisms*, 1(1), 37-42.
 30. Yoshida, K., Sanada, M., Shiraishi, Y., Nowak, D., Nagata, Y., Yamamoto, R., ... & Ogawa, S. (2011). Frequent pathway mutations of splicing machinery in myelodysplasia. *Nature*, 478(7367), 64-69.
 31. Wahl, M. C., Will, C. L., & Lührmann, R. (2009). The spliceosome: design principles of a dynamic RNP machine. *Cell*, 136(4), 701-718.
 32. Zamore, P. D., Patton, J. G., & Green, M. R. (1992). Cloning and domain structure of the mammalian splicing factor U2AF. *Nature*, 355(6361), 609-614.
 33. Zhang, M., Zamore, P. D., Carmo-Fonseca, M., Lamond, A. I., & Green, M. R. (1992). Cloning and intracellular localization of the U2 small nuclear ribonucleoprotein auxiliary factor small subunit. *Proceedings of the National Academy of Sciences*, 89(18), 8769-8773.
 34. Singh, R., Valcarcel, J., & Green, M. R. (1995). Distinct binding specificities and functions of higher eukaryotic polypyrimidine tract-binding proteins. *Science*, 268(5214), 1173-1176.
 35. Valcárcel, J., Gaur, R. K., Singh, R., & Green, M. R. (1996). Interaction of U2AF65 RS region with pre-mRNA of branch point and promotion base pairing with U2

- snRNA. *Science*, 273(5282), 1706-1709.
36. Abovich, N., Liao, X. C., & Rosbash, M. (1994). The yeast MUD2 protein: an interaction with PRP11 defines a bridge between commitment complexes and U2 snRNP addition. *Genes & development*, 8(7), 843-854.
 37. Abovich, N., & Rosbash, M. (1997). Cross-intron bridging interactions in the yeast commitment complex are conserved in mammals. *Cell*, 89(3), 403-412.
 38. Sridharan, V., Heimiller, J., & Singh, R. (2011). Genomic mRNA profiling reveals compensatory mechanisms for the requirement of the essential splicing factor U2AF. *Molecular and cellular biology*, 31(4), 652-661.
 39. Sridharan, V., & Singh, R. (2007). A conditional role of U2AF in splicing of introns with unconventional polypyrimidine tracts. *Molecular and cellular biology*, 27(20), 7334-7344.
 40. MacMillan, A. M., McCaw, P. S., Crispino, J. D., & Sharp, P. A. (1997). SC35-mediated reconstitution of splicing in U2AF-depleted nuclear extract. *Proceedings of the National Academy of Sciences*, 94(1), 133-136.
 41. Imai, H., Chan, E. K., Kiyosawa, K., Fu, X. D., & Tan, E. M. (1993). Novel nuclear autoantigen with splicing factor motifs identified with antibody from hepatocellular carcinoma. *Journal of Clinical Investigation*, 92(5), 2419.
 42. Hastings, M. L., Allemand, E., Duelli, D. M., Myers, M. P., & Krainer, A. R. (2007). Control of pre-mRNA splicing by the general splicing factors PUF60 and U2AF65. *PLoS One*, 2(6), e538.
 43. Page-McCaw, P. S., Amonlirdviman, K. E. V. I. N., & Sharp, P. A. (1999). PUF60: a novel U2AF65-related splicing activity. *Rna*, 5(12), 1548-1560.
 44. Tronchre, H., Wang, J., & Fu, X. D. (1997). A protein related to splicing factor U2AF35 that interacts with U2AF65 and SR proteins in splicing of pre-mRNA. *Nature*, 388(6640), 397-400.
 45. Shepard, J., Reick, M., Olson, S., & Graveley, B. R. (2002). Characterization of U2AF6, a splicing factor related to U2AF35. *Molecular and cellular biology*, 22(1), 221-230.

46. Mollet, I., Barbosa - Morais, N. L., Andrade, J., & Carmo - Fonseca, M. (2006). Diversity of human U2AF splicing factors. *FEBS Journal*, 273(21), 4807-4816.
47. Zarnack, K., König, J., Tajnik, M., Martincorena, I., Eustermann, S., Stévant, I., ... & Ule, J. (2013). Direct competition between hnrnp c and u2af65 protects the transcriptome from the exonization of Alu elements. *Cell*, 152(3), 453-466.
48. Reed, R. (1989). The organization of 3'splice-site sequences in mammalian introns. *Genes & development*, 3(12b), 2113-2123.
49. Zamore, P. D., & Green, M. R. (1991). Biochemical characterization of U2 snRNP auxiliary factor: an essential pre-mRNA splicing factor with a novel intranuclear distribution. *The EMBO journal*, 10(1), 207.
50. Wu, S., Romfo, C. M., Nilsen, T. W., & Green, M. R. (1999). Functional recognition of the 3' splice site AG by the splicing factor U2AF35. *Nature*, 402(6763), 832-835.
51. Merendino, L., Guth, S., Bilbao, D., Martínez, C., & Valcárcel, J. (1999). Inhibition of msl-2 splicing by Sex-lethal reveals interaction between U2AF35 and the 3' splice site AG. *Nature*, 402(6763), 838-841.
52. Pacheco, T. R., Coelho, M. B., Desterro, J. M., Mollet, I., & Carmo-Fonseca, M. (2006). In vivo requirement of the small subunit of U2AF for recognition of a weak 3' splice site. *Molecular and cellular biology*, 26(21), 8183-8190.
53. Soares, L. M. M., Zanier, K., Mackereth, C., Sattler, M., & Valcárcel, J. (2006). Intron removal requires proofreading of U2AF/3' splice site recognition by DEK. *Science*, 312(5782), 1961-1965.
54. Tavanez, J. P., Madl, T., Kooshapur, H., Sattler, M., & Valcárcel, J. (2012). hnRNP A1 proofreads 3' splice site recognition by U2AF. *Molecular cell*, 45(3), 314-329.
55. Park, J. W., Parisky, K., Celotto, A. M., Reenan, R. A., & Graveley, B. R. (2004). Identification of alternative splicing regulators by RNA interference in *Drosophila*. *Proceedings of the National Academy of Sciences of the United States of America*, 101(45), 15974-15979.

56. Moore, M. J., Wang, Q., Kennedy, C. J., & Silver, P. A. (2010). An alternative splicing network links cell-cycle control to apoptosis. *Cell*, 142(4), 625-636.
57. Le Guiner, C., Lejeune, F., Galiana, D., Kister, L., Breathnach, R., Stévenin, J., & Del Gatto-Konczak, F. (2001). TIA-1 and TIAR activate splicing of alternative exons with weak 5' splice sites followed by a U-rich stretch on their own pre-mRNAs. *Journal of Biological Chemistry*, 276(44), 40638-40646.
58. Xue, Y., Zhou, Y., Wu, T., Zhu, T., Ji, X., Kwon, Y. S., ... & Zhang, Y. (2009). Genome-wide analysis of PTB-RNA interactions reveals a strategy used by the general splicing repressor to modulate exon inclusion or skipping. *Molecular cell*, 36(6), 996-1006.
59. Wang, Z., Kayikci, M., Briese, M., Zarnack, K., Luscombe, N. M., Rot, G., ... & Ule, J. (2010). iCLIP predicts the dual splicing effects of TIA-RNA interactions. *PLoS biology*, 8(10), e1000530.
60. Lim, K. H., Ferraris, L., Filloux, M. E., Raphael, B. J., & Fairbrother, W. G. (2011). Using positional distribution to identify splicing elements and predict pre-mRNA processing defects in human genes. *Proceedings of the National Academy of Sciences*, 108(27), 11093-11098.
61. Yoshida, K., Sanada, M., Shiraishi, Y., Nowak, D., Nagata, Y., Yamamoto, R., ... & Ogawa, S. (2011). Frequent pathway mutations of splicing machinery in myelodysplasia. *Nature*, 478(7367), 64-69.
62. Thol, F., Kade, S., Schlarman, C., Löffeld, P., Morgan, M., Krauter, J., ... & Heuser, M. (2012). Frequency and prognostic impact of mutations in SRSF2, U2AF1, and ZRSR2 in patients with myelodysplastic syndromes. *Blood*, 119(15), 3578-3584.
63. Cazzola, M., Della Porta, M. G., & Malcovati, L. (2013). The genetic basis of myelodysplasia and its clinical relevance. *Blood*, 122(25), 4021-4034.
64. Danckwardt, S., Kaufmann, I., Gentzel, M., Foerstner, K. U., Gantzer, A. S., Gehring, N. H., ... & Kulozik, A. E. (2007). Splicing factors stimulate polyadenylation via USEs at non-canonical 3' end formation signals. *The EMBO journal*, 26(11), 2658-2669.
65. Zhang, C., & Darnell, R. B. (2011). Mapping in vivo protein-RNA interactions at single-

- nucleotide resolution from HITS-CLIP data. *Nature biotechnology*, 29(7), 607-614.
66. Yeo, G., & Burge, C. B. (2004). Maximum entropy modeling of short sequence motifs with applications to RNA splicing signals. *Journal of Computational Biology*, 11(2-3), 377-394.
67. Murray, J. I., Voelker, R. B., Henscheid, K. L., Warf, M. B., & Berglund, J. A. (2008). Identification of motifs that function in the splicing of non-canonical introns. *Genome Biol*, 9(6), R97.
68. Huelga, S. C., Vu, A. Q., Arnold, J. D., Liang, T. Y., Liu, P. P., Yan, B. Y., ... & Yeo, G. W. (2012). Integrative genome-wide analysis reveals cooperative regulation of alternative splicing by hnRNP proteins. *Cell reports*, 1(2), 167-178.
69. Aguilera, A. (2005). Cotranscriptional mRNP assembly: from the DNA to the nuclear pore. *Current opinion in cell biology*, 17(3), 242-250.
70. Gama-Carvalho, M., Barbosa-Morais, N. L., Brodsky, A. S., Silver, P. A., & Carmo-Fonseca, M. (2006). Genome-wide identification of functionally distinct subsets of cellular mRNAs associated with two nucleocytoplasmic-shuttling mammalian splicing factors. *Genome biology*, 7(11), R113.
71. Xiao, R., Tang, P., Yang, B., Huang, J., Zhou, Y., Shao, C., ... & Fu, X. D. (2012). Nuclear matrix factor hnRNP U/SAF-A exerts a global control of alternative splicing by regulating U2 snRNP maturation. *Molecular cell*, 45(5), 656-668.
72. Zhou, Z., Qiu, J., Liu, W., Zhou, Y., Plocinik, R. M., Li, H., ... & Fu, X. D. (2012). The Akt-SRPK-SR axis constitutes a major pathway in transducing EGF signaling to regulate alternative splicing in the nucleus. *Molecular cell*, 47(3), 422-433.
73. Wei, W. J., Mu, S. R., Heiner, M., Fu, X., Cao, L. J., Gong, X. F., ... & Hui, J. (2012). YB-1 binds to CAUC motifs and stimulates exon inclusion by enhancing the recruitment of U2AF to weak polypyrimidine tracts. *Nucleic acids research*, 40(17), 8622-8636.
74. Shen, H., Zheng, X., Luecke, S., & Green, M. R. (2010). The U2AF35-related protein Urp contacts the 3' splice site to promote U12-type intron splicing and the second step of U2-type intron splicing. *Genes & development*, 24(21), 2389-2394.

75. Han, J., Ding, J. H., Byeon, C. W., Kim, J. H., Hertel, K. J., Jeong, S., & Fu, X. D. (2011). SR proteins induce alternative exon skipping through their activities on the flanking constitutive exons. *Molecular and cellular biology*, 31(4), 793-802.
76. Han, J., Xiong, J., Wang, D., & Fu, X. D. (2011). Pre-mRNA splicing: where and when in the nucleus. *Trends in cell biology*, 21(6), 336-343.
77. Przychodzen, B., Jerez, A., Guinta, K., Sekeres, M. A., Padgett, R., Maciejewski, J. P., & Makishima, H. (2013). Patterns of missplicing due to somatic U2AF1 mutations in myeloid neoplasms. *Blood*, 122(6), 999-1006.
78. van Helden, J., André, B., & Collado-Vides, J. (1998). Extracting regulatory sites from the upstream region of yeast genes by computational analysis of oligonucleotide frequencies. *Journal of molecular biology*, 281(5), 827-842.
79. Kahvejian, A., Quackenbush, J., & Thompson, J. F. (2008). What would you do if you could sequence everything?. *Nature biotechnology*, 26(10), 1125-1133.
80. Marx, V. (2013). Biology: The big challenges of big data. *Nature*, 498(7453), 255-260.
81. Quiñones-Mateu, M. E., Avila, S., Reyes-teran, G., & Martinez, M. A. (2014). Deep sequencing: Becoming a critical tool in clinical virology. *Journal of Clinical Virology*.
82. Waern, K., Nagalakshmi, U., & Snyder, M. (2011). RNA sequencing. *Yeast Systems Biology* (pp. 125-132). Humana Press.
83. Kodzius, R., Kojima, M., Nishiyori, H., Nakamura, M., Fukuda, S., Tagami, M., ... & Carninci, P. (2006). CAGE: cap analysis of gene expression. *Nature methods*, 3(3), 211-222.
84. Fullwood, M. J., Wei, C. L., Liu, E. T., & Ruan, Y. (2009). Next-generation DNA sequencing of paired-end tags (PET) for transcriptome and genome analyses. *Genome research*, 19(4), 521-532.
85. Chu, C., Qu, K., Zhong, F. L., Artandi, S. E., & Chang, H. Y. (2011). Genomic maps of long noncoding RNA occupancy reveal principles of RNA-chromatin interactions. *Molecular cell*, 44(4), 667-678.

86. Core, L. J., Waterfall, J. J., & Lis, J. T. (2008). Nascent RNA sequencing reveals widespread pausing and divergent initiation at human promoters. *Science*, 322(5909), 1845-1848.
87. Churchman, L. S., & Weissman, J. S. (2011). Nascent transcript sequencing visualizes transcription at nucleotide resolution. *Nature*, 469(7330), 368-373.
88. Ingolia, N. T., Ghaemmaghami, S., Newman, J. R., & Weissman, J. S. (2009). Genome-wide analysis in vivo of translation with nucleotide resolution using ribosome profiling. *Science*, 324(5924), 218-223.
89. Robertson, G., Hirst, M., Bainbridge, M., Bilenky, M., Zhao, Y., Zeng, T., ... & Jones, S. (2007). Genome-wide profiles of STAT1 DNA association using chromatin immunoprecipitation and massively parallel sequencing. *Nature methods*, 4(8), 651-657.
90. Hesselberth, J. R., Chen, X., Zhang, Z., Sabo, P. J., Sandstrom, R., Reynolds, A. P., ... & Stamatoyannopoulos, J. A. (2009). Global mapping of protein-DNA interactions in vivo by digital genomic footprinting. *Nature methods*, 6(4), 283-289.
91. Crawford, G. E., Holt, I. E., Whittle, J., Webb, B. D., Tai, D., Davis, S., ... & Collins, F. S. (2006). Genome-wide mapping of DNase hypersensitive sites using massively parallel signature sequencing (MPSS). *Genome research*, 16(1), 123-131.
92. Giresi, P. G., Kim, J., McDaniell, R. M., Iyer, V. R., & Lieb, J. D. (2007). FAIRE (Formaldehyde-Assisted Isolation of Regulatory Elements) isolates active regulatory elements from human chromatin. *Genome research*, 17(6), 877-885.
93. Wang, Z., Zang, C., Cui, K., Schones, D. E., Barski, A., Peng, W., & Zhao, K. (2009). Genome-wide mapping of HATs and HDACs reveals distinct functions in active and inactive genes. *Cell*, 138(5), 1019-1031.
94. Smith, Z. D., Gu, H., Bock, C., Gnirke, A., & Meissner, A. (2009). High-throughput bisulfite sequencing in mammalian genomes. *Methods*, 48(3), 226-232.
95. Dostie, J., Richmond, T. A., Arnaout, R. A., Selzer, R. R., Lee, W. L., Honan, T. A., ... & Dekker, J. (2006). Chromosome Conformation Capture Carbon Copy (5C): a massively parallel solution for mapping interactions between genomic elements. *Genome research*, 16(10), 1299-1309.

96. Fullwood, M. J., Liu, M. H., Pan, Y. F., Liu, J., Xu, H., Mohamed, Y. B., ... & Ruan, Y. (2009). An oestrogen-receptor-bound human chromatin interactome. *Nature*, 462(7269), 58-64.
97. Soon, W. W., Hariharan, M., & Snyder, M. P. (2013). High - throughput sequencing for biology and medicine. *Molecular systems biology*, 9(1).
98. Cock, P. J., Fields, C. J., Goto, N., Heuer, M. L., & Rice, P. M. (2010). The Sanger FASTQ file format for sequences with quality scores, and the Solexa/Illumina FASTQ variants. *Nucleic acids research*, 38(6), 1767-1771.
99. Li, H., Ruan, J., & Durbin, R. (2008). Mapping short DNA sequencing reads and calling variants using mapping quality scores. *Genome research*, 18(11), 1851-1858.
100. Andrews, S. (2010). FastQC: A quality control tool for high throughput sequence data.
101. Langmead, B., Trapnell, C., Pop, M., & Salzberg, S. L. (2009). Ultrafast and memory-efficient alignment of short DNA sequences to the human genome. *Genome Biol*, 10(3), R25.
102. Li, H., & Durbin, R. (2009). Fast and accurate short read alignment with Burrows–Wheeler transform. *Bioinformatics*, 25(14), 1754-1760.
103. Langmead, B., & Salzberg, S. L. (2012). Fast gapped-read alignment with Bowtie 2. *Nature methods*, 9(4), 357-359.
104. Zhang, C., & Darnell, R. B. (2011). Mapping in vivo protein-RNA interactions at single-nucleotide resolution from HITS-CLIP data. *Nature biotechnology*, 29(7), 607-614.
105. Zhang, Y., Liu, T., Meyer, C. A., Eeckhoute, J., Johnson, D. S., Bernstein, B. E., ... & Liu, X. S. (2008). Model-based analysis of ChIP-Seq (MACS). *Genome Biol*, 9(9), R137.
106. Yeo, G. W., Coufal, N. G., Liang, T. Y., Peng, G. E., Fu, X. D., & Gage, F. H. (2009). An RNA code for the FOX2 splicing regulator revealed by mapping RNA-protein interactions in stem cells. *Nature structural & molecular biology*, 16(2), 130-137.
107. Xue, Y., Zhou, Y., Wu, T., Zhu, T., Ji, X., Kwon, Y. S., ... & Zhang, Y. (2009). Genome-wide analysis of PTB-RNA interactions reveals a strategy used by the general splicing repressor to modulate exon inclusion or skipping. *Molecular cell*, 36(6), 996-1006.

108. Chi, S. W., Zang, J. B., Mele, A., & Darnell, R. B. (2009). Argonaute HITS-CLIP decodes microRNA–mRNA interaction maps. *Nature*, 460(7254), 479-486.
109. Hsu, F., Kent, W. J., Clawson, H., Kuhn, R. M., Diekhans, M., & Haussler, D. (2006). The UCSC known genes. *Bioinformatics*, 22(9), 1036-1046.
110. Pruitt, K. D., Tatusova, T., & Maglott, D. R. (2007). NCBI reference sequences (RefSeq): a curated non-redundant sequence database of genomes, transcripts and proteins. *Nucleic acids research*, 35(suppl 1), D61-D65.
111. Hubbard, T., Barker, D., Birney, E., Cameron, G., Chen, Y., Clark, L., ... & Clamp, M. (2002). The Ensembl genome database project. *Nucleic acids research*, 30(1), 38-41.
112. Harrow, J., Denoeud, F., Frankish, A., Reymond, A., Chen, C. K., Chrast, J., ... & Guigo, R. (2006). GENCODE: producing a reference annotation for ENCODE. *Genome Biol*, 7(Suppl 1), S4.
113. Burge, C., & Karlin, S. (1997). Prediction of complete gene structures in human genomic DNA. *Journal of molecular biology*, 268(1), 78-94.
114. van Helden, J., André, B., & Collado-Vides, J. (1998). Extracting regulatory sites from the upstream region of yeast genes by computational analysis of oligonucleotide frequencies. *Journal of molecular biology*, 281(5), 827-842.
115. Durbin, R. (Ed.). (1998). *Biological sequence analysis: probabilistic models of proteins and nucleic acids*. Cambridge university press.
116. Yeo, G., & Burge, C. B. (2004). Maximum entropy modeling of short sequence motifs with applications to RNA splicing signals. *Journal of Computational Biology*, 11(2-3), 377-394.
117. Barrett, T., Wilhite, S. E., Ledoux, P., Evangelista, C., Kim, I. F., Tomashevsky, M., ... & Soboleva, A. (2013). NCBI GEO: archive for functional genomics data sets—update. *Nucleic acids research*, 41(D1), D991-D995.
118. Metzker, Michael L. "Sequencing technologies—the next generation." *Nature Reviews Genetics* 11.1 (2010): 31-46.

119. Brusic, Vladimir, et al. "Data learning: understanding biological data." Knowledge sharing across biological and medical knowledge based systems: Papers from *the 1998 AAAI Workshop*. 1998.
120. Cohen-Boulakia, Sarah, Alain Denise, and Sylvie Hamel. "Using medians to generate consensus rankings for biological data." *Scientific and Statistical Database Management*. Springer Berlin Heidelberg, 2011.
121. DeConde, Robert P., et al. "Combining results of microarray experiments: a rank aggregation approach." *Statistical Applications in Genetics and Molecular Biology* 5.1 (2006).
122. Gao, Jun, et al. "Comparison of different ranking methods in protein-ligand binding site prediction." *International journal of molecular sciences* 13.7 (2012): 8752-8761.
123. Sengupta, Debarka, et al. "Reformulated Kemeny Optimal Aggregation with Application in Consensus Ranking of microRNA Targets." (2013): 1-1.
124. Dwork, Cynthia, et al. "Rank aggregation methods for the web." *Proceedings of the 10th international conference on World Wide Web*. ACM, 2001.
125. Kendall, Maurice G. "A new measure of rank correlation." *Biometrika* (1938).
126. Fagin, Ronald, Ravi Kumar, and Dandapani Sivakumar. "Efficient similarity search and classification via rank aggregation." *Proceedings of the 2003 ACM SIGMOD international conference on Management of data*. ACM, 2003.
127. Diaconis, P., & Graham, R. L. (1977). Spearman's footrule as a measure of disarray. *Journal of the Royal Statistical Society. Series B (Methodological)*, 262-268.
128. Fagin, Ronald, et al. "Comparing and aggregating rankings with ties." *Proceedings of the twenty-third ACM SIGMOD-SIGACT-SIGART symposium on Principles of database systems*. ACM, 2004.
129. Kemeny, John G., and James Laurie Snell. *Mathematical models in the social sciences*. Vol. 9. Boston: Ginn, 1962.
130. Farah, M., & Vanderpooten, D. (2007, July). An outranking approach for rank aggregation in

- information retrieval. In *Proceedings of the 30th annual international ACM SIGIR conference on Research and development in information retrieval* (pp. 591-598). ACM.
131. Dwork, Cynthia, et al. "System and method for aggregating ranking results from various sources to improve the results of web searching." *U.S. Patent* No. 7,188,106. 6 Mar. 2007.
 132. Conitzer, Vincent, Andrew Davenport, and Jayant Kalagnanam. "Improved bounds for computing Kemeny rankings." *AAAI*. Vol. 6. 2006.
 133. Meila, Marina, et al. "Consensus ranking under the exponential model." *arXiv preprint arXiv:1206.5265* (2012).
 134. Brusica, Vladimir, et al. "Data learning: understanding biological data." Knowledge sharing across biological and medical knowledge based systems: Papers from *the 1998 AAAI Workshop*. 1998.
 135. Risse, Mathias. "Why the count de Borda cannot beat the Marquis de Condorcet." *Social Choice and Welfare* 25.1 (2005): 95-113.
 136. Young, H. Peyton, and Arthur Levenglick. "A consistent extension of Condorcet's election principle." *SIAM Journal on Applied Mathematics* 35.2 (1978): 285-300.
 137. De Grazia, Alfred. "Mathematical derivation of an election system." *Isis* 44.1/2 (1953): 42-51.
 138. Blin, Guillaume et al. "Medians of an odd number of permutations." *Pure Mathematics and Applications* 21, 2 (2011) 161 – 175.
 139. Ailon, Nir. "Aggregation of partial rankings, p-ratings and top-m lists." *Algorithmica* 57.2 (2010): 284-300.
 140. Ailon, Nir, Moses Charikar, and Alantha Newman. "Aggregating inconsistent information: ranking and clustering." *Journal of the ACM (JACM)* 55.5 (2008): 23.
 141. Van Zuylen, Anke, and David P. Williamson. "Deterministic pivoting algorithms for constrained ranking and clustering problems." *Mathematics of Operations Research* 34.3 (2009): 594-620.
 142. Schalekamp, F., & van Zuylen, A. (2009). Rank Aggregation: Together We're Strong.

- In *ALENEX* (pp. 38-51).
143. Qin, T., Geng, X., & Liu, T. Y. (2010). A new probabilistic model for rank aggregation. In *Advances in neural information processing systems* (pp. 1948-1956).
144. Ali, Alnur, and Marina Meilă. "Experiments with Kemeny ranking: What works when?." *Mathematical Social Sciences* 64.1 (2012): 28-40.
145. Young, H. Peyton. "An axiomatization of Borda's rule." *Journal of Economic Theory* 9.1 (1974): 43-52.
146. Cohen, William W., Robert E. Schapire, and Yoram Singer. "Learning to order things." *arXiv preprint arXiv:1105.5464* (2011).
147. de Borda, Jean C. "Mémoire sur les élections au scrutin." (1781).
148. Ailon, N. (2010). Aggregation of partial rankings, p-ratings and top-m lists. *Algorithmica*, 57(2), 284-300.
149. Khachiyan, L. G. (1980). Polynomial algorithms in linear programming. *USSR Computational Mathematics and Mathematical Physics*, 20(1), 53-72.
150. Makhorin, A. (2008). GLPK (GNU linear programming kit).

Appendix: List of the publications

Huang, C., Xie, M. H., Liu, W., **Yang, B.**, Yang, F., Huang, J., ... & Zhang, Y. (2011). A structured RNA in hepatitis B virus post - transcriptional regulatory element represses alternative splicing in a sequence - independent and position - dependent manner. *FEBS Journal*, 278(9), 1533-1546.

Xiao, R., Tang, P., **Yang, B.**, Huang, J., Zhou, Y., Shao, C., ... & Fu, X. D. (2012). Nuclear matrix factor hnRNP U/SAF-A exerts a global control of alternative splicing by regulating U2 snRNP maturation. *Molecular cell*, 45(5), 656-668.

Wang, Y., Jiang, L., Ji, X., **Yang, B.**, Zhang, Y., & Fu, X. D. (2013). Hepatitis B viral RNA directly mediates down-regulation of the tumor suppressor microRNA miR-15a/miR-16-1 in hepatocytes. *Journal of Biological Chemistry*, 288(25), 18484-18493.

Zhang X., Zuo X., **Yang B.**, Li Z., Xue Y., Zhou Y., Huang J., Zhao X., Zhou J., Yan Y., Zhang H., Guo P., Sun H., Guo L., Zhang Y., Fu X. (2014). MicroRNA Directly Enhances Mitochondrial Translation during Muscle Differentiation. *Cell*, 158(3), 607-619.

Shao C., **Yang B.**, Wu T., Huang J., Tang P., Zhou Y., Zhou J., Qiu J., Jiang L., Li H., Chen G., Sun H., Zhang Y., Denise A., Zhang D., and Fu X-D. (2014). Mechanisms for U2AF to Define 3' Splice Sites and Regulate Alternative Splicing in the Human Genome. *Nature Structure & Molecular Biology*. (Co-first author)

Acknowledgement

I would have not been able to finish this dissertation without the help and support of many people through these years.

First, I would like to express my deepest gratitude to my two advisors, Professor Xiangdong Fu and Professor Alain Denise, for their excellent guidance, enthusiasm, patience, and immense knowledge. Professor Denise is always so kind, precise and full of patience to me. He led me into the exciting field of combinatorial algorithms, trained me on algorithms and programming, taught me how to write and present, and usually concerned about my life in France. And Professor Fu is full of enthusiasm and knowledge. He taught me how to think independently in a biological view, and usually gave me profound insight or advice. I learned a lot from them and I am sure this will benefit me in the future. I also would like to thank to Yi Zhang, for her guide and kind help.

I would also like to thank the members of this thesis committee, Stéphane Vialette, and Jérôme Waldispühl, for their reviews of my work and their helpful comments.

Special thanks to all my collaborators: Changwei Shao, Bryan Brancotte, Xiaorong Zhang, Yanling Wang, Rui Xiao, Chen Huang and Qijia Wu, Peng Tang, Li Jiang. Many good ideas come out from discussion with them about the details, and they told me a lot of the experiments with patience.

I wish to thank all of the members of labs in Wuhan and Orsay, for their tremendous concern and help, as Feng Lou, Cong Zeng and Cécile Pereira usually discussed with me about our projects in Orsay. I would like to thank Yu Zhou. He taught me a lot and helps me in many aspects.

Last but not the least I would like to thank my family. Thanks to my parents for their always supporting and encouraging me with their best wishes. And I would like to thank my wife, Wei Zhou, for her love and unwavering support through the good times and bad.